TURUN YLIOPISTON JULKAISUJA
ANNALES UNIVERSITATIS TURKUENSIS

SARJA - SER. D OSA - TOM. 904

MEDICA - ODONTOLOGICA

EARLY DETECTION OF ALZHEIMER'S DISEASE β-AMYLOID PATHOLOGY

Applicability of Positron Emission Tomography with the Amyloid Radioligand ^{11}C-PIB

by

Noora Scheinin

TURUN YLIOPISTO
UNIVERSITY OF TURKU
Turku 2010

From Turku PET Centre / Department of Clinical Physiology and Isotope Medicine,
University of Turku, Turku, Finland

Supervised by

Professor Juha O. Rinne
Turku PET Centre
University of Turku
Turku, Finland

Reviewed by

Professor Aapo Ahonen
Department of Clinical Physiology and Nuclear Medicine
University of Helsinki
Helsinki, Finland

and

Professor Raimo Sulkava
Institute of Public Health and Clinical Nutrition
University of Eastern Finland
Kuopio, Finland

Dissertation Opponent

Professor Agneta Nordberg
Division of Alzheimer Neurobiology, Department of Neurobiology, Care Sciences and Society, Karolinska Institute
Karolinska University Hospital Huddinge
Stockholm, Sweden

ISBN 978-951-29-4287-9 (PRINT)
ISBN 978-951-29-4288-6 (PDF)
ISSN 0355-9483
Painosalama Oy – Turku, Finland 2010

To your mental health

Cover illustration: ^{11}C-PIB PET images of an elderly individual with an AD-like cognitive impairment (left above) and his/her cognitively healthy same-sexed monozygotic co-twin (right above) compared with another elderly individual with an AD-like cognitive impairment (left below) and his/her cognitively healthy same-sexed dizygotic co-twin (right below). Note the similarly increased ^{11}C-PIB uptake within the monozygotic twin pair as opposed to the dizygotic pair with increased ^{11}C-PIB uptake seen only in the cognitively impaired co-twin.

ABSTRACT

Noora M. Scheinin

EARLY DETECTION OF ALZHEIMER'S DISEASE β-AMYLOID PATHOLOGY

Applicability of positron emission tomography with the amyloid radioligand ^{11}C-PIB

From Turku PET Centre and Department of Clinical Physiology and Nuclear Medicine, University of Turku, Turku, Finland
Annales Universitatis Turkuensis Ser. D
Painosalama Oy, Turku, Finland 2010

Accumulation of beta amyloid (Aβ) in the brain is characteristic for Alzheimer's disease (AD). Carbon-11 labeled 2-(4'-methylaminophenyl)-6-hydroxybenzothiazole (^{11}C-PIB) is a novel positron emission tomography (PET) amyloid imaging agent that appears to be applicable for *in vivo* Aβ plaque detection and quantitation.

The biodistribution and radiation dosimetry of ^{11}C-PIB were investigated in 16 healthy subjects. The reproducibility of a simplified ^{11}C-PIB quantitation method was evaluated with a test-retest study on 6 AD patients and 4 healthy control subjects. Brain ^{11}C-PIB uptake and its possible association with brain atrophy rates were studied over a two-year follow-up in 14 AD patients and 13 healthy controls. Nine monozygotic and 8 dizygotic twin pairs discordant for cognitive impairment and 9 unrelated controls were examined to determine whether brain Aβ accumulation could be detected with ^{11}C-PIB PET in cognitively intact persons who are at increased genetic risk for AD.

The highest absorbed radiation dose was received by the gallbladder wall (41.5 μGy/MBq). About 20 % of the injected radioactivity was excreted into urine, and the effective whole-body radiation dose was 4.7 μSv/MBq. Such a dose allows repeated scans of individual subjects. The reproducibility of the simplified ^{11}C-PIB quantitation was good or excellent both at the regional level (VAR 0.9-5.5 %) and at the voxel level (VAR 4.2-6.4 %). ^{11}C-PIB uptake did not increase during 24 months' follow-up of subjects with mild or moderate AD, even though brain atrophy and cognitive decline progressed. Baseline neocortical ^{11}C-PIB uptake predicted subsequent volumetric brain changes in healthy control subjects ($r = 0.725$, $p = 0.005$). Cognitively intact monozygotic co-twins – but not dizygotic co-twins – of memory-impaired subjects exhibited increased ^{11}C-PIB uptake (117-121 % of control mean) in their temporal and parietal cortices and the posterior cingulate ($p<0.05$), when compared with unrelated controls. This increased uptake may be representative of an early AD process, and genetic factors seem to play an important role in the development of AD-like Aβ plaque pathology. ^{11}C-PIB PET may be a useful method for patient selection and follow-up for early-phase intervention trials of novel therapeutic agents. AD might be detectable in high-risk individuals in its presymptomatic stage with ^{11}C-PIB PET, which would have important consequences both for future diagnostics and for research on disease-modifying treatments.

Key words: ^{11}C-PIB, PET, Alzheimer's disease, radiation dosimetry, reproducibility, early disease detection, twin study, follow-up.

TIIVISTELMÄ

Noora M. Scheinin

ALZHEIMERIN TAUDIN β-AMYLOIDIPATOLOGIAN VARHAINEN TOTEAMINEN

^{11}C-PIB-amyloidimerkkiaineella tehtävän positroniemissiotomografian soveltuvuus

Valtakunnallinen PET-keskus, Kliinisen fysiologian ja isotooppilääketieteen oppiaine, Kliininen laitos, Turun yliopisto
Annales Universitatis Turkuensis Ser. D
Painosalama Oy, Turku, 2010

Beeta-amyloidin (Aβ) kertyminen aivoihin on tyypillistä Alzheimerin taudille (AT). Hiili-11-isotoopilla leimattu 2-(4'-metyyliaminofenyyli)-6-hydroksibentsotiatsoli (^{11}C-PIB) on uusi positroniemissiotomografiassa (PET) käytettävä merkkiaine, joka vaikuttaa soveltuvan amyloidiplakkien toteamiseen ja niiden määrän arvioimiseen.

^{11}C-PIB:n jakautumista kehossa ja sen aiheuttamaa säderasitusta tutkittiin 16 terveellä henkilöllä. Yksinkertaistettujen ^{11}C-PIB-analyysimenetelmien toistettavuutta selvitettiin toistomittausasetelmalla 6 AT-potilaalla ja 4 terveellä verrokilla. ^{11}C-PIB-kertymän muutosta sekä ^{11}C-PIB-kertymän ja aivojen kutistumisnopeuden välistä suhdetta mitattiin kahden vuoden seurantatutkimuksella, jossa oli 14 AT-potilasta ja 13 tervettä verrokkia. Tutkimalla 9 samanmunaista ja 8 erimunaista muistihäiriön suhteen toisistaan poikkeavaa kaksosparia sekä 9 iäkästä verrokkihenkilöä ^{11}C-PIB PET:lla selvitettiin, voisiko aivoamyloidia olla havaittavissa sellaisilla kognitiivisesti terveillä henkilöillä, joilla on suurentunut riski sairastua AT:iin.

Sappirakon seinämä sai elimistä suurimman määrän säteilyä, 41.5 μGy/MBq. Noin 20 % annetusta radioaktiivisuusannoksesta erittyi virtsaan. Efektiivinen sädeannos oli 4.7 μSv/MBq. Tämä annos mahdollistaa toistetut tutkimukset samoilla henkilöillä. Yksinkertaistettujen ^{11}C-PIB PET –analyysimenetelmien toistettavuus oli hyvää tai erinomaista sekä alueittain (VAR 0.9-5.5%) että kuva-alkioittain (VAR 4.2-6.4%) tarkasteltuna. ^{11}C-PIB-kertymä ei lisääntynyt AT-potilailla seuranta-ajan kuluessa, vaikka aivojen kutistuminen ja kognitiivinen heikentyminen etenivät. Alkutilanteen ^{11}C-PIB-kertymä vaikutti ennustavan terveiden verrokkien aivojen tilavuusmuutoksia seuranta-aikana ($r = 0.725$, $p = 0.005$). Kognitiivisesti terveillä muistihäiriöisten samanmunaisilla kaksosilla – mutta ei erimunaisilla kaksosilla - oli suurentuneita ^{11}C-PIB-kertymiä (117-121% verrokkien keskiarvosta) ohimo- ja päälakialueen aivokuorella sekä posteriorisessa cingulumissa ($p<0.05$), kun heitä verrattiin verrokkeihin. Tämä suurentunut kertymä voisi viitata varhaiseen AT-sairausprosessiin; perinnöllisillä tekijöillä on ilmeisesti merkitystä amyloidipatologian kehittymiselle aivoissa. ^{11}C-PIB PET voi olla käypä menetelmä tutkittavien valinnassa ja seurannassa, kun tehdään varhaisen sairausvaiheen tutkimuksia uusilla lääkkeillä. AT saatetaan voida todeta ^{11}C-PIB PET:n avulla täysin oireettomassa vaiheessa sellaisilla henkilöillä, joilla on suurentunut riski sairastua. Tällä voisi olla merkittäviä vaikutuksia taudinmääritykselle ja sellaisten hoitojen tutkimiselle, jotka tähtäävät taudin kulun muuttamiseen.

Avainsanat: ^{11}C-PIB, PET, Alzheimerin tauti, säderasitus, toistettavuus, varhainen taudin havaitseminen, kaksostutkimus, seurantatutkimus.

TABLE OF CONTENTS

ABBREVIATIONS

^{11}C-PIB	carbon-11 labeled 2-(4'-methylaminophenyl)-6-hydroxybenzothiazole
^{11}C-PK-11195	carbon-11 labeled 1-(2-chlorophenyl)-N-methyl-N-(1-methylpropyl)-3-isoquinole carboxamide
Aβ	beta amyloid
AD	Alzheimer's disease
ALL	Anatomical Labeling atlas
ALS	amyotrophic lateral sclerosis
aMCI	amnestic mild cognitive impairment
ANOVA	analysis of variance
ApoE	apolipoprotein E
APP	amyloid precursor protein
AutoROI	automated ROI analysis
BACE1	β-secretase
CAA	cerebrovascular amyloid angiopathy
CDR-SOB	Clinical Dementia Rating Sum of Boxes
CERAD	Consortium to Establish a Registry for Alzheimer's Disease
CJD	Creutzfeldt-Jakob disease
CRST	Clinical Research Services Turku
CSF	cerebrospinal fluid
CT	computed tomography
DLB	dementia with Lewy bodies
DSM-IV	Diagnostic and Statistical Manual of Mental Disorders version IV
DV(R)	distribution volume (ratio)
DZ	dizygotic
ED	effective dose
^{18}F-FDG	fluorine-18 labeled fluoro-2-deoxy-D-glucose
fMRI	functional magnetic resonance imaging
FTLD	frontotemporal lobe dementia
ICC	intra-class correlation coefficient
ICRP	International Commission on Radiological Protection
MCI	mild cognitive impairment
MMSE	Mini-Mental State Examination
MNI	Montreal Neurological Institute
MRI	magnetic resonance imaging
MTL	medial temporal lobe
MZ	monozygotic
NFT	neurofibrillary tangle
NINCDS-ADRDA	The National Institute of Neurological and Communicative Disorders and Stroke and the Alzheimer's Disease and Related Disorders Association

NMDA	N-methyl-D-aspartate
PBBR	peripheral benzodiazepine binding receptor
PCA	posterior cortical atrophy OR
PCA	principal component analysis
PDD	Parkinson's disease dementia
PET	positron emission tomography
PPA	primary progressive aphasia
PS or PSEN	presenilin
rCMRgluc	regional cerebral glucose metabolism
rmANOVA	repeated measurements analysis of variance
ROC	receiver operating characteristics
ROI	region-of-interest
SPET	single photon emission tomography
SPM	Statistical Parametric Mapping
SUV(R)	standardized uptake value (ratio)
T1	longitudinal relaxation
T2	transverse relaxation
TAC	time-activity curve
TELE	cognitive screen by telephone
TICS	telephone screen for cognitive status
TRT	test-retest
VAR	absolute variability
VBM	voxel-based morphometry

LIST OF ORIGINAL PUBLICATIONS

This thesis is based on the following original publications, which will be referred to by their Roman numerals:

I **Scheinin NM**, Tolvanen TK, Wilson IA, Arponen EM, Någren KA, Rinne JO: Biodistribution and radiation dosimetry of the amyloid imaging agent ^{11}C-PIB in humans. *Journal of Nuclear Medicine* 2007; 48 (1):128-133.

II Aalto S, **Scheinin NM**, Kemppainen NM, Någren K, Kailajärvi M, Scheinin M, Rinne JO: Reproducibility of automated simplified voxel-based analysis of PET amyloid ligand [^{11}C]PIB uptake using 30 min scanning data. *European Journal of Nuclear Medicine* 2009; 36(10):1651-60.

III **Scheinin NM**, Aalto S, Koikkalainen J, Lötjönen J, Karrasch M, Kemppainen N, Viitanen M, Någren K, Helin S, Scheinin M, Rinne JO: Follow-up of [^{11}C] PIB uptake and brain volume in patients with Alzheimer disease and controls. *Neurology* 2009; 73(15):1186-92.

IV **Scheinin NM**, Aalto S, Kaprio J, Koskenvuo M, Räihä I, Rokka J, Hinkka-Yli-Salomäki S, Rinne JO: Early detection of Alzheimer's disease – ^{11}C-PIB PET in monozygotic and dizygotic twins discordant for cognitive impairment. *Submitted for publication.*

 In addition, unpublished data are presented in this thesis.

1. INTRODUCTION

Deposits of beta-amyloid (Aß) in the brain are characteristic for Alzheimer's disease (AD). The amyloid cascade hypothesis suggests that Aß deposits are the actual main underlying cause for functional brain loss in AD (Hardy and Selkoe 2002). Positron emission tomography (PET) ligands have been developed so that Aß plaques and brain amyloid pathology can be studied *in vivo* in living humans, not only *post mortem* in brain samples [for a review, see *e.g.* (Nordberg 2004)].

Carbon-11 labeled 2-(4'-methylaminophenyl)-6-hydroxybenzothiazole (^{11}C-Pittsburgh Compound B or ^{11}C-PIB) is an amyloid imaging agent which has been shown to be applicable for *in vivo* Aβ plaque detection. The compound crosses the blood-brain barrier readily and has high selectivity for Aß (Klunk et al. 2001, Bacskai et al. 2003). Several ^{11}C-PIB PET studies have confirmed that patients with AD consistently show significantly greater, up to two-fold, ^{11}C-PIB uptake compared with age-matched healthy control subjects in the neocortical brain regions that are typically affected by Aβ accumulation (Buckner et al. 2005, Price et al. 2005, Archer et al. 2006, Engler et al. 2006, Kemppainen et al. 2006, Edison et al. 2007a, Edison et al. 2007b, Rowe et al. 2007).

Currently ^{11}C-PIB PET is being evaluated to determine whether it has value in differential diagnostics, early disease detection, monitoring of AD progression, and testing the efficacy of anti-amyloid therapies. Since amyloid accumulation in the brain is characteristic for AD and possibly also a very early event in AD (Braak and Braak 1991, Price and Morris 1999), the quantity and distribution pattern of Aβ is of great interest also in studies exploring genetic factors and the ultimate molecular pathophysiology of AD.

The present work assessed the radiation safety and reproducibility of practical ^{11}C-PIB PET imaging methods (studies **I** and **II**) in order to evaluate the applicability of and to validate repeated studies with ^{11}C-PIB PET. It was also examined whether ^{11}C-PIB PET would be useful in monitoring disease progression relative to other changes in AD with a follow-up design (study **III**) and monozygotic and dizygotic twins discordant for cognitive impairment were investigated in order to gain insight into the impact of genetic factors behind Aβ accumulation (study **IV**). The assessment of early AD detection value of *in vivo* amyloid imaging and an improved understanding of AD pathophysiology were more distant goals of this work throughout the practical investigations, and represented the ultimate motivation behind this thesis project.

2. REVIEW OF THE LITERATURE

2.1 ALZHEIMER'S DISEASE AND APPROACHES TO ITS EARLY DETECTION

2.1.1 Epidemiology, clinical features, diagnosis and treatment of AD

AD epidemiology

Alzheimer's disease is the most common neurodegenerative disorder and the most common cause of cognitive decline in the elderly – it accounts for 60-75 % of all cases of dementia. With increasing longevity, the number of persons with AD is likely to increase quite dramatically – the incidence of both dementia and AD has been shown to increase rather sharply up to the age of 90 years, with no sign of levelling off (Jorm and Jolley 1998). It has been estimated that 24 million people worldwide had dementia in 2005, and that 4.6 million new cases of dementia develop every year. The same study estimated that the number of affected people will double every 20 years, to reach 81 million by the year 2040. The rate of increase of dementia has also been predicted to be three or four times higher in developing than in developed regions of the world (Ferri et al. 2005).

The clinical course and diagnosis of AD

AD causes a progressive decline in cognitive functions. The first sign is most often an impairment of episodic memory, presenting as problems in learning, storing, and recalling new information. Later in the disease course, other cognitive domains are also involved. These symptoms then include deficits in executive functioning, failures in concentration, inability to recognize familiar things, disorientation both temporally and visuo-spatially, as well as problems with language and perception. Most AD patients also experience behavioural symptoms, such as depression, agitation and irritability. In later phases of the disease, delusions, wandering, paranoia and sleep disturbances are common. Sensory and motor functions are relatively well preserved until the later stages of the disease, although also these domains are ultimately affected in severe AD. Patients with severe AD are most often institutionalized for a long duration, and at some point become bedridden and completely dependent on others for basic daily activities, such as dressing and feeding. The most common immediate cause of death in AD is pneumonia, because swallowing and coughing become increasingly impaired in very severe AD. The time from AD diagnosis to death varies greatly, but based on available knowledge, the clinical disease duration is considered to be approximately 10 years on the average.

Currently, AD is diagnosed by evaluating marked episodic memory impairment characterized by a gradual, progressive decline over more than 6 months (as reported

by the patient or an informant). Structural brain imaging can support the diagnosis of AD by revealing hippocampal and other medial temporal lobe brain atrophy (see section *2.1.6 Magnetic resonance imaging in AD and its potential in predicting AD*). Other supporting features might include biochemical or imaging biomarkers (Dubois et al. 2007). Laboratory testing and brain imaging can be used to rule out other or concomitant causes of cognitive impairment. These include vitamin B12 deficiency, hypothyroidism, infection, normal pressure hydrocephalus, brain tumours and vascular dementia. However, currently no test has been found, whether be it a laboratory test (from blood or cerebrospinal fluid samples) or an imaging procedure, which can give a definite AD diagnosis, let alone predict that the disease will develop before the appearance of any symptoms.

Treatment of AD

To date, no treatment has been shown to halt or reverse the underlying pathological process of AD. Therapies are confined to symptomatic, palliative interventions (Barrow 2002). The present treatments target the cholinergic neurotransmitter system of the brain, because it is progressively disturbed in AD – concentrations of acetylcholine are decreased in synaptic clefts of the neuronal connections important for memory and other cognitive functions. Acetylcholinesterases are natural enzymes that break down acetylcholine, and most of the current AD drugs inhibit these enzymes, thus prolonging the biological half-life of the acetylcholine content in the synaptic cleft and therefore improving cholinergic neurotransmission. Drugs of this class are currently used to help especially patients with mild-to-moderate AD, but their effects are confined to the alleviation of symptoms, and none of the treatments has a major therapeutic impact. Furthermore, it is not possible to identify those patients who will respond favourably to cholinesterase inhibitor treatment before starting the medication. (Birks 2006) In addition to the acetylcholinesterase inhibitor drugs such as donepezil, rivastigmine and galantamine, another drug, memantine, is currently in wide clinical use. This is an antagonist of N-methyl-D-aspartate (NMDA) receptors that mediate glutamatergic neurotransmission. There appears to be relative glutamatergic overactivity in AD, and this has been associated with neuronal death – memantine is postulated to reversibly block the actions of glutamate. The drug has shown some degree of efficacy in the symptomatic treatment of moderate-to-severe AD, and therefore it is often combined with an acetylcholinesterase inhibitor drug when the disease progresses. However, memantine is also unable to halt the progression of the disease (Areosa and Sherriff 2003).

Several types of potential disease-modifying treatments with specific molecular targets in AD pathology are under development, such as immunotherapy evoking antibody-induced clearance of beta-amyloid (Aβ) (Bayer et al. 2005, Gilman et al. 2005). Other approaches include inhibition of the secretase enzymes that are responsible for releasing Aβ from its parent protein APP, inhibition of Aβ self-association to form oligomers or amyloid plaques, and inhibition of Aβ-associated neuronal toxicity (Barrow 2002). There are several on-going clinical trials on agents that are aimed to treat AD by targeting Aβ.

Since Aβ accumulation is an early-stage event that is central to the neuropathology of AD (see next section *2.1.2 Neuropathological features of the disease*), there is hope that Aβ-related therapeutic strategies will lead to treatment options that target the underlying causes rather than the symptoms of AD.

2.1.2 Neuropathological features of the disease; neurofibrillary tangles, amyloid plaques and the amyloid cascade hypothesis

The neuropathological changes seen in AD include brain grey matter atrophy, accumulation of Aβ (as senile plaques and amyloid angiopathy) and neurofibrillary tangle formation. The loss of synapses and whole neurons leads to failure of important neural connections. The neurochemical changes associated with AD affect many neurotransmitters, *e.g.* the cholinergic, serotonergic, noradrenergic and dopaminergic systems. Morphologically, AD is primarily a degenerative disease of the supportive structures of the neuronal cells.

Neurofibrillary tangles

One reason for the degeneration of neurons in AD seems to be the appearance of intracellular neurofibrillary tangles (NFTs), which consist of hyperphosphorylated tau protein. Tau is normally a useful constituent of the neuronal cell structure because it supports microtubuli, which in turn have an important role in the cytoskeleton of the cellular transportation system. However, when tau is extensively phosphorylated, it forms paired helical filaments and detaches itself from the microtubuli. In AD, tau becomes hyperphosphorylated for currently unknown reasons, and the dimers that are generated in this way form NFTs. The tangles accumulate inside the neuron and this causes the intracellular connections to degenerate. (Brion 1998) NFTs are seen also in other dementing diseases as well as in the brains of healthy elderly subjects [*e.g.* (Price et al. 1991)].

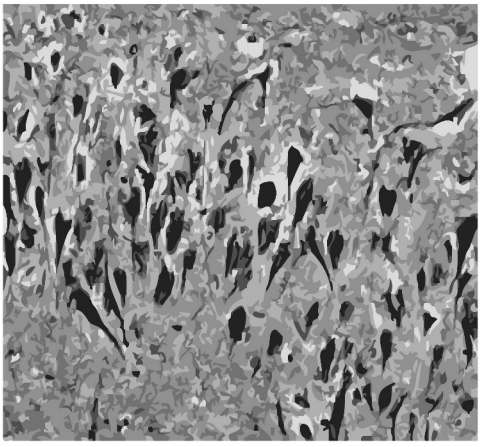

Figure 1. An illustration of neurofibrillary tangles, modified from an image of Bielschowski-stained brain tissue.

In AD, the accumulation of NFTs is nevertheless more abundant and their distribution in the brain follows a certain temporal and spatial pattern. NFTs first appear in the transentorhinal region of the brain, and then progress to affect the entorhinal region and the hippocampus (Braak and Braak 1991). The NFT distribution extends to the cerebral neocortex only during later phases (Braak stages V and VI) of NFT deposition, and these stages are associated with moderate-to-severe dementia symptoms. (Braak and Braak 1991, Price et al. 1991) AD can be distinguished from other diseases in a *post mortem* histopathological examination by determining the quantity and distribution of NFTs.

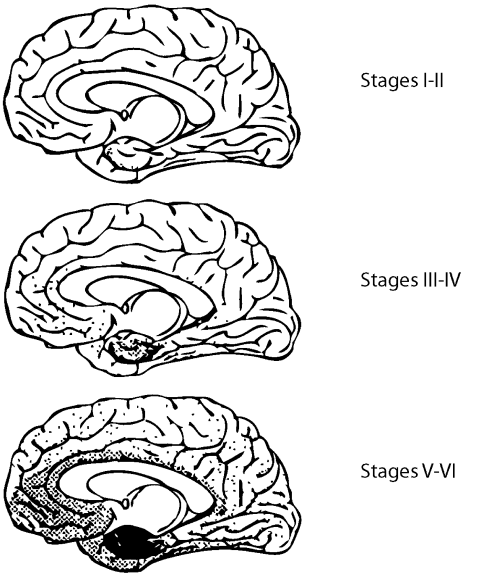

Figure 2. Braak stages of neurofibrillary tangle (NFT) distribution as modified from Braak and Braak 1991 (Braak and Braak 1991). Shaded areas represent relative density of NFTs. Note the very dense concentration of NFTs in the hippocampus.

Amyloid plaques and the amyloid cascade hypothesis

Another histopathologically observed difference between the brains of even mild AD patients and healthy subjects of the same age is the widely distributed Aβ plaque deposition in the neocortex of AD patients. The amyloid cascade hypothesis postulates that Aβ is the initial causative agent of the disease process (Hardy 1997, Hardy and Selkoe 2002). According to this hypothesis, the accumulation of Aβ triggers a series of events and as a consequence, the other pathological changes of AD evolve: NFT formation, oxidative stress, synapse loss, inflammatory responses, and ultimately, neuronal death.

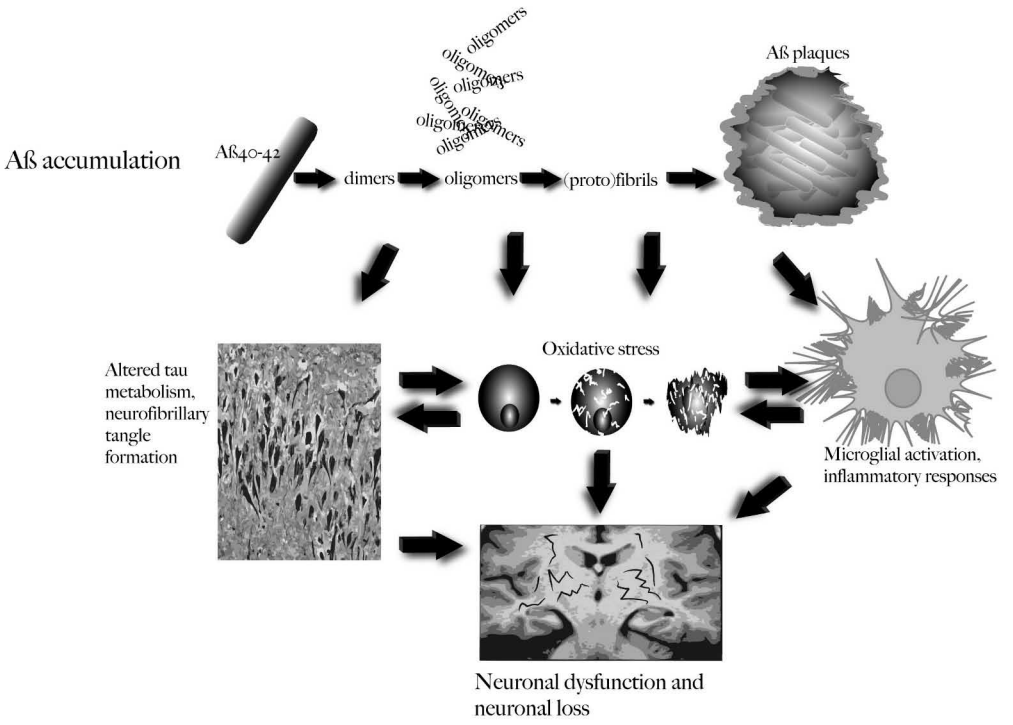

Figure 3. One version of the amyloid cascade hypothesis. This version takes into account the possibility that several forms of Aβ could be the toxic, initiating substances. The idea has been adapted from various sources in the literature [*e.g.* Mathis et al. 2007)].

The concept that several familial forms of AD are associated with mutations in genes affecting amyloid metabolism and thus causing increased brain Aβ load supports the amyloid cascade hypothesis (see more in section *2.1.3 Genetics of AD*). Other findings supporting the amyloid cascade hypothesis include the observation that Aβ induces NFT formation in transgenic mice [*e.g.* (Bolmont et al. 2007, Terwel et al. 2008)]. These results suggest that even though NFTs may be more directly associated with ultimate neuronal loss, Aβ accumulation would precede and accelerate NFT formation and would therefore be a more "upstream" process in AD pathophysiology. Furthermore, Aβ-induced oxidative stress has been demonstrated in both *in vitro* and *in vivo* studies [for a review, see (Sultana et al. 2009)].

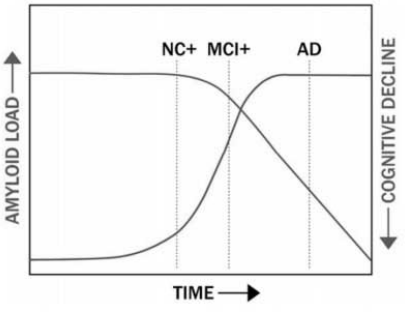

Figure 4. A proposition for the time course of amyloid deposition and cognitive decline in Alzheimer's disease, partly based on observations with ^{11}C-PIB PET, as suggested by Mathis *et al*. (Mathis et al. 2007). NC = normal cognition; MCI = mild cognitive impairment; AD = Alzheimer's disease.

Aβ is a polypeptide with multiple β-pleated sheets, and it consists of 39 – 43 amino acids. Two enzymes, β- and γ-secretases, cleave Aβ peptides proteolytically from the amyloid precursor protein (APP) (**Figure 5**), which is a glycoprotein abundantly expressed in neuronal cell membranes. In AD, Aβ accumulates abnormally in different forms, which can be divided for example into soluble and insoluble forms. Aβ can polymerize into dimers, oligomers, protofibrils, fibrils and plaques (see **Figure 5** for a schematic illustration of the amyloidogenic pathway of APP metabolism). Extracellularly situated amyloid plaques, containing insoluble fibrillary Aβ, are one of the most typical characteristics of AD, and these plaques can further be divided into different subtypes, such as diffuse and neuritic plaques. The neuritic plaques are traditionally considered to play an important role in AD pathophysiology. They have a hard core and the long form Aβ1-42 is overrepresented in these structures compared with other lengths of Aβ. Inflammatory changes such as activated microglial cells and astrocytes are associated with these plaques, and dystrophic axons and dendrites are seen in their proximity. Neuritic plaques are also surrounded by abundant NFTs and along with Aβ, several other proteins, such as apolipoprotein E (ApoE), can be found in the plaques.

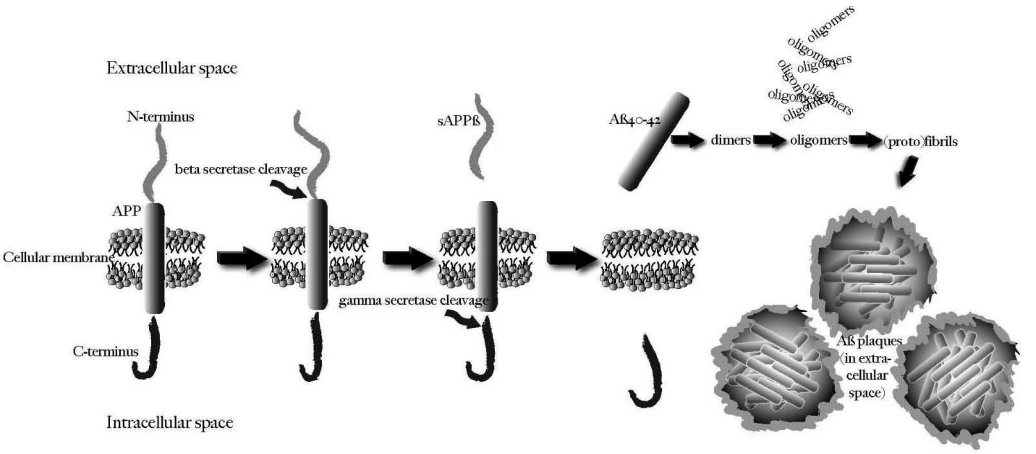

Figure 5. Schematic illustration of the amyloidogenic pathway of APP processing and the formation of Aβ plaques. Aβ monomers are thought to form oligomers in the extracellular space. Some of these oligomers polymerize further into protofibrils and fibrils, which are the main component of Aβ plaques. Both oligomers and fibrillar Aβ are believed to be initial toxic components evoking neurodegeneration in AD. This concept has been adapted from various published sources. [See *e.g.* (Mathis et al. 2007)].

Aβ plaque deposition appears to start in the neocortex, especially in the poorly myelinated regions of the basal neocortex. Subsequently, plaques can be found in the nuclei of the midbrain, as well as in the basal cholinergic nuclei of the forebrain, which is the site of origin of important cholinergic pathways to the hippocampus and neocortex. Finally, Aβ plaques become distributed in all of the basal nuclei and cortical regions – in the very late stages of AD, they can be found even in the cerebellum. (Braak and Braak 1991,

Braak and Braak 1997) AD-related Aβ deposition appears to advance anterogradely to structures that receive neural projections from sites of earlier Aβ deposition (Thal et al. 2002). More specifically, in the medial temporal lobe (MTL; an important brain region with regard to memory), amyloid plaques first develop in the temporal cortex and thereafter in the entorhinal cortex, followed later by different parts of the hippocampus. This concept highlights the importance of the neural connections between the entorhinal cortex and the hippocampus in the spread of Aβ pathology. (Thal et al. 2002) The temporal and spatial accumulation pattern of Aβ plaques resembles, at least to some extent, the distribution of NFTs in the same brain regions, such as in the MTL (Braak and Braak 1991). However, amyloid pathology can be seen in mild AD also in the frontal cortical regions, which is not typical for NFTs. (Braak and Braak 1997). In addition, histological studies suggest that NFTs are prominent in the MTL early in the disease and progress outwards; amyloid has a broader cortical distribution that includes, but is not especially prominent in, the MTL (Braak and Braak 1991, Price et al. 1991, Braak and Braak 1997).

The brain regions with the greatest grey matter atrophy (*i.e.* neuronal loss) and amyloid accumulation also seem to differ (Jack et al. 2008). In AD, profound cell loss is observed predominantly (and as a relatively early change) in the hippocampal region (for more information see section *2.1.6 MRI in AD in its potential in predicting AD*). As reviewed here, Aβ deposition is conversely predominantly seen in the neocortex. The discrepancies between the sites of the different measurable and characteristic pathological changes of AD naturally raise questions as to the nature of the relationships between Aβ load, NFTs and neuronal loss. Some of the possible explanations will be discussed later in this thesis, and further studies will no doubt shed light on these associations. Disruptions in Aβ metabolism are in any case present in AD, the accumulation of Aβ seems to be an early event [*e.g.* (Price and Morris 1999)], and Aβ plaques are quite specific for the disease, as opposed to some other neuropathological changes. Studies on Aβ accumulation in AD are therefore of great interest both in terms of early detection of the disease as well as for developing new therapeutic strategies to combat this devastating illness. Previously, it was possible to study Aβ accumulation in humans only by staining Aβ plaques with different histopathological dyes, such as Congo Red or thioflavine, in *post mortem* brain tissue or, rarely, in a brain biopsy. New *in vivo* amyloid imaging methods have the potential to markedly contribute to improving our understanding of Aβ pathology in AD and its relationship with the other neuropathological changes typical of this disease.

2.1.3 Genetics of AD: familial monogenic forms of AD, twin studies, effect of apolipoprotein E genotype

Genetics of AD – familial forms

A large number of autosomal dominant mutations in the gene that encodes APP (in chromosome 21) have been found to cause early-onset (at 40 – 65 years of age) familial

AD. These mutations cause disturbances in the processing of APP, which lead to increased Aβ accumulation in brain tissue. These mutations can cause either overproduction of Aβ or inappropriate cleavage of APP into longer, more easily precipitating forms of Aβ (Aβ1-42). [For a review, see *e.g.* (Lambert and Amouyel 2007).] Duplication of the APP gene locus also appears to cause autosomal dominant AD through overexpression of the gene (Rovelet-Lecrux et al. 2006, Sleegers et al. 2006). It has also been known for some time that an increased APP gene copy number in 21-trisomy, *i.e.* in Down's syndrome, is associated with increased brain Aβ load and AD with a substantially earlier disease onset than encountered in the general population [*e.g.* (Hof et al. 1995)]. At the moment, attempts are being made to characterize mutations or polymorphisms also in the promoter region of the APP gene and there are hints that genetic variation within this promoter may modify the risk of developing AD (Theuns et al. 2006).

Several autosomal dominant mutations in presenilin (PS or PSEN) genes (in chromosomes 14 and 1) have also been found to cause familial early-onset AD. These mutations in the genes PS1 and PS2 cause cleavage of Aβ into longer, accumulation-prone forms (Hardy 1997). The more frequently mutated gene, PS1, accounts for the majority of those AD cases with an onset before the age of 50 (Bertram and Tanzi 2005).

In all, the monogenic forms with mutations in the APP and PS genes have been estimated to account for as little as 1-5 % of all cases of AD (Campion et al. 1999, Bertram and Tanzi 2004b). All of the so far identified mutations in APP, PS1 and PS2 are on the other hand associated with early-onset AD. It is very plausible that there are other monogenic familial forms of AD that manifest as late-onset AD, but the genetic alterations behind these forms have not yet been clarified because many of the carriers of these mutations have died at a presymptomatic stage of the disease.

Sporadic AD, twin studies

Although additional forms of monogenic as well as multiple-gene familial AD are still expected to be identified, the vast majority of AD is currently at least apparently non-familial, and therefore classified as sporadic AD. However, family history is the second-greatest risk factor for the disease, being only second to age (Bertram and Tanzi 2005), which highlights the importance of genetic influences also in these cases. Twin studies have attempted to elucidate the extent of this – most likely very heterogenic - entity of genetic components as opposed to purely environmental factors. It has been estimated that in late-onset AD – if one tries to exclude familial forms of the disease - monozygotic (MZ) twins are on the average 31-67 % concordant for AD while the concordance rate of dizygotic (DZ) twins is 8.7-22 % (Räihä et al. 1996, Gatz et al. 1997, Pedersen et al. 2004) The finding that MZ twins (who share 100 % of their genes) show more AD concordance than DZ twins (who share on the average 50 % of their segregating genes) implies that genetics could play a dose-related role in the risk for AD. This conclusion is based on the assumption that twins, irrespective of their zygosity, more or less share their pre- and postnatal environments. One large twin study indicated that genetic factors

alone may explain 60–80 % of the risk of developing AD (Gatz et al. 2006). Longitudinal studies have, however, shown that the time of onset of AD symptoms between MZ co-twins who eventually become concordant for the disease can vary by several years (Cook et al. 1981, Räihä et al. 1996, Brickell et al. 2007) Additionally, the mere existence of discordance between genetically identical MZ twins already suggests that environmental factors also contribute at least to the disease phenotype and age of clinical onset. In short, the relationship between genetic and environmental factors is unclear in sporadic AD.

The role of apolipoprotein E genotype

Only one genetic factor has so far been found to clearly affect the risk for sporadic AD. It was discovered in 1993 that the apolipoprotein (ApoE) gene and more specifically its epsilon 4 allele is genetically associated with an increased risk for both sporadic and familial late-onset AD (Strittmatter et al. 1993). At present, ApoE epsilon 4 is considered the primary genetic risk factor associated with sporadic AD (Ritchie and Dupuy 1999, Martins et al. 2006). A dose-effect relationship exists between the number of epsilon 4 alleles and the risk for AD (Farrer et al. 1997) – see **Table 1** for the association of the different ApoE genotypes with the risk of developing AD.

Table 1. The association of the different ApoE genotypes with the risk of developing AD in Caucasian populations [from (Farrer et al. 1997)]. OR = odds ratio; IC = confidence interval.

	Autopsy and clinic studies	**Population-based studies**
ApoE	OR (IC 95%)	OR (IC 95%)
e2/e2	0.6 [0.2–2.0]	0.9 [0.3–2.8]
e2/e3	0.6 [0.5–0.8]	0.6 [0.5–0.9]
e3/e3	1 (reference)	1 (reference)
e2/e4	2.6 [1.6–4.0]	1.2 [0.8–2.0]
e3/e4	3.2 [2.8–3.8]	2.7 [2.2–3.2]
e4/e4	14.9 [10.8–20.6]	12.5 [8.8–17.7]

The ApoE epsilon 4 allele lowers the age of onset of AD and it is associated with increased Aβ deposition in brain parenchyma as well as in cerebral blood vessels (Schmechel et al. 1993, Olichney et al. 1996, Khachaturian et al. 2004). Even in elderly subjects without dementia, the ApoE genotype is related to the degree of deposition of Aβ in the cerebral cortex (Polvikoski et al. 1995). However, in recent longitudinal studies, epsilon 4 has shown only a slight effect on lifetime susceptibility to AD (Khachaturian et al. 2004) and it has been suggested that the epsilon 4 allele may actually predict only *when* but not *if* an individual is predisposed to AD (Meyer et al. 1998). This would mean that the epsilon 4 allele would only alter the age of onset as a function of other factors; these would be the factors that truly predispose an individual to the disease. Furthermore, both sex and ethnicity seem to greatly modify the effect of the ApoE genotype on the risk for AD (Farrer et al. 1997). Given these uncertainties and the concept that the role of ApoE in AD pathophysiology is still unclear (Bertram and Tanzi 2004a, Bertram and Tanzi 2005), ApoE genotyping is not at present considered a diagnostic or predictive investigation for AD.

Another potential genetic risk factor for late-onset AD that has recently received attention is the SORL1 gene, which encodes a sorting receptor involved in endosomal protein trafficking. The exact mechanisms through which SORL1 polymorphisms might be linked with AD are unclear, and conflicting results have been published as to its actual impact on the risk. [*e.g.* (Reitz and Mayeux 2009)] Nonetheless, other candidate genes for potentially important polymorphisms are anticipated to emerge as genetic mapping continues to develop.

2.1.4 Mild cognitive impairment *per se* and as a predictor of AD

MCI

Mild cognitive impairment (MCI) is a condition in which the cognitive functions of a subject are subjectively and/or objectively worsened in comparison to healthy persons of the same age. The criteria of AD or any other dementia are, however, not fulfilled, because there are no significant problems encountered in the activities of daily living. The recently revised MCI criteria are more unambiguous: (i) the person is neither normal nor demented; (ii) there is evidence of cognitive deterioration shown by either an objectively measured decline over time and/or subjective report of decline by self and/or informant in conjunction with objective cognitive deficits; and (iii) activities of daily living are preserved and complex instrumental functions are either intact or minimally impaired (Winblad et al. 2004).

MCI is often conceptualized as a transitional state between healthy aging and dementia (Petersen 2000). However, it is a heterogenic syndrome rather than a disease. It can be categorized into three or more different subtypes according to the dimensions of memory impairment (amnestic *vs.* nonamnestic) and the number of cognitive domains involved (single *vs.* multiple). (Petersen 2004, Winblad et al. 2004) Amnestic MCI (single- or multi-domain) is considered to be the subcategory of MCI with the greatest risk of subsequent AD.

MCI as a predictor of AD

About 10-15 % of persons with MCI convert annually to AD, depending on the study and the criteria for MCI, whereas the proportion of cognitively healthy individuals of the same age is 1-2 % (Petersen 2000). More specifically, individuals who have amnestic MCI (aMCI) – although aMCI is considered to be the most likely form of MCI to represent early AD - have been reported to convert to AD with an annual rate of about 12 %. Perhaps more importantly, it has been estimated that up to about 80 % of these aMCI subjects will convert to AD within 6 years. (Petersen et al. 2001) The conversion rates of MCI to AD, however, display extensive variation between studies, with epidemiological studies generally showing smaller proportions than progressive studies conducted in specialty clinics (Larrieu et al. 2002, Ganguli et al. 2004). Furthermore, a number of studies suggest that a very substantial proportion of MCI subjects also remain stable

or even revert to normal cognition during follow-up (Larrieu et al. 2002, Ganguli et al. 2004, Hansson et al. 2006).

Post mortem studies on MCI subjects have reported varying degrees of AD pathology (Morris et al. 2001, Markesbery et al. 2006, Petersen et al. 2006). The MCI subjects that eventually convert to AD show more overall as well as greater focal brain atrophy (in the hippocampus, inferior and middle temporal gyrus, posterior cingulate and medial temporal region) measured with MRI than non-converters (Chételat et al. 2005). Furthermore, even when assessed visually, medial temporal atrophy rates in aMCI subjects are associated with a significantly increased risk of developing dementia in the subsequent 3 years (DeCarli et al. 2007). Poorer performance on a combination of neuropsychological test measures has also been claimed to predict conversion to AD with relatively good accuracy (80 % combined with ApoE carrier status) (Fleisher et al. 2007). Reduced cerebral glucose metabolism seen with ^{18}F-FDG PET (prediction sensitivity and specificity around 80-90 %) (Mosconi et al. 2004, Drzezga et al. 2005) as well as low cerebrospinal fluid Aβ and increased tau levels (both combined: sensitivity 95 % and specificity 83 %) (Hansson et al. 2006) and ApoE epsilon 4 carrier status (possession of an epsilon 4 allele was associated with a 93 % increase in the risk of developing AD during follow-up) (Aggarwal et al. 2005) have also been identified as potential predictors of conversion. The sensitivity and specificity of these additional predictive factors have, however, varied substantially depending on the study and so far, it is impossible to predict reliably which subjects with MCI are most prone to later convert to AD. Thus, one could argue that it would be useful to abandon the diagnosis of MCI and to try to otherwise identify the true features that would predict which subjects with memory impairment will develop AD in the future.

The pathological changes in AD may start even decades before clinical symptoms are detectable (Price and Morris 1999). MCI is therefore an interesting condition and better understanding of the syndrome could be expected to aid in understanding the etiology of AD, and in developing tools for the early detection of AD. However, given the heterogeneity of the research results described above, the common criteria for MCI still have limited specificity for the early detection of AD. Thus it is essential to understand why MCI conversion rates differ so much between studies and it is also important to improve both the specificity and sensitivity of the diagnostics. Although it cannot be expected that MCI (or its subtypes) could be the only measure of conversion risk to AD, one can hope that research on MCI could provide markers for the early identification of individuals with prodromal AD at a pre-dementia stage when potential disease-modifying therapies would be most likely to be efficacious and cost-effective.

2.1.5 Cerebrospinal fluid and blood biomarkers in AD and as its antecedent indicators

The typical changes found in the cerebrospinal fluid (CSF) of AD patients are decreased levels of Aβ1-42 and increased levels of tau and phosphorylated tau (p-tau) [*e.g.*

Sunderland et al. 2003, Hansson et al. 2006, Mattsson et al. 2009)]. However, these changes are detectable only in some AD patients, it seems especially in those who carry the ApoE epsilon 4 risk allele (Sunderland et al. 2004). None of the investigated CSF biomarkers have to date fulfilled the criteria needed for diagnostic testing. However, some CSF biomarkers have shown potential in identifying persons at an increased risk for AD. Recent studies have implied that reduced CSF Aβ1-42 and increased total tau and p-tau (Ewers et al. 2007, Mattsson et al. 2009), or β-secretase (BACE1) activity (Zetterberg et al. 2008) as single biomarkers, as well as the combination of tau and Aβ1-42 or tau and Aβ1-42/p-tau (Hansson et al. 2006), could predict conversion from MCI to AD. However, inter-site assay variability in these CSF measures represents a significant challenge (Mattsson et al. 2009). Many questions also remain unanswered behind these findings, such as why and how Aβ1-42 and tau concentrations and BACE1 activity are associated with the ApoE epsilon 4 allele (Sunderland et al. 2004, Ewers et al. 2008). Other candidates for early biomarkers of AD pathophysiology in the CSF are also under study. The relationships between CSF biomarkers and brain Aβ plaques will be discussed later in this thesis.

Blood biomarkers would be a very interesting possibility for early AD detection in terms of feasibility. The studies on plasma Aβ are not consistent, but recent findings have indicated that decreased plasma Aβ1-42 concentrations relative to the amounts of Aβ1-40 might increase the risk of AD (Hampel et al. 2008). The development of plasma-based biomarker assays may also be possible, but again, details on their predictive value are inconclusive (Ray et al. 2007, Hansson et al. 2010). These methods are still novel and will require further investigation and optimization before any conclusions can be made about their applicability.

2.1.6 Magnetic resonance imaging in AD and its potential in predicting AD

Structural magnetic resonance imaging (MRI) is often used in assessing patients with cognitive decline, to exclude structural lesions and for differential diagnosis as well as for the confirmation of the putative diagnosis. With MRI, one can rule out brain tumours as the reason of cognitive decline, as well as possibly detect vascular lesions, normal pressure hydrocephalus, and both global and focal grey matter atrophy. Computed tomography (CT) has poorer sensitivity in detecting medial temporal lobe (MTL) atrophy, which is a characteristic of AD, and therefore MRI is the imaging modality of choice in dementia, when there are no contraindications (*e.g.* metallic objects in the body). Structural MRI can help to support the clinical diagnosis of AD, but so far MRI alone is insufficient to provide a definitive diagnosis. This is mostly accounted for by the marked overlap in the atrophy findings between AD, many other types of dementia [*e.g.* (Barber et al. 2000, Fein et al. 2000, Boccardi et al. 2003)], and so called healthy aging (van de Pol et al. 2006). Some functional MRI (fMRI) techniques show more promise in the early detection of AD [*e.g.* (Dai et al. 2009)]. Functional imaging is indeed a logical approach, because alterations in neuronal functions are likely to precede neuronal loss

in AD. fMRI methods are, however, both quite novel as well as very diverse and are beyond the scope of this literature review.

MTL atrophy, or more specifically atrophy of the hippocampus, parahippocampal gyrus and amygdala as well as the entorhinal cortex, can be studied with structural MRI. Hippocampal atrophy, present even in early AD, can be readily detected in thin coronal T1 or FLAIR slices through the MTLs [*e.g.* (Likeman et al. 2005)]. In the visual inspection of brain MRIs, grading (0-4) of hippocampal atrophy is widely used and this has been validated in the evaluation of severity of AD-like volume reductions (Scheltens et al. 1992, Wahlund et al. 1999, Wahlund et al. 2000). The cerebral ventricles also often appear dilated in AD MRIs because of the atrophy of the MTL structures (see **Figure 6**).

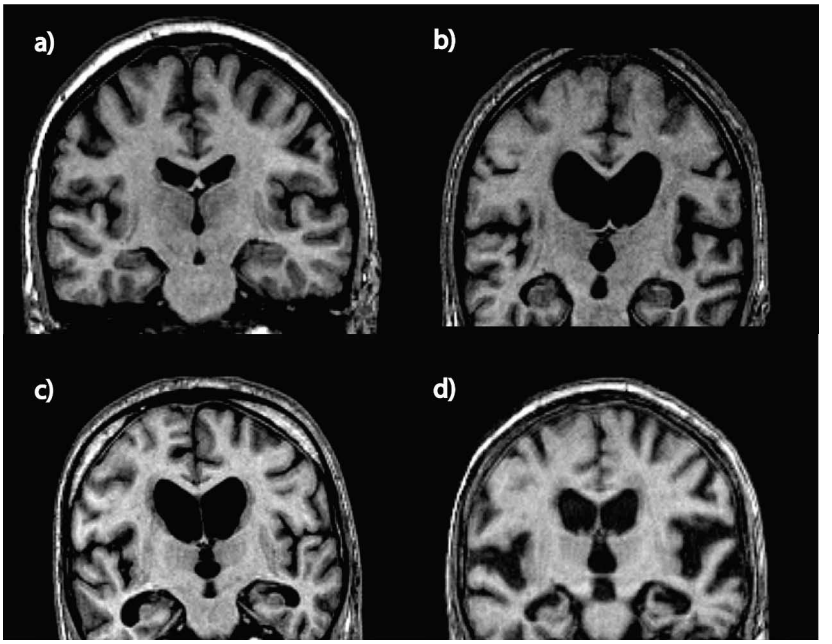

Figure 6. Coronal sections of T1 weighted MRI images depicting a healthy elderly subject (a) and patients with AD with mild (b), moderate (c) and severe (d) hippocampal atrophy. The images are courtesy of Timo Erkinjuntti.

In addition to visual evaluation of brain MRIs, volumetric MRI techniques are useful in AD studies, because they enable the quantitation of regional brain atrophy. Furthermore, more automated analytic methods such as voxel-based morphometry (VBM) allow for an unbiased examination of anatomical group differences across the whole brain and at a fine degree of spatial resolution. The advantage of whole-brain VBM is that it does require any pre-existing assumptions about the size, location or shape of the brain regions of interest. VBM also allows quantitation of brain changes that are not easily appreciated by visual inspection. (Ries et al. 2008) However, visual assessment and computed methods have both had their challenges with reproducibility. Fortunately methodological development

is intense in this field, recently including *e.g.* the optimization of both accuracy as well as speed of assessment through multi-atlas brain MRI segmentation (Lötjönen et al. 2010).

VBM assessments of MRIs have shown diagnostic accuracy of 83 % in very mild AD patients, although it should be noted that in the same study, ^{18}F-FDG-PET (see section *2.2.4 ^{18}F-FDG PET in AD and in the early detection of AD*) had slightly higher accuracy (Kawachi et al. 2006). Modern volumetric MRI techniques also seem to be able to predict, at least to some extent (29 % of MCI subjects with atrophy converted *versus* 8 % who did not show measurable atrophy), the conversion of MCI to AD in longitudinal studies [*e.g.* (McEvoy et al. 2009, Misra et al. 2009)]. Furthermore, longitudinal studies on cognitively intact subjects with an autosomal dominant AD-causing mutation have demonstrated serial volumetric MRI to show progressive hippocampal and whole-brain atrophy already at a presymptomatic stage (Ridha et al. 2006). However, large sample sizes have been required to confirm the predictive value in MCI studies, and reductions in cerebral volume appear to be detectable only relatively shortly before clinical symptoms become evident [*e.g.* (Ridha et al. 2006)]. On the other hand, combining MRI with other biomarkers could prove to be a feasible approach for early AD risk assessment.

In correlation studies of MRI findings and other AD-related pathological brain changes, the rates of brain atrophy seem to predict specific *post mortem* AD pathology (Silbert et al. 2003). In MCI subjects, longitudinal hippocampal volume loss has been closely associated with increasing hyperphosphorylated tau and a decline in the Aβ1-42 levels in CSF (de Leon et al. 2006, Schuff et al. 2009). Associations between the rate of brain atrophy and amyloid accumulation (shown by ^{11}C-PIB PET), in AD patients as well as in healthy elderly subjects, have also been suggested (Archer et al. 2006, Mormino et al. 2009) (see section *2.3.6 ^{11}C-PIB PET in relation to CSF biomarkers, MRI findings, ^{18}F-FDG PET findings, inflammation markers and cognitive measures*), but the brain regions with greatest grey matter atrophy and amyloid accumulation seem nevertheless to be different [*e.g.* (Jack et al. 2008)]. For instance, it has been proposed that different brain regions could be differentially susceptible to the toxic effects of Aβ (Frisoni et al. 2009).

2.2 EMISSION TOMOGRAPHY IMAGING IN ALZHEIMER'S DISEASE

Positron emission tomography (PET) and single-photon emission tomography (SPET) are virtually non-invasive radioisotope imaging methods that enable the *in vivo* investigation of a number of physiological and biochemical events in human tissues. The methods utilize positron-emitting (PET) or gamma-emitting (SPET) imaging tracers. The radiopharmaceuticals, that are synthesized with high radiopurity, are administered into the bloodstream of the subject, from where they are distributed into tissues, and tracer distribution is ultimately visualized in PET or SPET images. The benefits of nuclear imaging with PET or SPET include high sensitivity in very low (nano- or

even picomolar) concentrations, allowing for relatively weak signals (*i.e.* binding of a tracer reflecting tissue biochemistry) to be detected without having to administer the radiopharmaceuticals in quantities that could evoke adverse effects.

2.2.1 The PET principle

PET imaging compounds are labeled with a radioactive, positron-emitting isotope. The radioactive decay of the radioisotope component of the tracer molecule is detected by the PET scanner. As a result, one attains quantitative cross-sectional images of the concentration of the tracer in tissues, reflecting various physiological and pathophysiological processes.

Several endogenous biological compounds and therapeutic agents can be labeled with different radioisotopes, which have to be manufactured in a cyclotron. These unstable isotopes have a relatively short half-life (^{11}C 20.4 min, ^{18}F 110 min and ^{15}O 2.1 min). PET radioisotopes have an excess of protons in their nuclei and for the atom to reach equilibrium (*i.e.* for a proton to become a neutron), the proton emits a positron, which is a positively charged beta-particle. When the positron leaves the nucleus of the atom, it travels a distance of typically a couple of millimeters, depending on the radioisotope and the density of the tissue (*e.g.* the average distance from an ^{11}C-nucleus is only 0.56 mm and the maximum distance is 4.1 mm). The positron travels in the tissue until it has lost enough of its kinetic energy and its velocity decreases to a level where the positron ends up in an interaction with a nearby electron. In this interaction, a phenomenon called annihilation occurs. In annihilation, the masses of the positron and the electron are transformed into energy in the form of two gamma rays, *i.e.* photons. The masses of the particles are converted to energy resulting in two 511 keV photons that depart the annihilation site in practically opposite directions (180 ° ± 0.25) at the speed of light.

The PET scanner identifies the coinciding photons resulting from the annihilation event.. The PET scanner is a ring that surrounds the scanned target (the subject), and it consists of radiation detectors. It registers the two coincidental photons arriving at opposing detectors simultaneously (within 8-12 nanoseconds) and a decay event is thus recorded. Thus, the scanner determines the trajectory line on which the annihilation must have occurred. Each detector pair converts the photon information from the coinciding detections to electrical impulses and an image can be formed when enough of these impulses have been collected. The reconstruction of the impulse data into an image happens through mathematical processing. The time during which the impulses were gathered in each angle has also been registered. In this respect, the information is actually 4-dimensional. In other words, the spatial distribution of radioactivity concentration of (*e.g.* in kBq/ml) in an object can be observed as a function of time.

In brain studies, PET enables the *in vivo* assessment of regional blood flow, blood volume, glucose metabolism, oxygen metabolism, the functioning of several neurotransmitter

systems (pre- and postsynaptic events) and nowadays also the measurement of pathophysiological changes such as amyloid plaques and neurofibrillary tangles [*e.g.* (Shoghi-Jadid et al. 2002, Klunk et al. 2004)]. **Table 2** shows examples of approaches which have been used in brain PET studies in dementia research. Future prospects also include the possibility to label nanoparticles (*i.e.* supramolecular structures) with a positron-emitting isotope to study phenomena related to dementia pathophysiology and progression.

Table 2. Approaches to dementia studies with PET: targets and examples of radiotracers and direction of uptake change in Alzheimer's disease.

Amyloid deposition	^{11}C-PIB, ^{18}F-FDDNP, ^{18}F-BAY… etc.	increase
Glucose metabolism	^{18}F-FDG	decrease
Cholinergic system		
Nicotinic receptors	^{11}C-nicotine, ^{18}F-A85380	decrease
Muscarinic receptors	^{11}C-NMPB, ^{18}F-FP-TZTP	decrease
AChE activity	^{11}C-MP4A, ^{11}C-MP4P	decrease
Serotonergic system		
5HT(1A) receptors	^{11}C-WAY-100635, ^{18}F-MPPF	decrease
5HT(2A) receptors	^{18}F- or ^{11}C-Altanserin, ^{11}C-MDL-100907	decrease
Serotonin transporter	^{11}C-DASB	decrease
Dopaminergic system		
Striatal dopamine D2 receptors	^{11}C-raclopride, ^{18}F-fallypride	no change
Extrastriatal dopamine D2 receptors	^{11}C-FLB 457	decrease
Dopa transporter	^{18}F- or ^{11}C-FP-CIT	virtually no change
Dopa decarboxylation and vesicular storage	^{18}F-fluorodopa	no change
GABA/benzodiazepine receptors	^{11}C-flumazenil	decrease
Inflammation (microglial activation)	^{11}C-PK-(R)-11195	increase
Cerebral blood flow	^{15}O-H_2O	decrease

2.2.2 PET tracer quantification

Detailed analysis (as opposed to visual inspection, which is sometimes sufficient) of PET data requires dynamic imaging (*i.e.* time data not discarded) and often blood sampling, as well as elaborate modelling.

Time-activity curves (TACs) reflect tissue characteristics; the TAC of tracer concentration in arterial blood versus the TAC of the tracer concentration in tissue measured by the

PET scanner tells about the properties of the tissue in question. The relationship between arterial and tissue concentration is naturally affected by many factors such as perfusion, endothelial permeability, vascular volume fraction, transport across cell membranes, specific binding to receptors, non-specific binding of the tracer, enzyme activity, etc.

The radioactivity concentration can be converted to the radioligand concentration through a simple equation: Radioligand concentration = radioactivity concentration (kBq/cm^3) / specific radioactivity (GBq/μmol). This radioligand concentration reflects the *in vivo* tissue function under study (*e.g.* perfusion, glucose consumption, receptor density). Physical decay during the PET study requires that all measured radioactivities need to be corrected to the time of injection.

The more advanced statistical methods that can be applied to quantitative PET data require using for instance parametric images. A parametric image represents the dynamic (time-activity) information converted to functional information with dedicated software. In a parametric image, each image voxel value represents the value of the studied physiological parameter (*e.g.* perfusion, glucose consumption, receptor density). This approach also requires careful evaluation of alternative models on how to convert the data into a parametric image.

There are alternatives for model calculation, *e.g.* compartmental models, spectral analyses, multiple-time graphical analyses (MTGA) (Logan or Gjedde-Patlak plot), and the standardized uptake value approach. The approaches that use compartmental models are often referred to as kinetic analyses. Graphical analysis (Logan 2000) is independent of compartments, and involves the application of a suitable transformation to the data so that a linear plot is attained. The two most frequently applied graphical methods are the Patlak plot (Patlak et al. 1983) for irreversible binding, and the Logan plot (Logan et al. 1990) for reversible binding (Logan 2000). The slope of the linear phase of the plot is used for the quantification of radioligand binding (the slope represents the distribution volume, DV, in the case of the Logan plot and the net influx rate, *i.e.* K_i values, in a Gjedde-Patlak plot). Logan analysis usually employs a plasma input for reference, yielding the distribution volume, *i.e.* DV: in the Logan plot, Y-axis is the integral of the tissue curve divided by tissue concentration and the X-axis is the integral of the plasma curve divided by tissue concentration. Therefore, the slope of the linear phase equals DV. A variation of the Logan graphical analysis allows for the substitution of image-derived reference tissue data in place of the plasma radioactivity input function (Logan et al. 1996) so that a distribution volume ratio, DVR, can be obtained.

The standardized uptake value (SUV) is a simple, semi-quantitative measure that can be expressed in g/ml. The SUV is obtained from the regional radioactivity concentration, which has been simply normalized to the injected dose and the subject weight so that the average SUV in the entire body would represent the body density. Blood sampling is not needed to obtain SUVs. Inter-individual differences *e.g.* in blood flow and metabolism mean that the SUV is not comparable between subjects *per se*. Therefore a ratio of the ROI SUV to a

reference SUV in the same individual is a more comparable parameter. In this context, to obtain a SUV ratio (SUVR) or, in other words, a region-to-reference ratio (because injected dose and subject mass cancel each other out), the reference input can sometimes be image-derived so that blood sampling is still not necessary. The requirement for a reference region in the same PET image is that it optimally contains only non-specifically bound tracer.

2.2.3 SPET

Single-photon emission tomography (SPET) is a tomographic imaging technique not unlike PET, except that it uses gamma-emitting isotopes instead of positron-emitting isotopes. On the other hand, the technique is, actually very similar to conventional nuclear medicine imaging with a gamma camera, with the important difference that SPET can produce three-dimensional information. One advantage of SPET over PET is that the employed radioisotopes generally have a relatively long half-life so that an expensive on-site cyclotron and a specialized radiochemistry laboratory are not needed. SPET is generally more available and less expensive than PET and it is undergoing rapid methodological development *e.g.* for utilization in early dementia detection (Matsuda et al. 2007). However, the spatial resolution of SPET is substantially poorer than what can be achieved with PET.

One SPET tracer commonly used in dementia research is ^{99m}Tc-HMPAO (hexamethylpropyleneamine oxime), where ^{99m}Tc (technetium-99m) is a metastable gamma-emitting nuclear isomer. ^{99m}Tc-HMPAO distribution represents blood flow, and in many ways ^{99m}Tc-HMPAO SPET can compete with ^{18}F-FDG (fluorodeoxyglucose) PET scanning of the brain *e.g.* in dementia research [*e.g.* (Kato et al. 2008, Zaknun et al. 2008)]. The similar SPET tracer ^{99m}Tc-ECD has also been used to assess regional blood flow, in an attempt to diagnose dementia, to differentiate alternative causes of dementia, and to predict which MCI patients are likely to convert to dementia (Caroli et al. 2007).

Ongoing dementia studies with SPET include the assessment of neuroinflammation and microglial activation with peripheral benzodiazepine receptor –binding SPET tracers such as ^{123}I-PK11195 (Versijpt et al. 2003) and ^{123}I-CLINDE (Arlicot et al. 2008). Furthermore, an amyloid imaging tracer for studying AD Aβ pathology, in particular, ^{123}I-IMPY, is also under evaluation for use in clinical SPET studies (Kung et al. 2004, Newberg et al. 2006). Interesting future prospects in SPET imaging of AD include the use of a dual isotope technique with both a blood flow tracer (^{99m}Tc-HMPAO or ^{99m}Tc-ECD) and an amyloid tracer (*e.g.* ^{123}I-IMPY).

2.2.4 ^{18}F-FDG PET in AD and in the early detection of AD

^{18}F-FDG PET in AD

PET imaging can be used to quantitatively measure regional cerebral glucose uptake and metabolism (rCMRgluc). In AD research, ^{18}F-FDG, *i.e.* a fluorine-18 labelled derivative

of glucose, fluorodeoxyglucose, is the most commonly employed PET tracer. Its uptake reflects the activity of glucose metabolism in the investigated tissues; brain glucose metabolism is regionally impaired in AD.

This technique is not simply confined to research but it can also been used in the clinic; ^{18}F-FDG PET can increase diagnostic confidence when one is evaluating the type of dementia in an individual patient. Different clinical syndromes show different patterns of brain hypometabolism (Ishii et al. 1998, Nestor et al. 2003, Diehl-Schmid et al. 2007). However, although AD can be detected with ^{18}F-FDG-PET with an average sensitivity of approximately 90 %, differentiation from other dementias is somewhat less reliable (Mosconi 2005). On the other hand, encouraging specificities for AD of up to 70-90 % have also been recently reported in relatively large samples and meta-analysis (Silverman et al. 2001, Silverman et al. 2004, Patwardhan et al. 2004). Be that as it may, ^{18}F-FDG PET is very applicable in some clinically unclear situations, and has recently been accepted as an insurance-covered diagnostic investigation in the United States (Centers for Medicare & Medicaid Services) to facilitate the differential diagnosis of AD, especially from frontotemporal dementia (FTD) (Mosconi et al. 2007).

In AD, ^{18}F-FDG-PET typically reveals reduced glucose metabolism predominantly in the parietal and superior/posterior temporal regions, posterior cingulate and the precuneus (Minoshima et al. 1997, Herholz 2003) (see **Figure 7**). Later in the disease course, AD patients also exhibit reduced glucose metabolism in their frontal lobes (Choo et al. 2007). The affected association cortices are those that become myelinated last during brain maturation. (Bartzokis et al. 2007). In AD, in contrast to some other dementias, the basal ganglia, the primary motor and visual cortices as well as the cerebellum typically show relatively normal levels of rCMRgluc. This is in line with the symptoms of AD, where primary motor and sensory functions are relatively well preserved as opposed to the deficits in memory, associative thinking and executive functions. (Herholz et al. 2007) It has been evaluated that the sensitivity and specificity of AD prediction with ^{18}F-FDG-PET are 93 % and 63 %, respectively (Hoffman et al. 2000), although much better

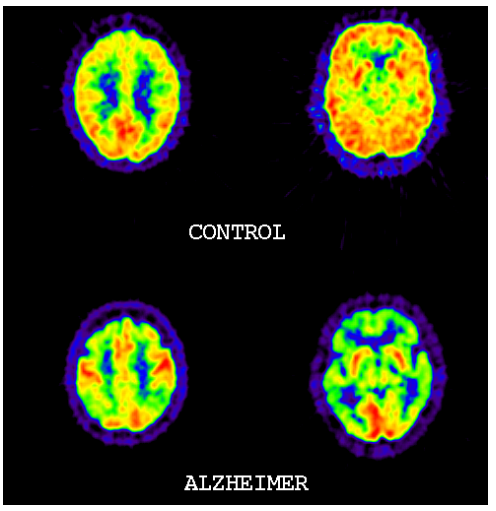

Figure 7. Typical ^{18}F-FDG PET images of a healthy elderly control subject (above) and of an AD patient (below). Note the temporal and parietal regional hypometabolism shown by reduced ^{18}F-FDG uptake in the AD patient.

specificities of up to 86 % have been attained in some recent and thoroughly conducted studies (Silverman et al. 2001, Silverman et al. 2004, Patwardhan et al. 2004). Limited specificity, in any case, seems to be the more obvious shortcoming of this approach.

In longitudinal studies, it has been shown that the reductions in rCMRgluc in the temporal and parietal cortices are progressive, and frontal lobe reductions become more evident over time (Jagust et al. 1988, Mielke et al. 1994). In AD patients, the association cortices typically show rCMRgluc reductions of about 15 to 20 % over 2 or 3 years (Smith et al. 1992, Engler et al. 2006), whereas healthy controls seem to display no significant reductions over the same period of time (Smith et al. 1992).

^{18}F-FDG PET in the early detection of AD

^{18}F-FDG PET also appears to have prognostic value in presymptomatic AD two or more years before the full clinical manifestation of dementia (Silverman et al. 2001, Chételat et al. 2003, Chang and Silverman 2004). This technique seems to be able to detect glucose hypometabolism in the inferior parietal, temporoparietal, posterior cingulate and precuneus regions in MCI patients who will subsequently convert to AD (Arnáiz et al. 2001, Chételat et al. 2003, Mosconi et al. 2004, Anchisi et al. 2005, Drzezga et al. 2005), suggesting that these glucose utilization changes are predictive of further progressive cognitive decline in individuals with a recognized but still not dementia-level cognitive impairment. The sensitivity and specificity for the prediction of MCI converting to AD were reported to be as high as 92 % and 89 %, respectively, in a longitudinal ^{18}F-FDG PET study (Drzezga et al. 2005). ^{18}F-FDG PET has also been indicated to be more accurate in predicting amnestic MCI subjects' conversion to AD than neuropsychological evaluation (Chételat et al. 2003).

Non-symptomatic persons with a high risk of AD because of a family history and ApoE epsilon 4 carrier status show reductions in rCMRgluc compared to matched low-risk subjects (Small et al. 1995, Reiman et al. 1996). Cognitively healthy persons who are homozygous for the ApoE epsilon 4 allele show reductions in rCMRgluc in the same regions in which they typically occur in AD (Small et al. 2000). A normal ^{18}F-FDG PET scan in MCI seems to indicate a low chance of progression to AD within one year, even when severe memory deficits are present in neuropsychological tests (Anchisi et al. 2005). Furthermore, a 3-year follow-up study on cognitively healthy subjects indicated that ^{18}F-FDG PET could have predictive value in the development of MCI in the first place (de Leon et al. 2001). Reduced rCMRgluc in the entorhinal cortex was reported to be able to predict the conversion from a healthy state to MCI with 83 % sensitivity and 85 % specificity over 3 years of follow-up (de Leon et al. 2001).

In studies with monozygotic (MZ) twins discordant for AD, non-demented MZ co-twins of AD patients have shown reductions in rCMRgluc in several cortical regions and the cingulate gyrus (Järvenpää et al. 2003, Virta et al. 2009). These results suggest that these metabolic changes are early indicators of the disease process and can be detected before the onset of clinical dementia, or alternatively that the changes are indicators of familial

susceptibility to AD, not necessarily the disease process itself. In dizygotic healthy co-twins of AD patients, no such findings were seen (Virta et al. 2008, Virta et al. 2009), which suggests that genetic factors rather than shared environmental factors are behind the familial susceptibility to reductions in rCMRgluc.

^{18}F-FDG-PET is nonetheless a somewhat non-specific AD research tool, because it does not directly reflect the specific disease process and because cerebral glucose metabolism is reduced also in many other diseases, not only in AD, and even in healthy aging. Reductions in rCMRgluc have been shown to correlate with some indices of dementia severity [*e.g.* (Bittner et al. 2005, Engler et al. 2006, Haense et al. 2008)] but not for instance with CSF tau concentrations (Haense et al. 2008) (see section *2.1.5 Cerebrospinal fluid and blood biomarkers in AD and as its antecedent indicators*). It is not unreasonable that reductions in rCMRgluc should correlate to some extent with cognitive decline and therefore ^{18}F-FDG PET might prove to be useful as a surrogate marker of disease progression. However, individual compensatory mechanisms and physiological differences will make these assessments not as straightforward as could be hoped. Even more importantly, the reductions in rCMRgluc are most likely to be consequences of a still more profound, earlier, and specific pathological process, and it would therefore be of great importance to discover more ”upstream” markers of the pathophysiological events occurring in AD.

2.2.5 Development of amyloid radiotracers for PET

It is important to assess the specific pathological processes in AD *in vivo* but this requires that there are valid biomarkers available, for instance radiotracers for PET, that can detect these specific changes in the living brain. Based on the current knowledge about AD pathophysiology, amyloid imaging would seem to represent a feasible means of investigating both the pathogenesis of AD and possibly disease-modifying treatment options [for a review, see (Mathis et al. 2007)]. There are, however, many requirements that a tracer for *in vivo* human amyloid imaging would have to fulfill: an ability to cross the blood-brain barrier, stability, lipophilicity, efficient clearance from tissues, and specific binding to amyloid in very small (nanomolar) concentrations. Radiation safety and the quantitative reproducibility of the method are also naturally very important issues, especially when longitudinal follow-up or intervention studies are planned. A number of amyloid ligand candidates have been developed, and these can be roughly categorized into three groups: antibodies [*e.g.* (Friedland et al. 1997)]; MRI agents [*e.g.* (Wadghiri et al. 2003)] and so called small-molecule compounds. Many tracers have failed because of high non-specific binding and insufficient distribution in brain tissue in experimental animals [for a review, see (Nordberg 2004)], but some compounds have passed these tests and now have an established place in human studies.

Research in this field has mainly focused on small-molecule compounds suitable for PET and SPET. The most promising of these compounds appear to be derivatives of

agents previously used as tissue stains in histopathology. These include derivatives of Congo Red (Styren et al. 2000, Link et al. 2001, Klunk et al. 2002), thioflavine (Klunk et al. 2001, Mathis et al. 2002, Bacskai et al. 2003, Mathis et al. 2003, Klunk et al. 2004) and stilbene (Verhoeff et al. 2004, Kudo et al. 2007. Rowe et al. 2008, Waragai et al. 2009), as well as FDDNP (or [^{18}F] 1,1-dicyano-2-[6-(dimethylamino)-2-naphthalenyl] propene) (Agdeppa et al. 2001, Shoghi-Jadid et al. 2002, Small et al. 2006, Boxer et al. 2007). Acridine orange and its analogues have also been investigated and for instance a compound named BF-108 has demonstrated efficient binding to brain amyloid in a study conducted with AD-transgenic mice (Suemoto et al. 2004).

With respect to the ligands that bind selectively to amyloid, the derivatives of the histological dye thioflavin T have been studied most extensively in humans. These compounds have been labeled with radioactive carbon (^{11}C) as well as with iodine (^{123}I), and recently also with ^{18}F. ^{123}I-IMPY (Kung et al. 2004) is a SPET radiotracer that will not be reviewed here in detail – the focus will be on PET radiotracers.

Thioflavin T (a benzothiazole salt obtained by the methylation of dehydrothiotoluidine with methanol in the presence of hydrochloric acid, see **Figure 8** for molecular structure) is an amyloid dye that is commonly used in histopathology. It is a positively charged molecule and it does not cross the blood-brain barrier. A number of uncharged derivatives of the compound have been developed in recent years (Klunk et al. 2001, Mathis et al. 2002). Of these compounds, N-methyl-2-(4'-methylaminophenyl)-6-hydroxybenzothiazole, *i.e.* 6-OH-BTA-1, was found to be the most promising (Bacskai et al. 2003, Mathis et al. 2003). This compound was subsequently labeled with ^{11}C, and the radiotracer was named Pittsburgh Compound B (PIB or ^{11}C-PIB) after its birthplace and for convenience. The molecular structure of ^{11}C-PIB is shown in **Figure 9**. Other new tracers for amyloid imaging are under active development (see section *2.3.7 Possibilities and prerequisites of in vivo amyloid imaging tracers*).

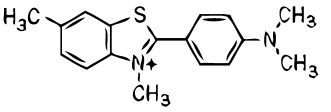

Figure 8. Thioflavin T, an amyloid binding dye used in histopathology.

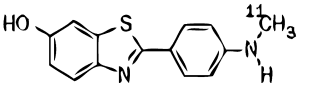

Figure 9. ^{11}C-PIB, a thioflavin T derivative developed for *in vivo* amyloid imaging.

2.3 ^{11}C-PIB PET

2.3.1 ^{11}C-PIB PET uptake analysis

Quantitation of PET tracer uptake is traditionally done through manual region-of-interest (ROI) analysis. ROIs are delineated either on corresponding and co-registered MRIs for clear visualization of anatomical structures, or in some cases, directly on the PET images.

ROIs may be imposed on either the whole dynamic PET image or on an integrated, averaged or summated image over a certain period of time of the emission scan, *i.e.* over certain time frames. Tracer kinetics affect which part of the emission scan is most representative and informative, *i.e.* during which time interval there is least non-specific binding or signal coming from the bloodstream as opposed to specific tracer binding. The ROIs are implemented on the PET data, and time-activity curves (TACs) can be calculated from the serial ROIs, giving radioactivity concentration values for the brain regions (radioactivity per volume at a certain time) that the ROIs represent. An appropriate model for the tracer, to enable between-subjects and between-groups comparisons, must then be applied to the data. This kind of normalization is done in order to obtain comparable data on the *specific* binding of the radiotracer in the investigated region. Image-driven methods – *e.g* as opposed to. using a plasma input function for reference – are a tempting approach to this end because of their non-invasiveness and convenience. In practice, this usually means the use of tracer uptake measurements of a reference region (with no or little specific tracer binding) of the same individual. The cerebellum has proven to contain only small quantities of fibrillar Aβ plaques in *post mortem* studies [*e.g.* (Joachim et al. 1989)] and has therefore been chosen as a candidate for an ^{11}C-PIB uptake reference region, with similarly low binding in AD patients and controls (Klunk et al. 2003, Klunk et al. 2004, Price et al. 2005). Late-scan region-to-cerebellum ratios of ^{11}C-PIB uptake have subsequently been demonstrated to effectively differentiate AD patients from controls with acceptable test-retest reproducibility (Lopresti et al. 2005).

As is evident, when one includes all preprocessing phases (*e.g.* image frame summations, co-registrations of PET images with MRIs), the manual ROI method is very laborious, and also prone to investigator-induced bias. There is a need for more standardized and automated methods. Automated ROI analysis using a similar ROI set for every subject is one way to achieve this goal. Since the individual images must be in the same stereotactic space if one wishes to use this approach, one needs common templates to which the individual images are spatially normalized. Even after this procedure, a standard automated ROI set might not suit the brain anatomy of every subject, especially if there is marked brain atrophy. In other words, the quality of the spatial normalization significantly affects the sensitivity and specificity of the method. However, there are advantages to this method: it is standardized and inaccuracies can even be thought to rule out each other, at least in larger samples. Furthermore, the time-activity calculations may be performed in a fully automated manner. Nonetheless, a thorough validation of this automated ROI analysis approach to ^{11}C-PIB uptake data needs to be conducted before it can enter into wider use.

Another more automated and bias-reducing approach for exploring tracer uptake in PET images is voxel-based analysis, *e.g.* with Statistical Parametric Mapping (SPM) (Friston et al. 1995). In this analysis method, the uptake in the whole brain may be investigated voxel by voxel, without any *a priori* hypotheses concerning the locations of the differences in tracer uptake *e.g.* between patient and control groups. SPM utilizes

parametric images, *i.e.* images to which modelling in terms of uptake value normalization has already been applied, and the tracer uptake has thus been rendered comparable between different subjects. Parametric images can be obtained *e.g.* by dividing the uptake in each voxel by the radioactivity concentration of a reference region. In a SPM analysis, the parametric images are spatially normalized into a common stereotactic space, and smoothed to reduce residual anatomical variance and to improve the signal-to-noise ratio. Then, subtraction analysis can be applied to the images, to explore, voxel by voxel, the statistical significance of the differences in tracer uptake between groups. This method achieves improved sensitivity in the statistical analysis and is more objective than manual ROI analysis. SPM of course only provides a map of statistically significant changes and is not a quantitative method of tracer uptake measurement. Thus it can be used to explore between-group differences, and as a guide for the selection of brain regions where ROIs should be delineated. Furthermore, and quite importantly, automated ROI analysis can also be applied to the parametric images obtained through the same image-preprocessing methods. Recent studies have provided support for the use of automated ROI analysis of spatially normalized parametric images also in ^{11}C-PIB uptake quantitation (Kemppainen et al. 2006, Ziolko et al. 2006, Mikhno et al. 2008). The reliability of voxel-based methods to study ^{11}C-PIB uptake can be assessed by measuring the signal in each voxel and comparing that with the corresponding voxels of different ^{11}C-PIB PET images of the same subjects. In this case, as in any test-retest setting, it is important to also evaluate whether within-subject variability is assuredly smaller than the between-subjects variability. Only if this is the case can the method be considered reliable *e.g.* for studies with repeated ^{11}C-PIB PET scans of the same subjects.

Future possibilities of ^{11}C-PIB PET image interpretation in clinical settings also include the visual assessment of images instead of quantitative analysis (Ng et al. 2007a, Suotunen et al. 2010), although that approach cannot currently be applied in scientific research and is therefore not reviewed here in more detail.

2.3.2 Findings in Alzheimer's disease

The first clinical PET study with ^{11}C-PIB was performed in a collaboration between the Pittsburgh and Uppsala research groups. Sixteen AD patients and 9 healthy controls were investigated with ^{11}C-PIB PET and ^{18}F-FDG PET. ^{11}C-PIB entered the brain rapidly and in an unchanged form, and was bound significantly more to the frontal, temporal, parietal and occipital cortices as well as the striata of AD patients, in comparison to the controls - the differences between patients and controls were 1.9-1.5-fold. In contrast, no differences were observed between young and elderly healthy controls. In this study, ^{11}C-PIB uptake was also inversely correlated with ^{18}F-FDG uptake in the same brain regions. The increase in ^{11}C-PIB uptake in the AD patients relative to the healthy age-matched controls was greater than the decrease in ^{18}F-FDG uptake. No significant correlation was found between ^{11}C-PIB uptake and cognitive performance (as assessed by the MMSE), although a trend towards an inverse correlation was observed. (Klunk et al. 2004)

Post mortem correlates were eagerly awaited after these initial findings with ^{11}C-PIB PET. Positive associations have, indeed, been demonstrated between the ^{11}C-PIB PET signal and biochemically measured brain Aβ levels (Bacskai et al. 2007, Ikonomovic et al. 2008). In a study with several regions examined in one AD brain, ^{11}C-PIB binding *in vivo* appeared to be highly selective for insoluble (fibrillar) Aβ deposits *post mortem* (Ikonomovic et al. 2008). Furthermore, in another study using *ex vivo* frontal brain biopsy specimens of patients with normal pressure hydrocephalus, there was a strong positive correlation between *in vivo* ^{11}C-PIB uptake and the amount of amyloid in the biopsy tissue (Leinonen et al. 2008).

Several subsequent ^{11}C-PIB PET studies have confirmed that patients with AD consistently show significantly greater, up to two-fold, ^{11}C-PIB uptake compared with controls in neocortical brain regions typically affected by Aβ accumulation (Buckner et al. 2005, Price et al. 2005, Archer et al. 2006, Engler et al. 2006, Kemppainen et al. 2006, Edison et al. 2007a, Edison et al. 2007b, Rowe et al. 2007) (see also **Figure 10**). Around 90 % of patients with probable AD show this increased cortical ^{11}C-PIB uptake (Klunk et al. 2004, Price et al. 2005, Archer et al. 2006, Edison et al. 2007a, Rowe et al. 2007). Based largely on these and other experiments with ^{11}C-PIB PET and MR imaging, it has been proposed that the research criteria for probable AD diagnosis should be revised to include imaging-confirmed brain Aβ accumulation (Dubois et al. 2007).

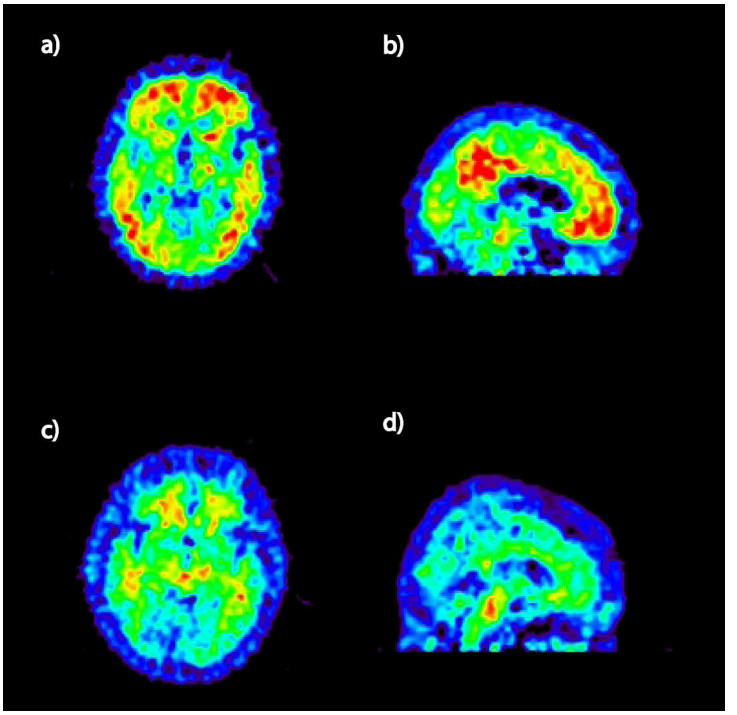

Figure 10. Typical coronal (a and c) and sagittal (b and d) image slices of ^{11}C-PIB PET images of an AD patient (a and b) and a healthy elderly control (c and d). Note the marked uptake increase *e.g.* in the AD patient's frontal and parietal cortices.

The concept that the difference between AD patients and controls in ^{11}C-PIB uptake is typically greater than the difference in ^{18}F-FDG uptake has also been reinforced since the first clinical study. ^{11}C-PIB scans have higher accuracy than ^{18}F-FDG scans for distinguishing AD patients from healthy controls. The sensitivity and specificity of ^{11}C-PIB PET for clinically probable AD seem to be high with a reported accuracy of 90 % (Ng et al. 2007a). Also visual assessment (as opposed to a quantitative analysis of a 90 min scan) of ^{11}C-PIB images seems to be reliable (Ng et al. 2007a, Suotunen et al. 2010), because agreement between readers appears to be excellent and ^{11}C-PIB images seem more accurate than ^{18}F-FDG scans both in ROC analysis as well as upon visual inspection (Ng et al. 2007a). In the older group of subjects in that study, accuracy declined more with ^{18}F-FDG than it did with ^{11}C-PIB. (Ng et al. 2007a) The pattern of regional involvement for ^{18}F-FDG and ^{11}C-PIB differs in AD, but the two techniques have shown up to 94 % case-by-case agreement (Li et al. 2008).

However, while ^{18}F-FDG uptake continues to decrease and brain atrophy advances when AD progresses, at least at a group level, AD patients have shown no significant increases in ^{11}C-PIB uptake over either a one-year or a two-year follow-up (Engler et al. 2006, Jack et al. 2009). There is a plausible explanation for this discrepancy; Aβ plaque accumulation could reach some sort of a plateau already before clinical symptoms become evident. This would in turn reinforce the hypothesis that amyloid pathology precedes deficits in brain energy metabolism, neurodegeneration (atrophy) and impairment of cognitive functions. Where applied to therapeutic studies, this would mean that drugs targeted at amyloid metabolism would have to be administered very early in the disease course to be able to modify or halt disease progression. Such drugs would also have to be very effective in clearing brain Aβ for the changes to be detectable with ^{11}C-PIB PET. At present, several clinical studies on anti-amyloid therapies in AD are ongoing, and in these trials, one of the outcome measures will be the possible change in Aβ load measured by ^{11}C-PIB PET (Rinne et al. 2010).

^{11}C-PIB, in addition to binding to neuritic Aβ plaques, delineates diffuse plaques and cerebrovascular amyloid angiopathy (CAA) (Bacskai et al. 2007, Lockhart et al. 2007). Studies on patients with non-AD dementia show that increased ^{11}C-PIB uptake can be seen *e.g.* in some Lewy body dementia (DLB) patients as well (see section *2.3.3 ^{11}C-PIB PET in other dementias*). ^{11}C-PIB uptake is also not strongly associated with dementia severity (see section *2.3.6 ^{11}C-PIB PET in relation to CSF biomarkers, MRI findings, ^{18}F-FDG PET findings, inflammation markers and cognitive measures*). These results suggest that there are limitations to the specificity of ^{11}C-PIB PET in diagnosing and monitoring disease progression in AD, and that the ligand could rather be a non-specific marker of Aβ-related cerebral amyloidosis. (Lockhart et al. 2007) The accuracy of ^{11}C-PIB PET in diagnosing clinical AD is also limited by the cortical binding seen in some healthy elderly subjects, which is consistent with *post mortem* studies of cerebral Aβ in aging [*e.g.* (Davies et al. 1988)], and could indicate presymptomatic AD (Mintun et al. 2005, Pike et al. 2007, Villemagne et al. 2008, Reiman et al. 2009). In conclusion, ^{11}C-PIB PET is not unambiguously associated with the cognitive state or clinical diagnosis of a given subject at a particular moment.

On the other hand, this is exactly why it could prove to be an antecedent marker of brain Aβ pathology prior to and irrespective of the symptoms being suffered by the individual. ^{11}C-PIB PET could benefit not only subjects with AD or with susceptibility to develop AD but other disease groups as well, and it could assist in choosing persons who would benefit from anti-amyloid therapies regardless of the clinical diagnosis.

2.3.3 ^{11}C-PIB PET in other dementias

Amyloid imaging is an interesting possibility, which may help in differentiating other, more rare causes of cognitive impairment from AD. There is a great deal of overlap between the clinical phenotypes of different dementias, and the demand for objective measures in differential diagnostics is evident. ^{11}C-PIB PET has recently shown potential in the segregation of AD from other dementing diseases, although increased ^{11}C-PIB uptake cannot currently be considered specific for AD.

In short, ^{11}C-PIB PET seems to be unable to differentiate AD from dementia with Lewy bodies (DLB) in the majority of cases, but shows promise in being an ideal means of differentiating AD from frontotemporal lobe degeneration (FTLD) (Rabinovici et al. 2007, Rowe et al. 2007, Drzezga et al. 2008, Edison et al. 2008b, Engler et al. 2008, Gomperts et al. 2008). In Parkinson's disease dementia (PDD), ^{11}C-PIB uptake is rarely increased (Rowe et al. 2007, Edison et al. 2008b, Gomperts et al. 2008, Maetzler et al. 2008, Maetzler et al. 2009). In rare forms of non-AD dementia as well as in familial forms of amyloid metabolism deficits, ^{11}C-PIB uptake is heterogeneous, with the absence of notable tracer uptake in some conditions and with distinct patterns of increased uptake in others (Johnson et al. 2007, Ng et al. 2007b, Koivunen et al. 2008b, Remes et al. 2008, Villemagne et al. 2009). Due to the overlapping or concomitant pathologies and uncertainties in clinical diagnoses, *post mortem* examinations are needed to confirm these findings and to further unravel the role of Aβ in non-AD dementias. Since AD is so common, it could be that longitudinal and *post mortem* studies would reveal mixed pathology *e.g.* in the minority of FTLD and PDD patients that have increased ^{11}C-PIB uptake. Although ^{11}C-PIB PET is unlikely to unambiguously differentiate AD and DLB from one another, it does seem to be a promising technique in identifying which patients, *e.g* with DLB or PDD, have concomitant brain amyloid pathology. This could have important implications in the future, both in terms of advanced understanding of neurodegenerative disorders as well as when new therapies targeted at amyloid metabolism are introduced into clinical practice. The allocation of these modern therapies to subjects who have imaging-confirmed amyloid pathology could prove important with regard to patient safety and cost-effectiveness of treatment strategies.

2.3.4 ^{11}C-PIB uptake in mild cognitive impairment

At a group level, ^{11}C-PIB uptake is increased in amnestic MCI (aMCI) in the frontal, parietal and lateral temporal cortices as well as in the posterior cingulate (Kemppainen

et al. 2007, Forsberg et al. 2008). This distribution resembles that seen in AD. At an individual level, about half of MCI patients have ^{11}C-PIB uptake in the AD range (Kemppainen et al. 2007, Okello et al. 2009a, Okello et al. 2009b, Wolk et al. 2009), which can be interpreted to be suggestive of an early AD state.

Increased ^{11}C-PIB uptake has been indicated to be predictive of conversion to AD in MCI subjects (Forsberg et al. 2008, Koivunen et al. 2008a, Okello et al. 2009b, Wolk et al. 2009) (see **Figure 11**). In one of these studies, a significant correlation between episodic memory impairment and ^{11}C-PIB uptake was seen (Forsberg et al. 2008). In another study, all of the 6 subjects who converted to AD during a two-year follow-up had PIB-positive brain scans at the MCI stage. In that same study, CSF Aβ1-42 was abnormal in only 54 % of the subjects, indicating that ^{11}C-PIB PET may also be more sensitive in detecting disrupted amyloid metabolism in MCI subjects than this CSF biomarker. (Koivunen et al. 2008a) In another MCI follow-up of 21 months, 5 out of 13 PIB-positive subjects converted to AD whereas none of the 10 PIB-negative subjects converted. Furthermore, 3 out of 10 of the amyloid-negative subjects reverted to normal cognitive functioning. (Wolk et al. 2009) In a longitudinal study over 1 to 3 years, as many as 82 % of the PIB-positive MCI subjects clinically converted to AD during the follow-up, and only one of the PIB-negative MCI cases converted to AD (Okello et al. 2009b).

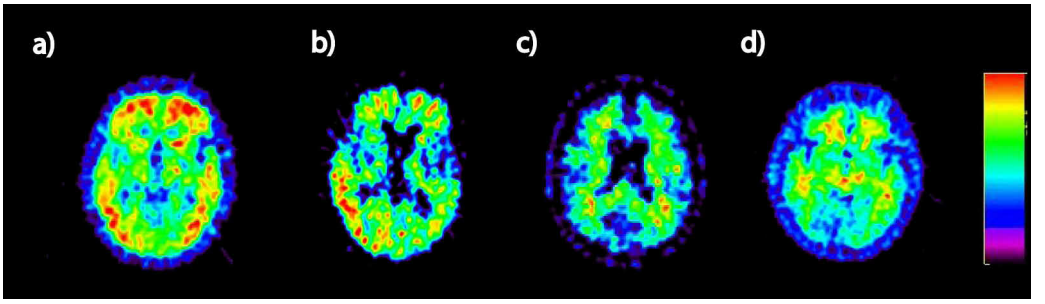

Figure 11. ^{11}C-PIB PET images of an AD patient (a), MCI patient who later converted to AD (b), MCI patient who did not convert to AD (c) and a healthy elderly control subject (d). Note the increased tracer signal in the MCI converter (b) *vs*. the MCI non-converter (c). The image is modified from (Rinne and Någren 2010).

When investigating healthy controls, AD patients, non-amnestic and amnestic MCI subjects, ^{11}C-PIB PET and ^{18}F-FDG PET showed similar significant group separation, with only ^{11}C-PIB PET showing significant separation of the non-amnestic and amnestic MCI subject groups (Lowe et al. 2009). This observation may have important implications, because amnestic MCI in particular is considered to represent a pre-dementia stage of AD (see section *2.1.4 Mild cognitive impairment per se and as a predictor of AD*). In another study, for the classification of MCI and healthy controls, ^{18}F-FDG was superior to ^{11}C-PIB, but there was only 54 % agreement at the individual level. Therefore combining the two modalities was suggested as a way to improve the diagnostic accuracy for MCI. (Li et al. 2008)

A major challenge in determining the value of ^{11}C-PIB PET in MCI comes from the heterogeneity of the MCI population. It cannot be anticipated at present that ^{11}C-PIB PET would have a revolutionary impact on the diagnostics of MCI itself but rather it may have a greater impact in understanding the presymptomatic or the symptomatic but non-dementia stage of AD and its amyloid pathology. Longer follow-ups and larger sample sizes will be needed to conclude whether ^{11}C-PIB PET can indeed identify those MCI patients who will develop AD from those who will not.

2.3.5 ^{11}C-PIB PET in normal aging and in healthy subjects with increased risk for AD

In studies with cognitively healthy elderly individuals, *i.e.* those with neither an AD nor MCI diagnosis, ^{11}C-PIB PET has appeared to be able to detect AD already at its preclinical stage (Mintun et al. 2005, Pike et al. 2007, Villemagne et al. 2008, Reiman et al. 2009). Subtle memory problems seem to be associated with increased ^{11}C-PIB uptake in seemingly cognitively healthy individuals in some studies (Pike et al. 2007, Mormino et al. 2009), although contradictory results exist as well (Aizenstein et al. 2008, Jack et al. 2008). In a longitudinal study where neuropsychological test results were available on the preceding years before ^{11}C-PIB PET, 70 % of the cognitively declining but originally healthy subjects had PIB-positive scans, compared with only 17 % of the cognitively stable subjects (Villemagne et al. 2008). More studies and time are needed to conclude whether PIB-positive scans can indeed detect prodromal AD in clinically cognitively normal persons.

Rather a large proportion of healthy elderly subjects do seem to show AD-like ^{11}C-PIB binding, about 10-30 % depending on the study (Klunk et al. 2004, Mintun et al. 2006, Pike et al. 2007, Rowe et al. 2007, Aizenstein et al. 2008, Jack et al. 2008). In short, due to the brief history of *in vivo* amyloid imaging, it is at present unclear whether a person can display increased ^{11}C-PIB uptake indicative of marked brain Aβ load without ever developing clinical symptoms of AD. However, for purely "diagnosing" normal aging, at least the prognostic value of a PIB-negative scan may have important clinical implications – it seems unlikely that a person would develop AD in the near future without demonstrating any cortical Aβ deposits in a ^{11}C-PIB PET scan.

Healthy individuals with an increased genetic risk for future AD are interesting study subject candidates within the group of cognitively normal subjects. Two different pedigrees of PS1-mutation carriers were investigated in one study, showing that at least with this kind of familial predisposition for AD, increased ^{11}C-PIB uptake is present during the asymptomatic stage (Klunk et al. 2007). However, as reviewed earlier, so called sporadic AD is much more common than the known familial forms of AD.

The effect of the apolipoprotein E genotype on the risk for brain amyloidosis and for developing sporadic AD is intriguing, yet unclear (see section *2.1.3 Genetics of AD*). It has been observed that ApoE epsilon 4 –positive AD patients seem to have greater ^{11}C-PIB uptake compared to age-matched epsilon 4 –negative patients with similar levels

of cognitive impairment and brain atrophy (Drzezga et al. 2009). The ApoE epsilon 4 allele has previously been shown to be associated with neuropathological AD also in nondemented individuals (Polvikoski et al. 2006). In a longitudinal study on a non-demented population, 54 % of ApoE epsilon 4 carriers were PIB-positive as opposed to only 19 % of non-carriers, although there was no difference in epsilon 4 prevalence between the cognitively stable and declining groups (Villemagne et al. 2008). These results could be considered important in a wider sense, because the findings were interpreted to confirm ApoE's involvement in the economy of Aβ deposition and/or removal. In an evaluation of cognitively normal persons with a reported family history of AD and 2 copies, 1 copy, and no copies of the ApoE epsilon 4 allele, ^{11}C-PIB uptake was again significantly associated with ApoE epsilon 4 carrier status, and furthermore, with epsilon 4 allele dose (heterozygosity *vs.* homozygosity) in frontal, temporal, posterior cingulate-precuneus, parietal, and basal ganglia areas, which are typically affected in AD (Reiman et al. 2009). Further studies on ApoE genotype, ^{11}C-PIB uptake and cognitive performance in originally healthy subjects will hopefully elucidate the links between ApoE genotype, brain amyloid accumulation, and clinically manifest AD.

2.3.6 ^{11}C-PIB PET in relation to CSF biomarkers, MRI findings, ^{18}F-FDG PET findings, inflammation markers and cognitive measures

^{11}C-PIB uptake and neuropsychological measures

Many research groups have tried to establish whether ^{11}C-PIB uptake is associated with the severity of dementia. Although there is extensive variability between studies, ^{11}C-PIB uptake does generally not appear to be strongly associated with cognitive measures in AD patients (Klunk et al. 2004, Engler et al. 2006, Edison et al. 2007a, Pike et al. 2007, Rowe et al. 2007, Grimmer et al. 2008). For example, ^{11}C-PIB uptake and Mini Mental State Examination (MMSE) scores, with some exceptions, have not shown significant negative correlations (Klunk et al. 2004, Engler et al. 2006, Rowe et al. 2007). Furthermore, disease duration does not appear to be associated with ^{11}C-PIB uptake (Klunk et al. 2004). The Clinical Dementia Rating Sum of Boxes (CDR-SOB) score has been reported to explain approximately 11-22 % of the variance of ^{11}C-PIB uptake, but when controlling for age, the association became even weaker (Grimmer et al. 2008). In one study, a greater cortical amyloid load correlated with lower scores on facial and word recognition tests (Edison et al. 2007a). In another study with a larger AD group (n = 31), however, no relationship was detected between measures of memory performance and ^{11}C-PIB uptake ($r = 0.04$, $p = 0.85$) (Pike et al. 2007).

In contrast, MCI subjects as well as healthy controls have demonstrated some associations between episodic memory and ^{11}C-PIB uptake (Pike et al. 2007, Mormino et al. 2009). It should be noted that when hippocampal volume and ^{11}C-PIB uptake were both included in the same model to predict episodic memory in the latter study, ^{11}C-PIB uptake no longer correlated with cognitive measures ($p = 0.50$) (Mormino et al. 2009). It was

hypothesized that the effect of brain Aβ is mediated by hippocampal atrophy, which is indeed plausible.

Another study employed a retrospective approach using clinical follow-up information on initially cognitively healthy subjects. Longitudinal data had been collected during the 6-10 preceding years before ^{11}C-PIB PET. Seven out of 10 of the cognitively declining subjects were PIB-positive, compared with only 4 out of 24 of the cognitively stable subjects – a significant difference was observed between the ^{11}C-PIB uptake of the stable and that of the declining group. In the cognitively declining group, Aβ load was strongly correlated with memory impairment and with word-recall slopes. By the time of the PET scan, 4 out of the 10 cognitively declining subjects had converted to MCI or AD and all of these were PIB-positive. However, only 3 out of the 6 remaining cognitively declining subjects (still with no diagnosis) were PIB-positive. This was interpreted to suggest that cognitive decline itself was not synonymous with prodromal AD, which is in line with previous MCI studies – not all declining subjects ever convert to AD [*e.g.* (Busse et al. 2006)]. Furthermore, the results could be interpreted to mean that ^{11}C-PIB PET could be sensitive at detecting AD-prone individuals from other cognitively declining subjects. (Villemagne et al. 2008)

^{11}C-PIB uptake and brain atrophy measured with MRI

In contrast to ^{11}C-PIB uptake and dementia severity, a positive correlation has been demonstrated between ^{11}C-PIB binding and the rate of cerebral atrophy in AD subjects ($n = 9$) (Archer et al. 2006). Associations were found between rates of whole brain atrophy calculated over a mean follow-up of 13 months, and whole brain ($p = 0.019$) as well as regional ^{11}C-PIB uptake. The relationships between atrophy rate and anterior ($r^2 = 0.59$; $p < 0.05$) and posterior cingulate ($r^2 = 0.57$; $p < 0.05$) ^{11}C-PIB uptake were quite robust, although the small sample size needs to be kept in mind. A recent study with larger samples found a significant association between elevated ^{11}C-PIB uptake and smaller hippocampal volumes in PIB-positive MCI patients ($n = 39$) and in controls ($n = 37$) (Mormino et al. 2009). This was, however, a cross-sectional study, not providing any information on the *rate* of atrophy in relation to ^{11}C-PIB retention.

A recent follow-up report, where ^{11}C-PIB scans and MRI scans were performed at baseline and after approximately one year, has also been published. ^{11}C-PIB uptake did not increase significantly over time, while rates of brain atrophy were greater in the AD group than in the MCI group and greater in the MCI group than in the control group, as expected. ^{11}C-PIB uptake and atrophy rates were, however, not compared with each other in that study, meaning that possible individual associations remained undetected. (Jack et al. 2009) It would be of great importance to study this possible association between brain Aβ load and volumetric brain changes with larger sample sizes, longer follow-ups and subjects with different levels of cognitive impairment and/or risk for AD.

^{11}C-PIB uptake and CSF biomarkers

Cerebrospinal fluid (CSF) biomarkers have recently been intensively investigated in the quest for early detection of AD (see section *2.1.5 CSF and blood biomarkers*). An association has been shown between ^{11}C-PIB uptake and decreased CSF Aβ1-42 levels in both demented and non-demented subjects (Fagan et al. 2006, Grimmer et al. 2009). In a study with MCI subjects, CSF Aβ1-42 was abnormal in only 53 % of the subjects, whereas ^{11}C-PIB uptake was increased in 87 %. Furthermore, only 54 % of the PIB-positive subjects exhibited AD-like CSF Aβ1-42 values. (Koivunen et al. 2008a) In another study, all participants with low CSF levels of Aβ1-42, irrespective of their cognitive state, were also PIB-positive (Fagan et al. 2006). These results together could indicate that ^{11}C-PIB PET is more sensitive at detecting disrupted amyloid metabolism than this CSF biomarker, and further imply that CSF levels of Aβ may decrease only after Aβ plaques are already detectable with ^{11}C-PIB PET.

^{11}C-PIB uptake and brain inflammation as assessed by ^{11}C-(R)-PK-11195 PET

A modified amyloid cascade–neuroinflammation hypothesis suggests that Aβ formation activates microglial cells which in turn release neurotoxic substances such as cytokines and that these inflammatory changes are responsible for the neurodegeneration encountered in AD [*e.g.* (McGeer and McGeer 2001)]. Microglial activation can be studied with PET using a tracer that binds to peripheral-type benzodiazepine binding receptors (PBBR), which are expressed in the mitochondria of activated microglia (Kreutzberg 1996). ^{11}C-PK-11195 [1-(2-chlorophenyl)-N-methyl-N-(1-methylpropyl)-3-isoquinole carboxamide] or its higher-affinity R-enantiomer ^{11}C-(R)-PK-11195 is this kind of a radiotracer, and it has shown increased uptake in the entorhinal, temporoparietal and posterior cingulate cortices of AD patients (Cagnin et al. 2001, Edison et al. 2008a). In recent studies combining ^{11}C-(R)-PK-11195 and ^{11}C-PIB PET imaging, the uptake of the two tracers did not seem to be quantitatively associated in patients with AD or MCI (Edison et al. 2008a, Okello et al. 2009a, Wiley et al. 2009). The absence of an association could partly be explained by the increases in ^{11}C-(R)-PK-11195 uptake being rather small in AD (Edison et al. 2008a, Wiley et al. 2009), and the observation that brain microglial activation and therefore ^{11}C-(R)-PK-11195 PET retention can be increased also in other types of brain injury [*e.g.* (Banati et al. 2000)]. In addition, it could be expected that immune responses to Aβ deposition would vary greatly from individual to individual, and the sample sizes in these studies have been rather small.

^{11}C-PIB uptake and ^{18}F-FDG PET findings

Another logical PET tracer to combine with ^{11}C-PIB imaging is ^{18}F-FDG (see section *2.2.4 ^{18}F-FDG PET in AD*). ^{11}C-PIB uptake was significantly correlated with impaired glucose metabolism as assessed by ^{18}F-FDG uptake in the first clinical ^{11}C-PIB PET study on AD patients (Klunk et al. 2004). A later follow-up report on these 16 patients again noted that reduced rCMRgluc was significantly associated with increased ^{11}C-PIB uptake in the

frontal, parietal and occipital cortex at baseline, but the relatively strong association did not, however, persist at follow-up (Engler et al. 2006). In another PET study combining these two tracers, greater ^{11}C-PIB uptake correlated with lower rCMRgluc in temporal and parietal cortices but not elsewhere (Edison et al. 2007a). The high frontal amyloid load detected by ^{11}C-PIB PET in AD in the presence of unimpaired glucose metabolism in the same region (Edison et al. 2007a) is an interesting phenomenon that should be studied further. This could indicate that (fibrillar) Aβ is not the cause of the hypometabolism in AD, or that different brain regions are differentially susceptible to the toxic effects of amyloid, or that Aβ causes hypometabolism indirectly in those regions that receive neuronal projections from sites of Aβ accumulation. It has also been discussed that soluble Aβ oligomers could be even mainly responsible for progressive synaptic and neuritic injury while insoluble amyloid deposits, to which ^{11}C-PIB binds (Ikonomovic et al. 2008), could be relatively inert [*e.g.* (Walsh and Selkoe 2007)]. Soluble Aβ levels also seem to correlate better with the cognitive impairment than do Aβ plaque quantities (Näslund et al. 2000). This Aβ oligomer hypothesis could potentially explain both the discrepancies between the brain sites of atrophy and ^{11}C-PIB binding as well as between regions of ^{18}F-FDG and ^{11}C-PIB uptake changes, but more studies are needed to unravel this puzzle.

2.3.7 Possibilities and prerequisites of *in vivo* amyloid imaging tracers

Amyloid imaging would potentially have a number of future applications (see **Table 3** below), which explains why research in this field is so dynamic. New amyloid-binding tracers emerge continuously; for example, ligands such as ^{18}F-AV-138 (Wey et al. 2009), ^{11}C-AZD2184 (Johnson et al. 2009) and the PIB-derivative ^{18}F-flutemetamol (Nelissen et al. 2009) have recently shown potential for clinical applications.

A prerequisite for any Aβ tracer for *in vivo* imaging is of course that it effectively illustrates brain Aβ deposits. To this end, it should bind specifically to Aβ at nanomolar concentrations and it should have a sufficient signal-to-noise ratio as a PET tracer. These properties should be studied properly using biochemical measurements in *post mortem* brain tissue before embarking on *in vivo* studies. Next, the *in vivo* tracer uptake and *post mortem* histochemical measures of Aβ should correspond well, which is not at all self-evident even if the two compounds show similar binding *e.g.* in brain histopathology, because of the effects of tracer kinetics in the human body. Toxicity and radiation safety of any radiotracer should also be assessed before its wider use. For example, the radiation burden resulting from an amyloid-imaging scan with a certain ligand is extremely important and has to be estimated before planning studies with repeated scanning of individual subjects with the tracer. Another practical prerequisite for the widespread usefulness of an amyloid imaging tracer is that the method should be highly reproducible, even across different institutes. Only in this way can important and unbiased collective knowledge be gained.

Table 3. Potential applications of *in vivo* amyloid imaging with PET.

• **Studying the pathophysiology of Alzheimer's disease** - The time course of Aβ plaque deposition - The temporal and causal relationships of Aβ plaques with other neuropathological findings (neurofibrillary tangles, synaptic loss, grey matter atrophy, neurotransmitter deficits, reduced metabolism, etc.)
• **Early detection of Alzheimer's disease** - Depiction of neuropathological changes before clinical symptoms occur - Research on the familial forms of AD as a disease model - Studies on monozygotic and dizygotic cognitively discordant twins - Investigation of changes related with healthy aging and distinguishing these from the AD disease process
• **Differential diagnostics** - The differential diagnosis of other dementing diseases from AD - The depiction of possible multiple pathologies such as the often-seen combination of vascular dementia with AD - Establishing possible Aβ accumulation patterns of atypical dementias
• **Development and efficacy assessment of new therapies** - Validation of the mechanisms of action of drugs that have an impact on amyloid metabolism - Assessments of the possible impact of current AD treatments on amyloid pathology - Efficacy assessments of putative disease-modifying therapies such as amyloid-degrading drugs or drugs that inhibit the accumulation of Aβ - Studying the effects of anti-amyloid immunotherapy with vaccinations and/or amyloid antibodies

The method should also be widely accessible and in this respect, ^{18}F-labelled amyloid ligands for PET are of great interest. Only a small minority – for instance <10 % in the US - of PET sites have the ability to manufacture ^{11}C-labeled compounds on site (Klunk and Mathis 2008). The short radiochemical half-life of ^{11}C requires an on-site cyclotron, whereas ^{18}F-labelled compounds can be produced in regional cyclotron facilities and distributed to imaging centres within a 2-4 h travel radius. In short, the discovery of an applicable ^{18}F-labelled amyloid imaging tracer could increase by one degree of magnitude the availability of *in vivo* amyloid imaging. A new tracer of this kind would likely attract marked commercial interest. ^{11}C-PIB, because of the widely gained knowledge on its properties, could function as a reference compound for the development of more readily available tracers. Furthermore, ^{11}C-PIB or another ^{11}C-labelled compound could turn out to be still the most specific Aβ radioligand and therefore a feasible tracer for research use in sites where it can be manufactured. The validation of ^{11}C-PIB PET itself is still also incomplete and needs a more thorough assessment. The detailed evaluation of all the properties, *e.g.* the radiation safety and reproducibility of the method, is a prerequisite before embarking on further studies which hopefully demonstrate whether ^{11}C-PIB PET is applicable for the diagnosis, differential diagnosis, monitoring and/or early detection of AD, as well as for efficacy assessments of future anti-amyloid treatments.

3. OBJECTIVES OF THE STUDY

One of the major mysteries of Alzheimer's disease (AD) is the evolution of brain amyloid pathology. How early in the disease course can Aβ accumulation be detected in the brain and how the Aβ-related pathology changes during the progression of the disease are important issues which need to be addressed in biomedical research on AD. Whether Aβ may be detected in completely non-symptomatic individuals who are at an increased risk for future AD is a key question also for new therapeutic strategies. Positron emission tomography (PET) has shown promise as a technology to monitor brain amyloid pathology in living humans. For follow-up studies, it is essential to determine whether a PET tracer is associated with an acceptable radiation burden and shows sufficient reproducibility. Furthermore, as follow-up studies often include seriously ill patients, simplified scanning protocols that still produce reliable results are desirable. In order to address these issues and to provide further validation of amyloid detection with the PET tracer compound ^{11}C-PIB, the four practical objectives of this series of studies were as follows:

I To study the biodistribution and radiation dosimetry of the PET amyloid imaging agent ^{11}C-PIB in humans for the radiation safety point-of-view validation of (clinical) ^{11}C-PIB PET studies.

II To evaluate the reproducibility and (clinical) applicability of simplified ^{11}C-PIB PET data analysis methods.

III To determine whether there is continuous, progressive Aβ accumulation, as assessed by ^{11}C-PIB PET, during the clinical progression of AD over a feasible (two-year) follow-up time and to compare ^{11}C-PIB uptake with brain atrophy rates assessed with repeated magnetic resonance imaging.

IV To investigate whether non-demented monozygotic and/or dizygotic co-twins of cognitively impaired persons display increased ^{11}C-PIB uptake compared to unrelated control subjects.

4. SUBJECTS AND METHODS

4.1 SUBJECTS

All study protocols were approved by the Ethics Committee of Southwest Finland Hospital District. All subjects and their next-of-kin, when applicable (for cognitively impaired subjects who were considered unable to provide valid informed consent on their own), gave written informed consent according to the Declaration of Helsinki. No one was included in the investigations against his or her own wish. The subjects were free to withdraw their consent at any time and to discontinue their participation in the studies. The cognitively impaired subjects and their next-of-kin were offered no monetary rewards for their participation.

4.1.1 Healthy young subjects (study I)

The original subject group of study **I**, the ^{11}C-PIB PET dosimetry study, consisted of 8 healthy male volunteers, who differed from the control subjects of the other studies in that they were young adults. The mean age of the subjects was 27.5 years (SD 6.7), the ages ranging from 22 to 42 years. This approach was employed because healthy young males were considered to give reliable input data for the MIRDOSE3.1 program (Stabin 1996) for the organ-wise absorbed dose estimates. It was also important to eliminate the effect of any local or systemic pathologies on the tracer biodistribution. All of the enrolled subjects were healthy in terms of both somatic and neuropsychological conditions, which was ensured by obtaining thorough medical history and conducting a clinical health examination. The MRI scans that were acquired to aid in the positioning of the subjects in the PET scanner and for anatomical reference when evaluating the PET data also confirmed that no anatomical brain abnormalities were present. The subjects' average weight was 76 kg (SD 11, range 65-96 kg), which is also close to the weight of the 70 kg Reference Man (Snyder et al. 1974) in the MIRDOSE3.1 software (Stabin 1996) that was utilized in study **I**. The brain scans and arterial blood and urine analysis data of 5 previously scanned healthy subjects (3 women, 2 men) were also included in study **I**. These subjects' mean (SD, range) age was 67 years (4.9, 59-73) and their mean weight was 79 kg (21, 59-101). Furthermore, during the data analysis of study **I**, it was observed that additional gallbladder scans were needed. Three healthy subjects of ages of 78, 78 and 82 years and weights of 68, 57 and 70 kg were included in the study. These additions resulted in a sample size of 16 subjects in study **I**.

4.1.2 Elderly subjects: patients and controls (studies II and III)

The patient groups in studies **II** and **III** were recruited through the Turku City Hospital geriatric clinic and consultant neurologists. All patients fulfilled the NINCDS-ADRDA

criteria for probable AD (McKhann et al. 1984) as well as the DSM-IV criteria for Dementia of the Alzheimer's type. In all cases the diagnosis was made by an experienced geriatrist or neurologist and the diagnosis was always based, in addition to a typical clinical picture, on neuropsychological evaluation, physical examination including full neurological examination, structural brain imaging with either CT or MRI, and laboratory tests. It was also confirmed after enrollment and before PET scanning that brain MRI did not reveal any findings that would conflict with the AD diagnosis.

For the 14 patients in study **III**, a thorough medical history and physical examination including neurological examination, blood pressure measurement, ECG and laboratory tests were performed as a part of this study, within one month before the PET scanning. This screening visit was also repeated before the follow-up scans to confirm that each subject was still well enough to participate and had not developed marked concomitant illnesses. On both occasions the screening visits were conducted according to Good Clinical Practice (GCP) protocols at Clinical Research Services Turku, University of Turku. The 13 healthy control subjects of study **III** underwent the same screening procedures before participation on both occasions, at baseline and follow-up. **Figure 12** illustrates the visits of study **III.** No evidence of major neurological or psychiatric illness was present in these healthy subjects. They were – as were the AD patients of study **III** - also free of any other conditions –such as heart, lung or liver disease or taking concomitant medications - that could have affected the results of the PET scanning, MRI scanning

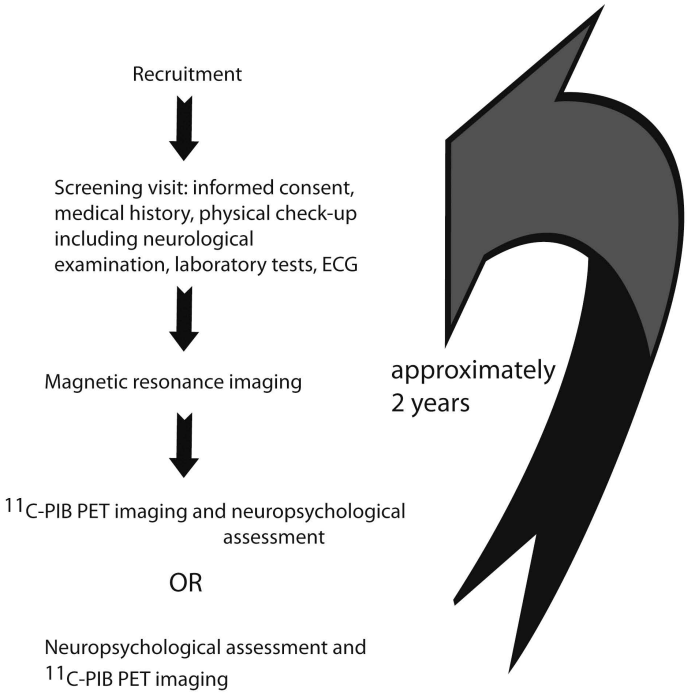

Figure 12. The steps of study **III**. The same procedures were conducted with each subject at baseline and at follow-up after an interval of approximately two years.

or neuropsychological testing. It was also confirmed that the healthy controls performed within the age-appropriate range in neuropsychological tests. The control subjects had to score a minimum 27 points in the MMSE at baseline of study **III**. One subject scored only 25 points at screening, but she underwent extensive neuropsychological assessments and in them performed within the age-appropriate range, and was therefore included in the healthy control group. The 4 elderly control subjects of study **II** were also deemed to be healthy on the basis of an interview about their medical history and were also subjected to a thorough physical examination. The patients of study **II** underwent the same check-up as the controls in order to exclude other (concomitant) illnesses and medications than AD that could have affected the results.

Four of the 6 patients and 3 of the 4 control subjects in study **II** were women. In study **III**, 6 of the 14 patients and 10 of the 13 control subjects were female. The mean (SD, range) age of the patient group at study **II** baseline was 71 years (7.6, 59-79), and the control subjects had a mean age of 64 years (9.2, 51-71). The mean age at baseline was 72 years (6.6, 55-84) for the patient group and 68 (5.4, 59-79) for the control group in study **III**.

In study **III (**and **IV**, see ahead), the educational background of each patient and control subject was also assessed and it was confirmed that the patient and control groups did not differ in terms of schooling. Furthermore, the educational level of the AD subgroups of progressors and nonprogressors did not differ from one another. See **Table 4** for the mean educational levels and other demographic information of study **III**.

Table 4. Demographical data [mean (SD) unless otherwise stated] on the Alzheimer's disease patients and the healthy controls of study **III**.

	AD patients (*n*=14)	AD progressors (*n*=8)	AD non-progressors (*n*=6)	Controls (*n*=13)
Men/women	8/6	4/4	4/2	3/10
Age at baseline, years	72.2 (6.6)	72.6 (4.0)	71.8 (9.6)	68.4 (5.4)
Age range at baseline, years	55.4-84.0	65.2-78.2	55.4-84.0	58.7-78.7
Time between scans, years	2.02 (0.20)	2.04 (0.25)	2.00 (0.11)	2.12 (0.57)
Range of time between scans, years	1.81-2.63	1.8-2.6	1.8-2.2	1.47-3.08
Educational level*	2.1 (0.8)	2.0 (0.8)	2.2 (1.0)	1.8 (0.7)
ApoE genotypes ε4ε4 / ε3ε4 / ε3ε3	3/10/1	3/5/0	0/5/1	0/7/6
MMSE at baseline	24.3 (3.1)	23.8 (3.7)	25.0 (2.3)	28.4 (1.5)
MMSE range at baseline	17-29	17-27	23-29	25-30
MMSE at follow-up	21.6 (3.9)	20.0 (3.9)	24.0 (2.4)	27.2 (1.8)
MMSE range at follow-up	12-28	12-25	21-28	23-30

AD = Alzheimer's disease

* The educational backgrounds of the subjects were classified into three categories according to the duration of their formal education: 1, basic education (6-8 years); 2, additional college or vocational education (8-15 years) and 3, higher academic education (≥ 15 years). The educational levels of the AD group and the control group did not differ (p = 0.325).

This data has been previously published in original publication **III**.

4.1.3 Twins and controls (study IV)

The elderly twins in study **IV** were recruited from the Finnish Twin Cohort (Kaprio and Koskenvuo 2002). During 1999-2001, all monozygotic (MZ) twin persons aged 65 years or more and having their co-twin alive in 1999 were asked to participate in a telephone screening of cognitive functioning. In 2003-2007, the study was amended to also include elderly same-sex dizygotic (DZ) twins and twins of uncertain zygosity. The TELE and the TICS questionnaires that have been described previously in more detail (Järvenpää et al. 2002, Järvenpää et al. 2003) were employed in the telephone screenings. The telephone interview was completed for 2483 twins of known zygosity (703 MZ twins and 1780 DZ twins) and 123 twins of uncertain zygosity with an overall response rate of 78.7 %. The zygosity of the twin pairs in the screening study was determined by using a previously validated questionnaire method (Sarna et al. 1978). The zygosity of the twin pairs that participated in the actual PET study were confirmed by genotyping of ten highly polymorphic markers at the Paternity Testing Unit of the National Public Health Institute, Helsinki, Finland.

In earlier studies the TELE interview has been shown to effectively differentiate probable AD patients from cognitively healthy individuals (Järvenpää et al. 2002). The twin pairs that showed discordance in their cognitive performance measured by the TELE interview were asked to participate in the PET study. The cognitive disorder of one of the co-twins and the intactness of the other were confirmed through neuropsychological testing with an extensive test battery for episodic and semantic memory, attention, language and visuospatial abilities. Based on these results, 8 MZ twin pairs and 9 DZ twin pairs were finally included in the PET study, because they were considered discordant for a memory disorder. In addition, 9 healthy elderly non-twin control subjects, who were unrelated to the twins, were recruited through advertisements in the local Alzheimer's disease association's magazine, and these subjects also underwent the same neuropsychological testing to confirm their normal cognitive performance. **Table 5** shows the gender distribution and age as well as educational level of the participants of study **IV**. There were no differences in the educational levels of the cognitively impaired and intact groups.

4.2 STUDY DESIGNS

Studies **I** and **IV** were cross-sectional. Study **II** included repeated ^{11}C-PIB PET scans, but the scans were performed within a short period, the mean scan interval being 34 days (SD 30) for the patient group and 58 days (SD 27) for the control group. Study **III** was a longitudinal study with an average time between the baseline and follow-up scans of 2.0 years (SD 0.2) for the patient group and 2.1 years (SD 0.6) for the control group. All studies included brain MRI scanning and PET scanning with ^{11}C-PIB as the radiotracer. Studies **II-IV** also assessed the cognitive performance of the participants, with Mini Mental State Examination (MMSE) as the minimum assessment (in study **II**). None of the studies can be considered as an intervention study, because no treatments were given to the subjects.

Table 5. Demographical information on the monozygotic and dizygotic twins and the healthy controls of study **IV**. The data are presented as mean (SD) unless otherwise stated.

	MZ-impaired (n=9)	MZ-preserved (n=9)	DZ-impaired (n=8)	DZ-preserved (n=8)	Controls (n=9)
Men/women	7/2	7/2	4/4	4/4	3/6
Age (years)	76.2 (4.3)	76.2 (4.3)	71.6 (0.5)	71.6 (0.5)	71.2 (3.4)
Educational level*	1.8 (1.1)	1.7 (1.0)	1.4 (0.5)	1.8 (1.0)	1.9 (0.6)
ApoE ε4 carriers	1 (11 %)	1 (11 %)	4 (50 %)	3 (38 %)	3 (33 %)
MMSE	20.9 (5.3)	27.9 (1.5)	22.6 (3.1)	27.5 (1.8)	28.3 (1.5)
Word list learning	16.5 (7.7)	21.2 (5.9)	16.3 (3.4)	19.0 (2.4)	21.3 (3.6)
Word list savings (%)	58.5 (30.1)	93.4 (16.6)	65.5 (19.0)	92.5 (8.5)	94.8 (6.2)
Trail making A (sec)	94.2 (50.6)	71.0 (25.6)	110.3 (59.2)	72.3 (18 .4)	61.9 (14.6)
Category fluency	19.3 (8.3)	24.0 (7.3)	20.6 (4.7)	25.6 (8.8)	22.2 (2.9)

* The educational backgrounds of the subjects were classified into three categories according to the duration of their formal education: 1, basic education (6-8 years); 2, additional college or vocational education (8-15 years) and 3, higher academic education (≥ 15 years).
MMSE = Mini-Mental State Examination; Word list learning: sum of three repetitions (maximum 10 words in each); Word list savings: the percentage of words remembered from the third repetition after delay; Trail making A: time (in seconds) needed to connect randomly placed numbered circles in correct order; Category fluency: sum of different animals the subject could list correctly in 60 seconds. The more extensive neuropsychological data was not available for one MZ twin pair but the discordance in cognitive abilities was evident clinically and according to the MMSE (23 vs. 29 points).

The health care of the subjects was totally independent of the studies. The main outcome measures were **I** the radiation burden of ^{11}C-PIB PET scanning in different organs of the body and in the human body as a whole (absorbed doses and effective dose); **II** the test-retest variability (VAR and ICC values) of ^{11}C-PIB uptake measurements obtained with simplified analysis methods; **III** the change in ^{11}C-PIB uptake (region-to-cerebellum ratios) over two years of follow-up (%) in the AD group compared with controls and the associations (correlation coefficients) of ^{11}C-PIB uptake ratios with brain atrophy rates; and **IV** the ^{11}C-PIB uptake ratios of cognitively intact subjects who had a monozygotic or dizygotic co-twin with AD-like cognitive impairment (stringent AD diagnostic criteria were not applied), compared with unrelated controls. The subject sample in study **I** consisted of healthy participants only, but in studies **II-IV**, both AD patients (or cognitively impaired subjects with AD-like symptoms) and healthy controls were investigated. The practical matters of studies **I-IV** are compared in **Table 6** (ahead).

4.3 IMAGING METHODS

4.3.1 MRI

The MRI scanning was always performed with a Philips Gyroscan Intera 1.5 T scanner (Philips, Best, The Netherlands). In study **I**, abdominal T1-weighted 3-dimensional

Table 6. Comparison of practical matters of studies **I-IV**.

	^{11}**C-PIB PET scans**	**PET scanner**	**MRI**	**Subjects' cognition (*n* preserved / impaired)**	**Neuropsychological assessments**
Study **I**	abdominal + whole body (+brain)	ECAT EXACT HR+	abdominal (+ brain) for reference	16 / 0	none
Study **II**	repeated (2) brain scans within 102 days	GE Advance	brain for reference	6 / 4	MMSE
Study **III**	repeated (2) brain scans with ~2 year interval	GE Advance	brain for screening + atrophy rate analyses	14 / 13	ADAS-Cog / CERAD
Study **IV**	single brain scan per subject	ECAT EXACT HR+	brain for screening	17 / 17 in twins + 9 / 0 in unrelated	ADAS-Cog / CERAD

scans with a voxel size of 1.56 x 1.57 x 4.00 mm were obtained for 6 subjects. The location of the kidneys was marked on the subjects' body according to these images to aid in the subsequent positioning into the PET scanner. In these abdominal scans, the subjects had to hold their breath. T1-weighted 3-dimensional brain MRIs with a voxel size of 0.50 x 0.50 x 1.00 mm were obtained with the same Philips scanner in all of the studies, **I-IV**. T2 sequences and FLAIR sequences were also obtained in all of the brain scans. These were used to exclude the presence of any brain pathologies that could have interfered with the results of the studies or resulted in the rejection of some subjects.

4.3.2 Radiotracer synthesis and administration

The radiotracer ^{11}C-PIB was in all studies manufactured in the same manner: by a reaction of 0.8 mg of 6-OH-BTA-0 and ^{11}C-methyl triflate in 100 µL of acetone, for 3 min at 80 °C. The crude product was then purified through high-performance liquid chromatography with a µBondapak column (Waters), using an eluent of 0.01 mol/L of phosphoric acid/acetonitrile (63:37) and a 5 mL/min flow rate. Then 0.3 mL of sterile propylene glycol/ethanol (7:3, v/v) was added and the fraction containing the product was evaporated and redissolved in a sterile medium [propylene glycol/ethanol (7:3, v/v)] / [physiologic phosphate buffer] (0.1 mol/L, pH 7.4; 1.5:8.0) and filtered through a 0.2 µm Acrodisc 4192 sterile filter (Gelman). The radioligand purity was In all studies the radioligand purity was 95 % at minimum, and the mean specific radioactivity ranged from 29 MBq/nmol to 32 MBq/nmol.

The mean (SD, range) injected radioactive dose of ^{11}C-PIB was 489 MBq (61, 416-606) in study **I**. In study **II**, the mean injected doses were 322 MBq (19.2, 295-345) for the AD patients and 301 MBq (10.1, 289-311) for the controls in the first scan and 301 MBq (23.4, 265-331) for the AD patients and 275 MBq (30.8, 236-309) for the controls in the second scan. For the ^{11}C-PIB PET scans of study **III**, the mean injected doses at baseline were 413 MBq (96.2, 282-521) for the patients and 397 MBq (104, 285-538) for the controls, and at follow-up, the mean doses were 436 MBq (75.4, 317-542) for the patients and 376 MBq (75.6, 289-502) for the controls. In study **IV**, the subjects received a radioactive dose of 470 MBq of ^{11}C-PIB on the average (67, 250-537). In all studies **I-IV**, the radiotracer was administered intravenously into an antecubital vein as a rapid bolus injection.

4.3.3 PET scanning

A transmission scan was always obtained before the injection of the radiotracer. In study **I**, when acquiring whole-body images of 2 subjects, a 2 min transmission scan was performed for each bed position. Otherwise the transmission scans of this study as well as study **IV** lasted 5 min. With the exception of the brain images of study **I** that were acquired previously with the GE Advance PET scanner (General Electric Healthcare) (and 10-15 min transmission scans), the PET scans of study **I** were performed with the ECAT EXACT HR+ scanner (CTI/Siemens) (**Figure 13**), as were all of the PET scans in study **IV**. The GE Advance scanner (**Figure 14**) was, in turn, used in all PET scans of studies **II** and **III**. In both of these studies, the transmission scans lasted 8 min. All of the transmission scans, irrespective of the scanner, were performed with rotating ^{68}Ge/^{68}Ga rod sources.

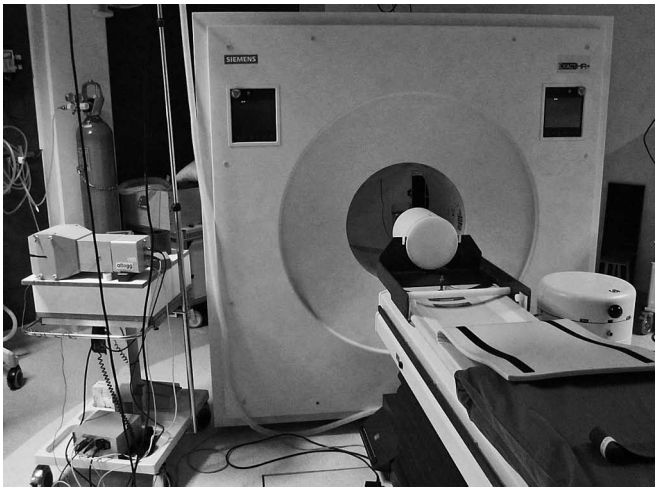

Figure 13. The ECAT EXACT HR+ scanner at Turku PET Centre.

The field of view of the ECAT EXACT HR+ scanner consists of 63 image slices in 15.5 cm, with 2.46 mm slice separation. The abdominal images and whole-body images in study **I** were obtained with the scanner in the 2-dimensional mode. Three subjects

underwent PET scanning of the upper abdomen and another 3 had their middle abdomens imaged. The former scans enabled the visualization and quantitation of ^{11}C-PIB uptake in the heart wall, stomach, spleen and intestine, whereas the latter provided data on the kidneys and back muscles. The ^{11}C-PIB uptake estimates of the vertebral bodies and the liver were obtained from both types of abdominal scans. Both types of abdominal scans consisted of 23 time frames (8 x 15, 6 x 30, 5 x 180 and 4 x 300 s), so that the emission scans lasted 40 min. Since it was observed that tracer uptake in the gallbladder was continuing at 40 min, another 3 subjects were scanned with their upper abdomen in the tomography field of view. These images were obtained at about 100 min after tracer injection, after these subjects had already undergone a 90 min brain scan. The 2 whole-body scans in study **I** were performed so that the first was started 5 min after tracer injection with the subject being imaged from the head to the upper thigh region and the second was started 11 min after tracer injection and the subject was imaged from the upper thigh region to the head. The emission scan for each bed position lasted 5 min. In contrast, in all of the other scans of studies **I-IV**, a stable bed position was used. The 3-dimensional (detector ring septa retracted) brain emission scans of study **I** as well as studies **II-IV**, lasted 90 min, with 28 time frames (4 x 30, 9 x 60, 3 x 180, 10 x 300 and 2 x 600 s), irrespective of the scanner employed. The GE Advance scanner used in the brain scanning of studies **I-III** yields 35 slices in a 15.2 cm long field of view, providing 4.25 mm slice separation.

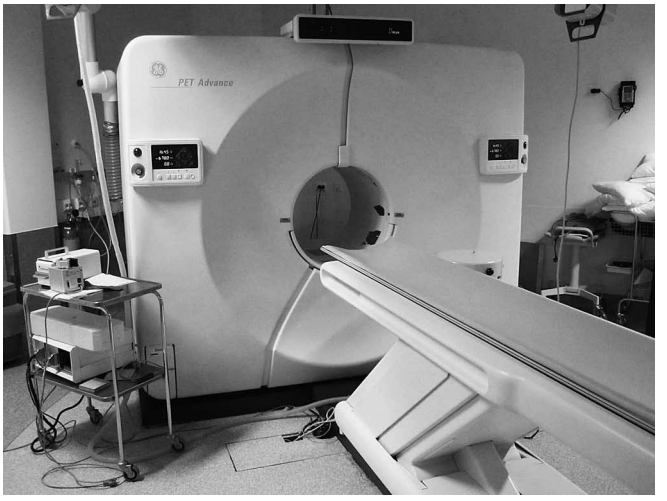

Figure 14. The GE Advance scanner at Turku PET Centre.

The images obtained with the ECAT EXACT HR+ scanner, *i.e.* those from the abdominal and whole-body scans of study **I** and all (brain) scans of study **IV**, were reconstructed with a filtered back projection algorithm using the Hann filter and a 4 mm cut-off frequency. The GE Advance scanner images of studies **I-III** were reconstructed with a transaxial Hann filter with a 4.6 mm cut-off frequency and an axial ramp filter with an 8.5 mm cut-off. All of the image data were reconstructed into a 128 x 128 matrix.

4.4 ARTERIAL AND URINE SAMPLING AND ANALYSES

4.4.1 Arterial input data

Arterial sampling was performed in study **I** to assess blood radioactivity. An arterial cannula was inserted in the radial artery of each subject by an experienced anesthesiologist for blood sampling during the PET scan. The cannula was always in the arm opposite to the venous cannula used for radiotracer administration. Radioactivity monitoring was performed continuously at 0-5 min post-injection with an online detector (ABSS, Allogg, on the HR+ scanner and FRQ, General Electric Healthcare, on the Advance scanner) with an automated blood flow pump (**Figure 15**) and then from blood samples manually collected at 3, 8, 12, 25 and 40 min during the abdominal scans and at 3, 8, 12, 25, 45, 60, 75 and 90 min after tracer injection during the brain scans. The online detectors as well as the automated gamma counter (Wizard 1480, Wallac) for manual sample measurements were cross-calibrated with the corresponding PET scanners with an ionization chamber (Veenstra Instruments). The data collected by the online detector and with manual sampling were combined to form a continuous curve representing blood radioactivity concentration (kBq/mL) as a function of time. For dosimetric studies the values were normalized to an injected activity of 1 MBq and the mass of the 70 kg Reference Man (Snyder et al. 1974) employed in the MIRDOSE3.1 software (Stabin 1996), and the decay correction was reversed. The descending part of the curve was fitted into a 2-exponential function and the curve was extrapolated to infinity.

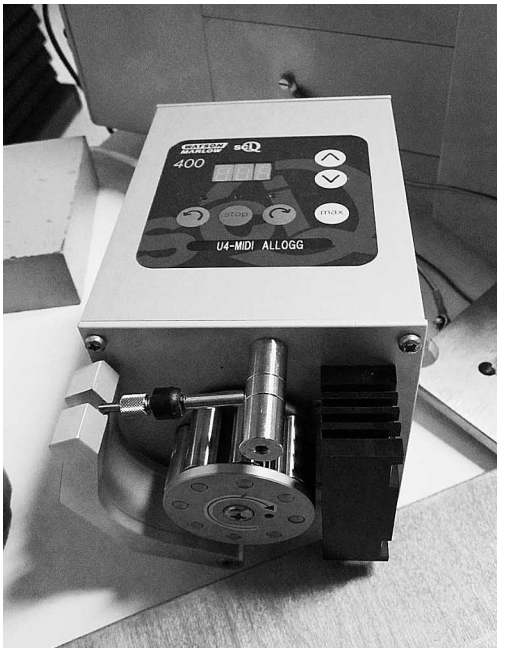

Figure 15. Automated pump to ensure constant blood flow through the online radioactivity concentration detector.

4.4.2 Urine input data

The subjects of study **I** were asked to void their bladder before the PET scans. Urination was then controlled during scanning, and the subjects were asked to urinate directly after the scan. These urine samples were collected and the time of urination was recorded by a time stamp system in the lavatory. Due to different PET scanning times between subjects, urine samples were obtained from 46 min post-injection to 141 min after the injection of ^{11}C-PIB. Altogether 16 urine samples, from subjects aged from 22 to 73 years, were obtained. The total volume of the urine was always measured first, after which a 2.5 mL sample was extracted with a dropper. This 2.5 mL sample was then measured in the ionization chamber and the time of this measurement was recorded to enable decay correction. The urine radioactivity at the time of voiding the bladder was estimated as the fraction of injected ^{11}C-PIB radioactivity. The data of these 16 subjects were combined into one dataset. The radioactivity in the residual or nonvoided urine could not be measured. Taking this into account, the radioactivity concentration values (in the voided urine) were modeled with the empiric formula of in-growth (Graham et al. 1997):

$$A(t) = A_B(1 - e^{-bt}).$$

This equation was thus used as a pattern of excretion of ^{11}C-PIB into urine. b was the rate coefficient for clearance, and it was estimated by adjusting the total excretion fraction of the injected radioactivity in urine, A_B, to different values between 15 % and 40 % to fit the measured data. (As a result of this fitting, the parameter A_B received the value 20 %, indicating that the renal system excretes about 20 % of the injected radioactivity.) To convert the fractional data to radioactivity concentration data, the mean sample volume of the measurements (V = 384 mL) and the mean injected radioactivity were employed.

4.5 ^{11}C-PIB IMAGE AND ABSORBED DOSE ANALYSES

^{11}C-PIB uptake was quantitatively evaluated through manual region-of-interest (ROI) analysis in study **I** and partly (as a comparison method) in study **II**, whereas in a part of study **II** as well as in all tracer uptake analyses of studies **III** and **IV**, an automated ROI analysis method was employed. In study **IV**, Statistical Parametric Mapping was performed in addition. In studies **II-IV** the only part of the body under evaluation was the brain, whereas in study **I**, the brain was only one of the evaluated organs and most ROIs were drawn on abdominal structures.

4.5.1 ^{11}C-PIB uptake analysis for dosimetry calculations

In the image analysis of study **I**, ROIs were drawn on either a summed image of the first 4 min of the dynamic scan (frames 1-12) or a summed image of the last 20 min (frames 20-23), depending on which part of the scan best illustrated the selected organs. Some

organs were better visualized early in the scan due to vascular activity and others in the later time frames due to tracer uptake or metabolism. ROIs were drawn on the PET images with the image analysis software Imadeus Academic 1.10 (Forima Inc.), on representative parts of the liver, heart, kidney cortex, kidney pelvis, spleen, gallbladder, lungs, stomach, large intestine, back muscles and vertebral bodies. In bilateral organs, ROIs were drawn bilaterally (kidney cortex and pelvis, and lungs). The anatomical location of the ROIs was confirmed by viewing the corresponding MRI simultaneously, and in the case of the lung ROIs, the ROIs were delineated with the aid of the transmission scans because contour visibility was best in these images. In the case of vertebral bodies, which represented cortical bone in the absorbed radioactivity dose estimates, the anatomical location was confirmed by both the MRI and the transmission PET image.

In study **I**, the ROIs for each source organ were drawn on 4 consecutive image planes and on a minimum of 3 different subjects' images, individually for each subject and for each plane. The ROIs were finally imposed on the dynamic ^{11}C-PIB PET images of the subjects, and through the Imadeus Academic software, time-activity curves, *i.e.* representations of the radioactivity concentration in a ROI-defined structure as a function of time, were calculated for each source organ. The time-activity curves were normalized to express radioactivity in the given organs after a 1 MBq dose (division by injected dose) of ^{11}C-PIB and in a 70 kg body (division by mass of subject x 70 to fit the MIRDOSE3.1 program). The decay corrections that had been part of the reconstruction algorithm were then reversed and the resulting non-decay-corrected, normalized curves were fitted with 3-exponential functions and extrapolated to infinity. In the case of the gallbladder and upper large intestine radioactivity concentration curves, the dynamic acquisition time of 40 min had not been sufficient to determine the clearance of ^{11}C-PIB from these organs. With the upper large intestine, the curve was nevertheless descending at 40 min, and a feasible approach was therefore to extrapolate the curve with the physical decay function of ^{11}C-PIB according to the half-life of ^{11}C (20.4 min). However, the radioactivity concentration of the gallbladder still seemed to be increasing at 40 min, and physical decay could not be assumed to represent the clearance of the radioactivity after the last measurement. As described in the section *4.1 Subjects*, three additional data points were therefore acquired for the gallbladder curve. These three extra measurements at approximately 100 min after tracer injection resulted in a representative radioactivity concentration curve that could be fitted to a 3-exponential function and handled in the subsequent analyses like the rest of the source organ curves.

4.5.2 Brain ^{11}C-PIB uptake analyses: ROI and SPM analyses

For the brain ^{11}C-PIB PET images of studies **II-IV**, automated ROI analysis was employed. In study **II**, the manual method was used for comparison to validate the automated method. In all of the brain ^{11}C-PIB uptake analyses, a summated image of the last 30 minutes of the emission scan (*i.e.* frames 25-28) was employed, because this time period (60 to 90 min post-injection) was deemed to best illustrate specific tracer uptake.

Manual ROI analysis

In the manual process in study **II**, the first and the second (the test and the re-test) ^{11}C-PIB PET images of each subject were realigned with one another with the Statistical Parametric Mapping software, version 2 (SPM2). The corresponding MRI was then coregistered with the (individual) mean image of the realigned images. ROIs were delineated manually on each of these combination images (with the MRI predominant, showing the anatomy), in the following structures: anterior and posterior cingulate cortices, lateral prefrontal and lateral temporal cortices, mesial temporal cortex (including amygdala, hippocampus and parahippocampal gyrus), occipital and inferior parietal cortices, caudate nucleus and putamen. The drawing on the coregistered MRIs was done with the Imadeus software, as were the time-activity calculations from the summated ^{11}C-PIB PET images. The regional uptakes were assessed by dividing the average ROI radioactivity concentration values by the same individual's average cerebellar radioactivity concentration value, resulting in estimates of region-to-cerebellum ratios.

Automated ROI analyses

The automated ROI analyses of studies **II-IV** were enabled by procedures conducted in a common stereotactic space. For this end, summated (60 to 90 min post-injection) ^{11}C-PIB PET images were first normalized using a common ^{11}C-PIB image template and written using bilinear interpolation. (The ligand-specific template had been created using 14 previously acquired ^{11}C-PIB scans, which included the images of 5 healthy control subjects, 4 MCI patients and 5 AD patients. The procedures involved in generating the template are described in detail in the original publication **II**.) To enable the calculation of parametric images representing ^{11}C-PIB region-to-cerebellum ratios in each voxel, the cerebellar (cortex) radioactivity concentration was evaluated through automated ROI analysis (described below) of the normalized summated images. The normalized summated images were divided by the cerebellar radioactivity concentration values, this procedure resulting in parametric images. A standardized set of ROIs (see **Figure 16** for examples) was defined on an MRI template image (the mean image of 12 spatially normalized MRIs, described in more detail in publication **II**), representing brain anatomy in accordance with the Montreal Neurological Institute database (MNI) space. When this ROI set, including the same regions as described above for the manual analysis, was imposed on the spatially normalized parametric images, regional average region-to-cerebellum ratios were obtained. The left and right sides of each brain region were averaged to result in region-specific uptake ratios, because no differences in ^{11}C-PIB uptake between the two hemispheres were observed, as has also previously been reported (Raji et al. 2008). In studies **III** and **IV**, a composite neocortical score, representing global cortical ^{11}C-PIB uptake, was also calculated. This score was the un-weighted average of the uptake ratios of the medial and lateral frontal cortices, the temporal and parietal cortices, and the posterior cingulate. In study **III**, in order to confirm the integrity of the cerebellum as a reference region, cerebellar standardized uptake values (SUVs) were also

calculated and the baseline values were compared with the follow-up values in both study groups. There were no differences between baseline and follow-up cerebellar SUVs.

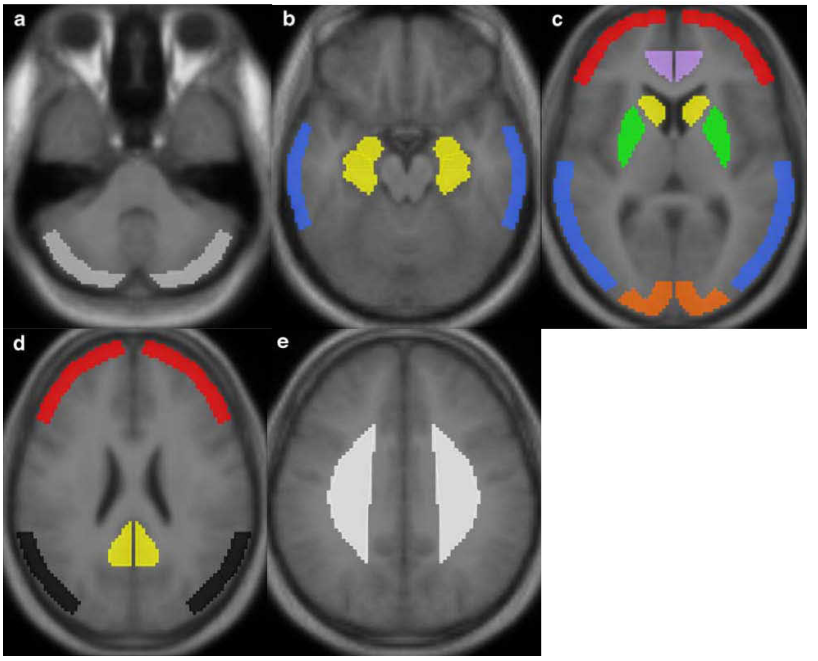

Figure 16. Examples of ROIs used in studies **II-IV**. A) Cerebellar cortex, the reference region. B) Lateral temporal cortex and medial temporal cortex. C) Lateral frontal cortex, anterior cingulate, caudate nucleus, putamen, lateral temporal cortex, and occipital cortex. D) Posterior cingulate and parietal cortex. E) White matter.

Statistical Parametric Mapping (SPM) analysis

Study **IV** included Statistical Parametric Mapping (SPM) analyses, performed with Statistical Parametric Mapping (Friston et al. 1995) software version 2 (SPM2) and Matlab 6.5 for Windows (Math Works, Natick, MA, USA). This method addresses the parametric ^{11}C-PIB PET images, *i.e.* the spatially normalized images where the ^{11}C-PIB signal in each voxel has been divided by the cerebellar ^{11}C-PIB signal of the same individual. The process enables the exploration of between-group differences without spatial constraints and thus without any *a priori* hypotheses concerning the locations of possible differences. It results in maps illustrating the brain regions where statistically significant ^{11}C-PIB uptake differences are present. In study **IV**, the different subgroups were compared with each other by SPM using one-way analysis of variance (ANOVA) and *t*-contrasts. The parametric images that were compared were smoothed with a 12 mm Gaussian kernel. Multiple comparison corrected p-values < 0.05 at cluster level were considered significant, and the non-significant clusters were discarded from the visualizations by adjusting the minimum cluster size. The SPM analysis results were also used to validate the choices for the regions-of-interest for the quantitative automated

ROI analysis of study **IV**. The regions of significant between-groups differences could be identified with the MNI Space Utility (http://www.ihb.spb.ru/~pet_lab/MSU/MSUMain.html), which converts the MNI coordinates given by SPM to Talairach coordinates (http://www.mrc-cbu.cam.ac.uk/Imaging/Common/mnispace.shtml) and enables identification of the location of each voxel according to the anatomic labels presented in the Talairach Daemon database (http://www.talairach.org/daemon.html).

4.6 MRI ANALYSES (study III)

The MRI analyses of study **III** were performed with the aim to compare the longitudinal changes in the groups (AD subjects and controls) both point-wise as well as ROI-wise.

To remove pose differences, the follow-up MRIs of all subjects were first rigidly registered onto the corresponding baseline images. Using non-rigid registration and an in-house tool, the baseline images were then coregistered onto the corresponding follow-up MRIs. This gave each point a deformation field, and the local volume change over the follow-up period was measured in each voxel by computing the determinant of the Jacobian matrix of the deformation field. For the point-wise comparison of the subjects, the data were normalized to a mean MRI template, previously created from the images of 14 healthy subjects. Thus, a point-correspondence was obtained, which enabled the comparison of local volume measures between different subjects. For the between-groups comparison, the local volume measures were smoothed 3 times with a Gaussian filter, after which the non-parametric Mann-Whitney U-test was applied for the volume change values of each voxel. The obtained voxel-wise between-groups differences in changes could then be visualized in colour on top of the MRI template. This is illustrated in **Figure 22** of the *Results* section.

To obtain regional results, ROI analysis was applied. The Anatomical Labeling (ALL) atlas (Tzourio-Mazoyer et al. 2002) was transformed onto the subjects' baseline MRIs and the average volume change in each ROI was computed. Principal component analysis (PCA) was finally applied to the ROI analysis data of the regions with the most significant between-groups differences, *i.e.* the hippocampus, the temporal cortex, the precuneus and the cerebral ventricles. The MRI score, to obtain a one-value representation of the magnitude of change in each subject, was derived from the weight of the Eigenvector that explained the largest share of the variance in the data (*i.e.* had the largest Eigenvalue).

4.7 NEUROPSYCHOLOGICAL ASSESSMENTS

The MMSE was carried out in all studies that included cognitively impaired subjects, *i.e.* in studies **II-IV**. More extensive neuropsychological testing was performed in studies **III** and **IV**. The test batteries included tests for episodic and semantic memory, attention, language and visuospatial abilities. All tests were performed by trained personnel, either

certified psychologists or advanced students of psychology. The testing was performed at Clinical Research Services Turku, at Åbo Akademi University facilities, or at Turku PET Centre.

4.7.1 The formation of AD progressor and nonprogressor subgroups

In study **III**, the AD subject group was *post hoc* subdivided into two groups with regard to estimated disease progression. Five neuropsychological measures were used in making the division into "progressors" and "nonprogressors"; the MMSE and four CERAD/ADAS-COG tests: word list learning, picture naming, word recognition and category fluency. These tests were considered to reflect the cognitive domains that typically change in AD (episodic and semantic memory) (Collie and Maruff 2000). Word list learning points were the sum of three repetitions (maximum 10 words in each). The picture naming score was the percentage of correctly named images and the word recognition score was the percentage of correctly recognized words from a previously introduced list. Category fluency was assessed as the number of different animals the subject could list correctly in 60 seconds. Subjects who had either a decline of 3 or more points in the MMSE or <3 points decline in the MMSE but ≥15 % decline in all other neuropsychological tests were considered to have more progressive AD, *i.e.* they were considered "AD progressors" whereas the rest, who had less dramatic changes in their test scores, were considered nonprogressors. **Table 2** of Original Publication **III** lists the mean values of the neuropsychological measures of the AD nonprogressor and progressor subgroups both at baseline and at two-year follow-up.

4.7.2 The assessment of discordance between co-twins in cognitive performance

The twin participants of study **IV** first underwent telephone screening of cognitive status using the TELE and the TICS instruments described previously in more detail (Järvenpää et al. 2002, Järvenpää et al. 2003). The twin pairs who were discordant for cognitive impairment, according to TELE, were asked to participate in a detailed neuropsychological examination. This test battery measured episodic and semantic memory, attention, language and visuospatial abilities. These tests confirmed the discordance in cognitive performance between the co-twins that were selected to participate in study **IV**. The cognitively impaired individuals had poor memory performance including episodic memory, when compared with non-impaired co-twins. In addition, they had impairment in at least two or more other cognitive domains. With these criteria and by exclusion of other causes of dementia, the cognitively impaired co-twins of study **IV** very likely had AD, although no stringent diagnostic algorithms were applied. In contrast, the cognitively preserved co-twins performed in the neuropsychological testing within age- and education-adjusted norms. The unrelated healthy control subjects of study **IV** also underwent the same neuropsychological tests,

which aided in selecting only cognitively preserved persons into the control sample. See **Table 1** in Original Publication **IV** for the mean scores of the study subgroups in the different neuropsychological tests.

4.8 STATISTICAL ANALYSES, DOSIMETRY CALCULATIONS AND EVALUATION OF REPRODUCIBILITY

The statistical analyses were performed with SPSS software versions 13.0, 15.0 and 16.0 (for Mac) (SPSS Inc., Chicago, IL, USA) and SAS software version 9.2 (SAS Institute Inc., Cary, NC, USA). nQuery Advisor software, version 7.0 (Statistical Solutions, Cork, Ireland) was also employed in study **II**. See section *4.5 ^{11}C-PIB image and absorbed dose analyses* for the description of Statistical Parametric Mapping. See section *4.6 MRI analyses* for the description of the point-wise comparison of the MRIs of the AD and control groups of study **III**. Parametric testing was valid for evaluating ^{11}C-PIB uptake differences between groups in all of the studies, because the results followed normal distributions and the variances were homogenous. $P < 0.05$ was considered significant when evaluating the between-groups differences.

4.8.1 Dosimetry calculations (study I)

As described above, the radioactivity concentration estimates for the dosimetry calculations of study **I** were obtained from ROI and urine and arterial blood analyses. Absorbed doses were thereafter calculated with the MIRD algorithm for radiation dose calculations in internal exposure, developed by the MIRD Committee of the Society of Nuclear Medicine (Howell et al. 1999). The mean absorbed dose (D) in a target organ (r_k) can be derived from the injected radioactivity (A_0) with the following equation:

$$\frac{\overline{D}(r_k)}{A_0} = \sum_h \tau_h S(r_k \leftarrow r_h)$$

Here S contains the physical characteristics (half-life, emission types and energies, penetration ability of the radiation) of ^{11}C as well as the specific fraction of energy absorbed in each source-target organ pair. Residence time τ_h includes the kinetics of the radionuclide in the source organ (r_h). The residence time, in turn, can be estimated by integrating the area under the corresponding (fitted) time-activity concentration curve and by multiplying that area by the source organ volume in the 70 kg Reference Man (Snyder et al. 1974) of the MIRDOSE3.1 software (Oak Ridge Institute for Science and Education, Oak Ridge, TN, USA) (Stabin 1996).

The MIRDOSE3.1 software thus calculated the absorbed doses in the target organs after the residence times for source tissues, including blood, were entered into the program. In order to obtain an estimate of the radioactivity in the remainder of the body, *i.e.*

in the tissues outside of the measured organs, the source organ dose estimates were subtracted from the total decayed value of the injected radioactivity. The effective dose was calculated from the target organ absorbed doses, to express radiation burden in the whole body as a summation of several different doses of radiation to differentially susceptible organs. This calculation was performed with specific tissue weighting factors, according to the International Commission on Radiological Protection (ICRP) 60 recommendations (ICRP publication 60, 1991).

4.8.2 Reproducibility evaluations of simplified voxel-based ^{11}C-PIB uptake analysis (study II)

Test-retest reproducibility was evaluated for the Automated ROI analysis method as well as the manual ROI method for comparison, in terms of absolute variability (VAR) and intra-class correlation coefficients (ICC). These values were calculated separately for the AD group and the control group because the reproducibility might vary between groups due to within-group differences in the extent of ^{11}C-PIB uptake and also in regional brain volumes. Variation in both of these measures was predicted to be greater in an AD patient group compared with a healthy control group.

The VAR value formula was the following:

$$VAR = \frac{|scan2 - scan1|}{0.5(scan1 + scan2)} x100\%$$

where scan1 and scan2 refer to parameter estimates of interest (in this case, region-to-cerebellum ratios of the corresponding test and retest scans) so that VAR reflects the difference of the two measurements as a percentage of the mean of the two measurements.

The ICC values were obtained with the equation:

$$ICC = \frac{BSMS - WSMS}{BSMS + (n-1)WSMS}$$

where BSMS is the between-subject mean square and WSMS is the within-subject mean square. *N* is the number of repeated observations, thus in this case, *n*=2. The ICC can receive a value between -1 and 1. Values close to 1 indicate that most variance is due to between-subject rather than within-subject variation. In contrast, values below zero imply greater within-subject than between-subject variation (i.e. poor reproducibility).

To evaluate reproducibility at the voxel level, the above equations were implied on each voxel of the spatially normalized and smoothed parametric ^{11}C-PIB PET images. This procedure produced 3D-maps of the ICC and VAR values' distributions in the MNI space. To obtain average voxel-level reproducibility values for given brain regions, the

same ROIs were applied for these ICC and VAR maps as were used in the automated ROI analysis.

To evaluate the test-retest reproducibility of the automated ROI analysis method, ROI-wise VAR and ICC values were calculated from the parametric, non-smoothed images. For comparison, the region-to-cerebellum ratios that were obtained with the manual ROI analysis were also subjected to VAR and ICC calculations.

4.8.3 Statistical analyses of reproducibility and power calculations (study II)

The comparisons of VAR and ICC values obtained with different image analysis methods were performed with SPSS for Windows (release 13.0.1, SPSS, Chicago, ILL). Student's *t*-test was employed to test for differences. The AD and control groups were evaluated separately. P-values < 0.05 were considered significant.

The rationale for the power calculations was to estimate sample sizes required to reveal significant differences between two study groups (*e.g.* AD subjects with an active intervention and AD subjects receiving no intervention) with two ^{11}C-PIB uptake measurements (*e.g.* baseline and follow-up). The power calculations were performed with nQuery Advisor software, version 7.0. The lateral frontal cortex was used as an example brain region, and it was assumed, for the calculations, that the average baseline region-to-cerebellum ratio (in two parallel AD patient groups) would be 1.505 and that its standard deviation would be 0.08 units. The sample size calculations were performed for 80 % and 90 % power so that the sample size could be estimated as a function of the difference between the two parallel groups in the change from baseline to follow-up (or baseline to post-intervention). For example, this simulates a situation where a 15 % change (or 0.226 units) is seen in one group, while the other group shows no change. The analysis was made using a *t*-distribution and a two-sided significance level of $p < 0.05$.

4.8.4 Comparisons of neuropsychological measures and MRI scores (studies III and IV)

For the neuropsychological measures of study **III**, within-group changes over time were evaluated with Wilcoxon's signed rank test and between-group differences were tested with the Mann-Whitney U-test for the difference variables (baseline score - follow-up score). The same testing was applied to the educational levels and cross-sectional neuropsychological test results in studies **III** and **IV**. The Mann-Whitney U-test was also applied in comparing the MRI scores (representing brain volumetric change) of the two study groups as well as those of the two AD subgroups (progressors and nonprogressors) of study **III**. In study **III**, SPSS software version 15.0 was employed. For study **IV**, these analyses were performed with SPSS v. 16.0 for Mac (Release 16.0.1).

4.8.5 Comparisons of ^{11}C-PIB uptake in repeated measurements (study III)

In study **III**, ^{11}C-PIB region-to-cerebellum ratios were analyzed first with repeated measurements ANOVA (rmANOVA), where time and region were used as repeated factors and group as the between-subjects factor. This analysis was performed to test whether possible between-groups differences in the changes in regional ^{11}C-PIB uptake ratios varied depending on the region of the brain (group*time*region interaction). This testing was performed with SAS version 9.2 software. Next, and to obtain the primary results of interest, ^{11}C-PIB uptake ratio results of each brain region were separately evaluated with rmANOVA with time as the repeated factor using SPSS version 15.0. This rmANOVA was done to estimate the interactions between time and group, *i.e.* to see whether there were between-groups or between-subgroups differences in the regional uptake changes over time. Within-group changes over time were analyzed with paired samples *t*-tests.

4.8.6 Comparisons of cross-sectional ^{11}C-PIB uptake (study IV)

Two-tailed two-sample *t*-tests were employed in study **IV** to test the primary issue of interest, *i.e.* whether or not the MZ-preserved subgroup differed from the controls. Also, as a comparison, the DZ-preserved subjects were also compared with the controls in the same manner. Other aims of study **IV** were to confirm that the cognitively impaired subjects (MZ and DZ combined as well as separately) showed greater ^{11}C-PIB uptake than the unrelated controls. Furthermore, it was of interest to see whether the MZ-preserved and the DZ-preserved co-twins differed from their corresponding cognitively impaired co-twins. These comparisons required taking into account the correlations between the corresponding co-twins, for which end a linear mixed model with an unstructured covariance structure was employed for these secondary analyses. The ages of the subjects were also included as a covariate in the linear mixed model, and the p-values were finally (Bonferroni) corrected for multiple comparisons. The linear mixed model also gave the results on the comparison of the MZ-preserved subgroup with the DZ-preserved subgroup.

The *t*-testing of study **IV** was performed with the SPSS v. 16.0 for Mac software (Release 16.0.1) and the linear mixed model analyses were conducted with SAS 9.2 for Windows.

4.8.7 Correlations

In study **III**, the correlations between ^{11}C-PIB uptake and MRI scores were evaluated with Spearman's rank-order correlation analysis, with SPSS version 15.0. The correlation coefficients were analysed separately for the AD and healthy control groups.

5. RESULTS

5.1 RADIATION DOSIMETRY OF ^{11}C-PIB PET (study I): ABSORBED DOSE ESTIMATES, CRITICAL ORGANS AND EFFECTIVE DOSE

The residence times in source regions were estimated as areas under the time-activity curves. Time-activity curves of organs of specific interest are presented in **Figure 17**. The urine time-activity values are shown in **Figure 18**. The residence times in the source regions are given in **Table 7**. The target organ absorbed dose estimates (calculated from the source organ residence times by the MIRDOSE software) are shown in **Table 8**. The effective dose, also given in **Table 8**, was calculated as the organ-weighted sum of target-organ absorbed doses, as described above (in the section *4.8.1 Dosimetry calculations*).

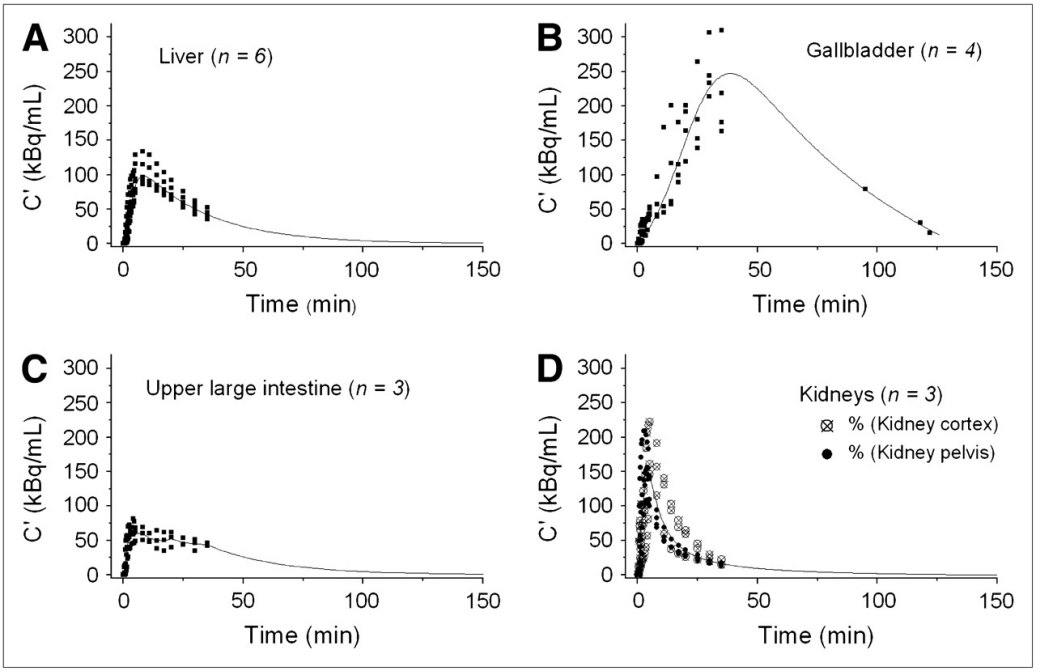

Figure 17. Time activity curves of the A) liver, B) gallbladder, C) upper large intestine and D) kidneys. The dots are individual measurements and the curves represent 3-exponential fitting to those measurements, except in C, where the curve is the average of measurements until 40 min and after that represents physical decay of ^{11}C. This image has been published in Original Publication **I**.

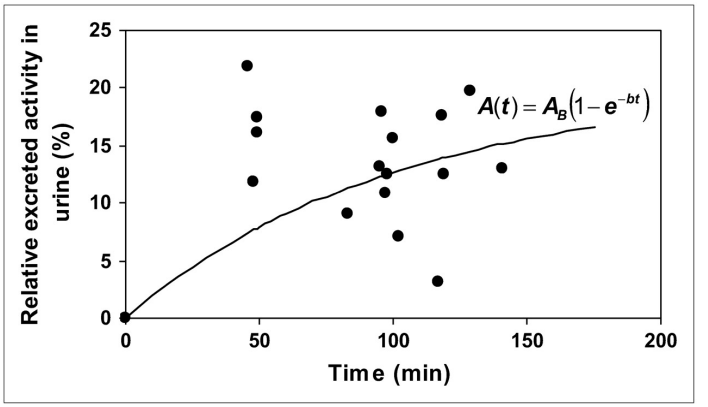

Figure 18. Excretion of ^{11}C-PIB into urine expressed as percentage of excreted radioactivity of the injected dose. The dots are individual measurements, and the curve is the fitted exponential in-growth formula. This image has been previously published in Original Publication **I**.

Table 7. The residence times of ^{11}C-PIB in source regions and numbers of subjects contributing to each source. This table was modified from a table that was published in Original Publication **I**.

Source organ	Residence time (h)	No. of subjects
Brain	0.012	5
Gallbladder content	0.016	7*
Stomach	0.002	3
Upper large intestine	0.011	3
Heart content	0.002	7
Heart wall	0.004	3
Kidneys	0.012	4
Liver	0.107	6
Lungs	0.008	3
Muscle	0.066	3
Cortical bone	0.021	6
Spleen	0.002	5
Urinary bladder content	0.022	16
Remainder of body	0.206	---

*Four subjects were imaged at 0-40 min to represent the dynamic phase and 3 subjects were scanned at steady state at approximately 100 min after tracer injection.

Table 8. The radiation doses for each target organ as well as the effective dose. This table was modified from data published in Original Publication **I**.

Radiation Doses in a 70 kg Reference Man	
Target organ	**μGy/Mbq**
Adrenals	3.97
Brain	3.10
Breasts	2.33
Gallbladder wall	41.5
Lower large intestine wall	3.00
Small intestine	3.62
Stomach	3.46
Upper large intestine wall	9.00
Heart wall	4.76
Kidneys	12.6
Liver	19.0
Lungs	3.39
Muscle	1.83
Ovaries	3.24
Pancreas	4.06
Red marrow	2.84
Bone surface	2.71
Skin	2.10
Spleen	4.31
Testes	2.44
Thymus	2.54
Thyroid	2.35
Urinary bladder wall	16.6
Uterus	3.52
Total body	2.83
Effective dose	4.74 μSv/MBq*

* Effective dose is the organ-weighted sum of target organ absorbed doses according to ICRP 60.

In summary, the greatest accumulation of ^{11}C-PIB was observed in the gallbladder, liver and urinary bladder (see **Figure 19**, whole body). The renal system was estimated to excrete about 20 % of the injected radioactivity (see *4.4 Arterial and urine sampling and analyses* for calculations). The organs with the greatest equivalent doses (absorbed doses weighted by radiation type, *i.e.* ß$^{+}$-radiation in this case) were the gallbladder wall, liver, urinary bladder wall, kidneys, and upper large intestine wall. The critical organ (the organ most vulnerable to irradiation) was the gallbladder wall, which received

0.041 mGy/MBq. The average effective radiation dose in a 70 kg adult male was 4.74 μSv/MBq. This means that *e.g.* a PET scan with a 500 MBq radioactive dose of ^{11}C-PIB injected intravenously would result in a radiation dose of 2.37 mSv.

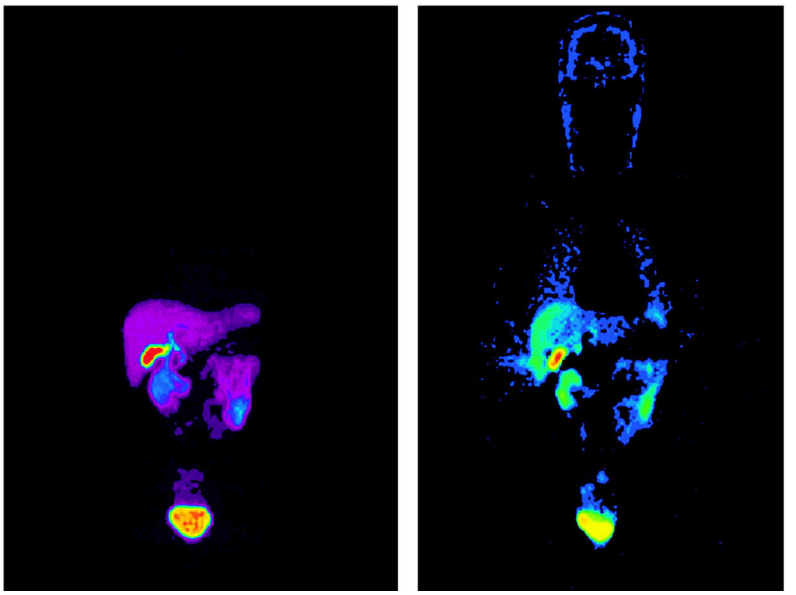

Figure 19. Whole body images of two subjects. The subject on the left was scanned from the head to the thighs and the subject on the right in the opposite direction. The radioactivity in the images is attributable to the biodistribution of the tracer during the course of its metabolism and elimination; no binding to amyloid deposits is seen. The images have different brightness levels and have been published previously in Original Publication **I.**

5.2 TEST-RETEST REPRODUCIBILITY OF SIMPLIFIED ^{11}C-PIB UPTAKE ANALYSIS METHODS

Tables 1 (for AD patients) and **2** (for healthy control subjects) of the Original Publication **II** display the regional ^{11}C-PIB uptake ratios and reproducibility measures of the analysis methods evaluated in study **II**. To summarize, excellent reproducibility was obtained regardless of the analysis method in both patients as well as healthy controls, and no significant differences were observed between the methods. The voxel-level reproducibility can be applied to SPM analyses (for evaluating between-groups differences with no spatial constraints) and the simplified Automated ROI method was validated, in terms of reproducibility, for the evaluation of regional quantitative ^{11}C-PIB uptake data from short (30 min) image acquisition protocols.

With the different brain regions of interest put together, average (range) region-level absolute variability (VAR) values of the Automated ROI analysis of the 30 min ^{11}C-PIB PET images were 4.3 % (3.3 – 5.1 %) for the AD group and 3.5 % (0.9 – 5.5 %) for the

controls. The average region-level VAR values of the manual ROI analysis method of the same images were 6.6 % (5.5 – 9.9 %) and 3.2 % (1.9 – 4.8 %) for the AD group and control group, respectively.

The voxel-level average VAR values of the parametric image analysis methods evaluated in study **II** were 5.3 % (4.2 – 6.4 %) for the AD patients and 5.3 % (4.2 – 6.4 %) for the control subjects.

Thus, in the AD group, the reproducibility of the Automated ROI method (average VAR 4.3 %) appeared to be slightly better than that of the manual method (average VAR 6.6 %), and the voxel level reproducibility of the parametric images was intermediate (average VAR 5.3 %). In the control group, manual ROI analysis (average VAR 3.2 %) was seemingly the better ROI method in terms of reproducibility, and the reproducibility at the voxel level was somewhat poorer than at the region level (average VAR 5.3 %). However, the Automated ROI method attained an average VAR of 3.5 %, so that the manual and automated methods were really comparable. Furthermore, the differences between the methods in the AD group as well as in the control group were altogether very small and as stated, statistically non-significant.

The ICC values were also quite homogenous across the different brain regions and analysis types. In the AD group, the average ICC of the Automated ROI analysis results was 0.92, ranging from 0.85 to 0.97. The control group received, across the different brain regions under evaluation, an average ICC value of 0.81 for the Automated ROI analysis method, with a range from 0.56 to 0.99. The voxel-level ICCs were of similar magnitude. Possible explanations for the lower values in the control group will be discussed later in this thesis.

5.3 APPLICABILITY FOR FOLLOW-UP STUDIES AND RELATIONSHIP OF ^{11}C-PIB UPTAKE AND BRAIN ATROPHY IN A TWO-YEAR LONGITUDINAL STUDY (studies II and III)

5.3.1 Power calculation results (study II)

The power calculation graph (**Figure 20**) displays the number of needed subjects per group as a function of the anticipated between-groups difference in the longitudinal within-group change in ^{11}C-PIB uptake. The curves are for 90 % and 80 % power. For example, the calculations indicated that when a 15 % change in ^{11}C-PIB uptake is predicted in one group and a 0 % change in the other, 90 % power could be achieved with sample sizes as small as five subjects per study group.

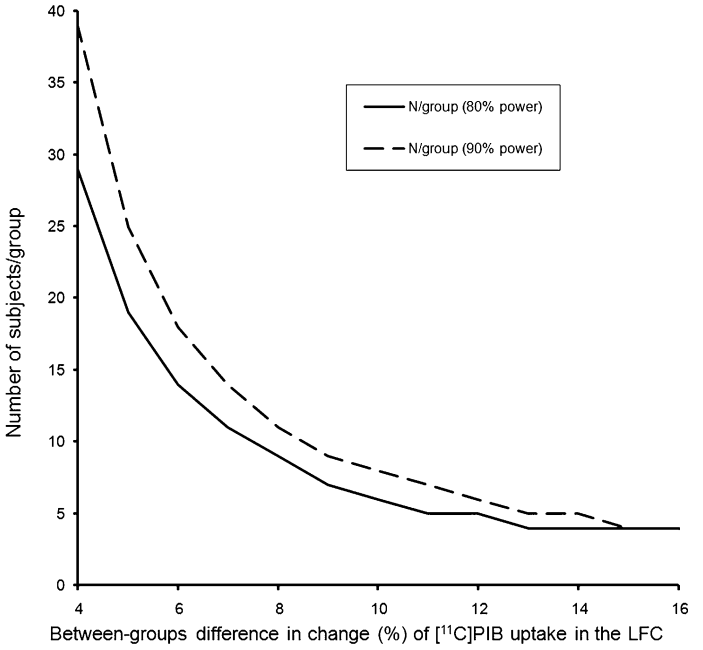

Figure 20. Power calculation graph to visualize estimated group sizes needed to demonstrate statistically significant differences in changes of tracer uptake over time. The graph has been previously published in Original Publication **II**.

5.3.2 Automated ROI analysis results: longitudinal changes in ^{11}C-PIB uptake and their between-groups comparisons (study III)

The ^{11}C-PIB uptake ratios at baseline and at follow-up and their changes are presented in **Table 3** of Original Publication **III**. When compared with baseline results, the ^{11}C-PIB uptake ratio of the medial frontal cortex had increased by 4.3 % during the follow-up in the AD group. However, medial frontal cortex ^{11}C-PIB uptake was increased also in the control group (by 3.3 %). Both of these changes were statistically significant on their own, but no difference was observed between the two groups in terms of the magnitude of this change. Furthermore, this average change falls within the range of test-retest variability that was demonstrated in study **II**. Overall, the rmANOVA revealed no differences between the AD group and the control group in longitudinal ^{11}C-PIB uptake changes in any of the examined brain regions.

When examined individually, most AD patients showed modest increases in their ^{11}C-PIB uptake ratios over time, but there were some AD subjects whose ^{11}C-PIB uptake ratios actually declined. In general, the average changes were thus within the test-retest variability range evaluated in study **II**. The direction of the change in all individual patients was similar in the medial and lateral frontal cortices as well as in the posterior cingulate. As examples, the individual ^{11}C-PIB uptake ratios and their changes in the posterior cingulate (a) and lateral frontal cortex (b) are illustrated in **Figures 21a and 21b**.

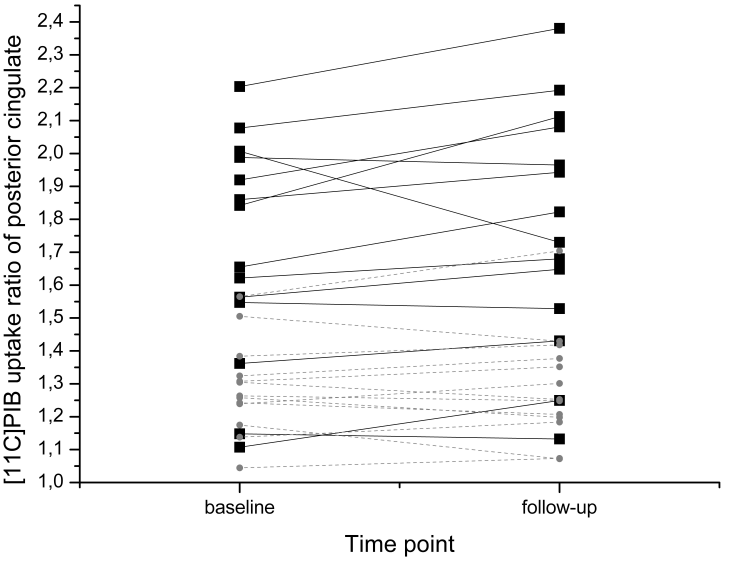

Figure 21a. ^{11}C-PIB region-to-cerebellum ratios of the posterior cingulate of every individual subject of study **III**. The black lines indicate Alzheimer's disease patients and the grey dashed lines represent healthy control subjects. A modified version of this graph has been previously published in Original Publication **III**.

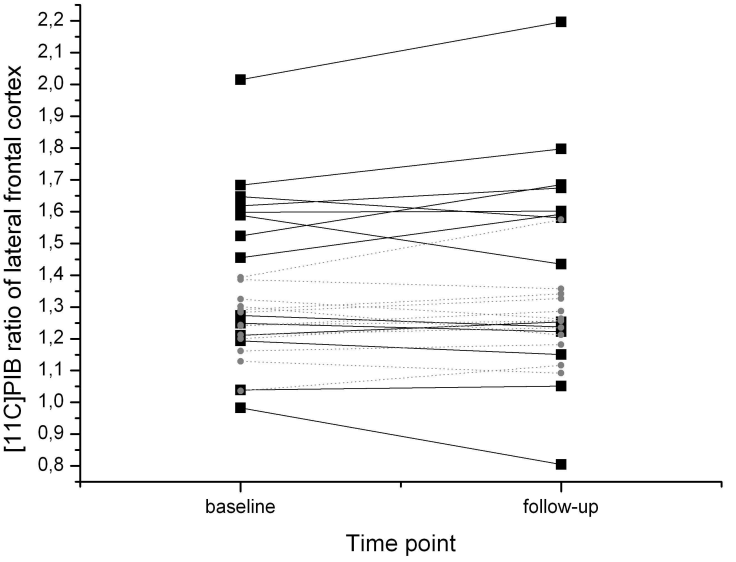

Figure 21b.^{11}C-PIB region-to-cerebellum ratios of the lateral frontal cortex of every individual subject of study **III**. The black lines indicate Alzheimer's disease patients and the grey dashed lines represent healthy control subjects.

5.3.3 MRI analysis results: longitudinal volumetric brain changes (study III)

The AD group displayed greater volumetric brain changes during the follow-up than the controls. Significant between-groups differences were observed in both hippocampi ($p = 0.02$ and $p = 0.01$), the right precuneus ($p = 0.03$) and left temporal cortex ($p = 0.01$). **Figure 22** illustrates the significant differences in changes between the AD group and the control group. No differences in volumetric brain changes were seen between the AD-progressor and AD-nonprogressor subgroups.

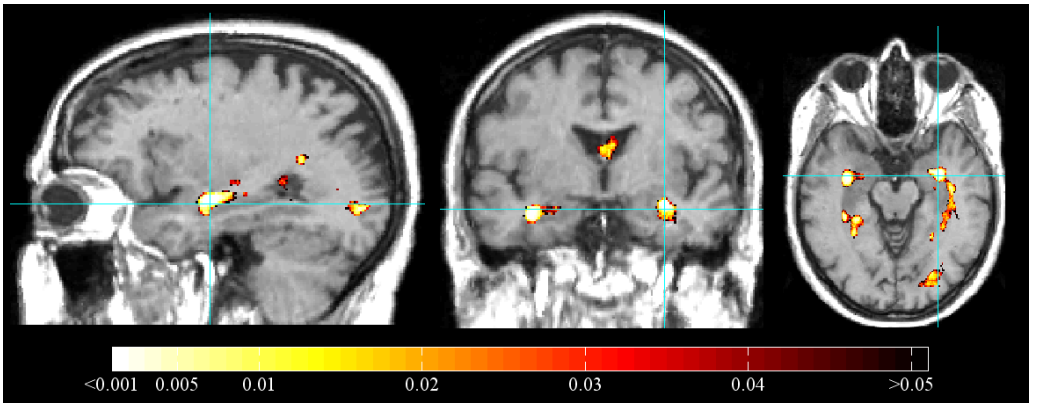

Figure 22. Graphical display of p-values from the statistical analysis of the group differences between Alzheimer's disease patients and control subjects in local longitudinal volume changes. The locations of statistically significant local volume changes and only continuous volumes larger than 500 mm^3 are shown in colour. This image has been published previously in Original Publication **III**.

5.3.4 ^{11}C-PIB uptake and volumetric brain change correlations (study III)

In the AD group of study **III** as a whole, a trend towards an association between baseline neocortical ^{11}C-PIB uptake (composite neocortical score) and subsequent volumetric brain change over time (MRI score) was observed ($r = 0.50$, $p = 0.072$). In the control group, this association was quite strong ($r = 0.73$, $p = 0.005$) (see **Figure 23**).

5.4 ^{11}C-PIB UPTAKE IN MONOZYGOTIC AND DIZYGOTIC TWINS DISCORDANT FOR COGNITIVE IMPAIRMENT (study IV)

The cognitively preserved MZ co-twins of the cognitively impaired subjects, as a group, had greater neocortical ^{11}C-PIB uptake than the unrelated controls, as assessed both with SPM and with quantitative ROI analyses. The DZ-preserved subgroup, in contrast, did not differ from the controls in their ^{11}C-PIB uptake in any of the examined brain regions, assessed either with SPM or ROI analysis.

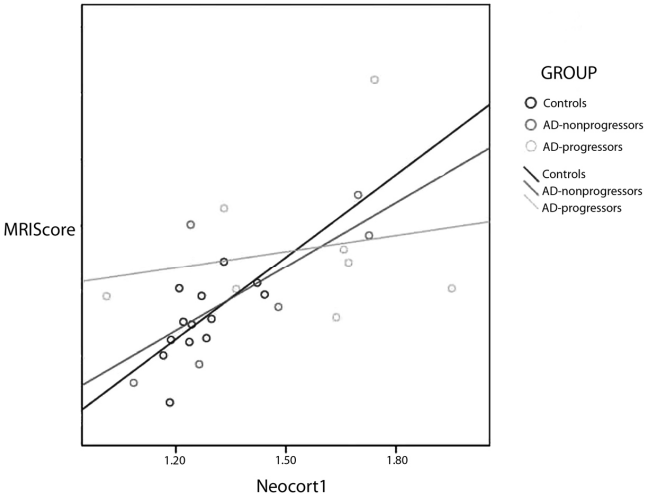

Figure 23. Regression lines showing the correlations between baseline neocortical composite scores (Neocort1) (representing ^{11}C-PIB uptake in the medial and lateral frontal cortices, the temporal and parietal cortices, and the posterior cingulate) and the MRI scores (representing global volumetric brain change over the two-year follow-up period). The regression is shown separately for the AD-nonprogressor and AD-progressor subgroups and for the controls.

The statistical parametric maps of between-group differences are shown in **Figure 24.**

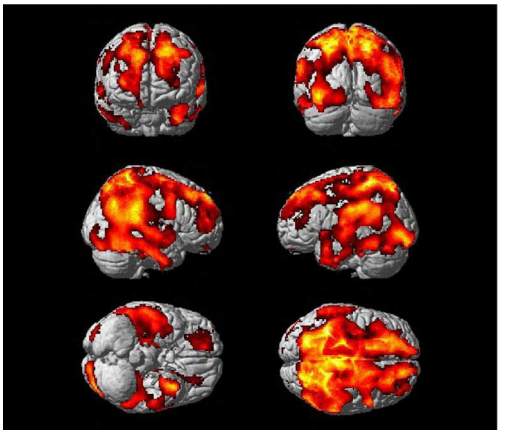

Figure 24a

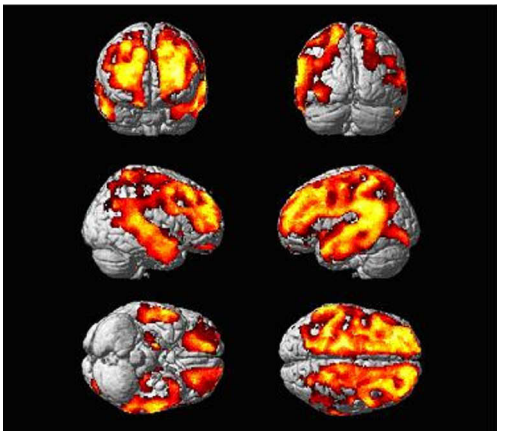

Figure 24b

Figures 24a and 24b. Statistical parametric (SPM) maps of between-groups ^{11}C-PIB uptake differences in study **IV**. **Figure 24a** represents the differences between the MZ-preserved group and the control group, whereas **Figure 24b** shows the differences between all of the cognitively impaired subjects (MZ- and DZ-impaired combined) and the controls. The map for the DZ-preserved / controls –contrast is not presented here because it illustrates no significant findings.

The ROI analysis demonstrated that the greatest regional differences in ^{11}C-PIB uptake between the MZ-preserved and the control group were in the posterior cingulate (21 % increase in the MZ-preserved) and in the parietal cortex (21 % increase). These were followed by the differences in the temporal cortex (17 % increase) and the putamen (15 % increase). In contrast, the ^{11}C-PIB uptake ratios of the DZ-preserved group varied between 96 % and 103 % of the control mean, *i.e.* no significant differences from the control group were observed. See **Figure 25** for the ^{11}C-PIB uptake neocortical scores (average of the region-to-cerebellum ratios of the medial frontal cortex, lateral frontal cortex, temporal cortex, parietal cortex and posterior cingulate) of all individual subjects of study **IV** and **Table 9** for the mean regional uptake ratios of the different subgroups of study **IV**. The impaired-all group showed 25 % to 28 % increases compared to the control means in the cortical regions where differences were anticipated, and a 22 % increase in the putamen. No significant differences were observed between the cognitively impaired and the unrelated controls in the occipital cortex or in the white matter.

The preserved MZ co-twins of the MZ-impaired showed ^{11}C-PIB uptake ratios which were *not* different (p>0.17 or greater) from those of the impaired (corresponding) co-twins in the temporal and parietal cortices and the posterior cingulate, as well as the grey and white matter reference regions, the occipital cortex and white matter. The DZ-preserved differed from their corresponding cognitively impaired co-twins in the same way as did the controls, although the difference in the ^{11}C-PIB uptake of the putamen did not reach statistical significance.

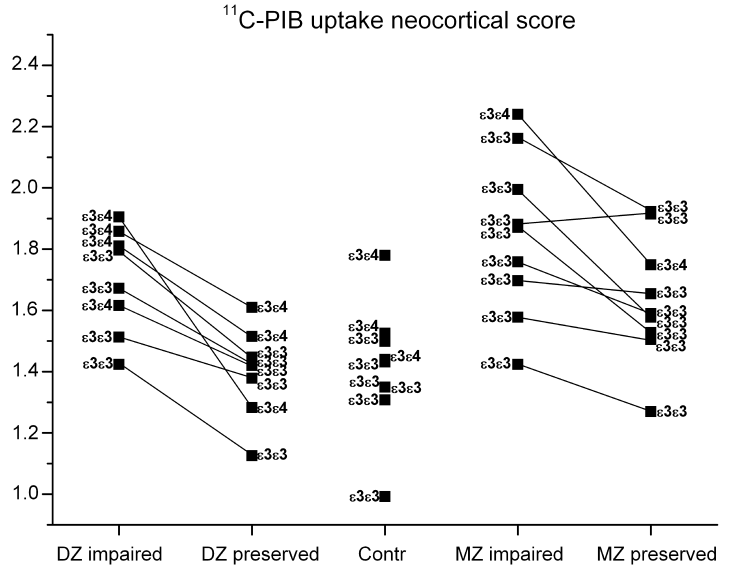

Figure 25. Graphical display of neocortical ^{11}C-PIB uptake scores of the subjects of study **IV**. The ApoE alleles of each subject are given and the corresponding co-twins' data points are connected with lines.

Table 9. ^{11}C-PIB region-to-cerebellum ratios (mean;SD) of dizygotic twin subjects (cognitively impaired and preserved), monozygotic twin subjects (cognitively impaired and preserved) as well as healthy controls and all subjects with impaired cognition.

	DZ-impaired (n=8)	**DZ-preserved (n=8)**	**MZ-impaired (n=9)**	**MZ-preserved (n=9)**	**Controls (n=9)**	**Impaired-all (n=17)**
Medial frontal cortex	1.66;0.28	1.35;0.16	1.82;0.36	1.56;0.20	1.38;0.26	1.75;0.33
Lateral frontal cortex	1.73;0.18	1.39;0.15	1.89;0.32	1.57;0.16	1.44;0.25	1.82;0.27 *
Temporal cortex	1.61;0.18	1.36;0.16	1.69;0.20	1.55;0.20 * °	1.32;0.16	1.65;0.19 *
Parietal cortex	1.71;0.17	1.43;0.17	1.82;0.17	1.70;0.22 * °	1.41;0.21	1.77;0.17 *
Posterior cingulate	1.78;0.23	1.47;0.21	2.00;0.34	1.80;0.31 * °	1.49;0.23	1.90;0.31 *
Occipital cortex	1.45;0.12	1.39;0.22	1.48;0.11	1.43;0.09	1.35;0.14	1.46;0.11
Putamen	1.65;0.08	1.45;0.14	1.83;0.21	1.65;0.16 *	1.43;0.14	1.74;0.18
White matter	1.89;0.13	1.59;0.34	1.83;0.22	1.66;0.16	1.66;0.23	1.86;0.18
Composite neocortical score	1.70;0.17	1.40;0.15	1.84;0.26	1.63;0.21 *	1.41;0.21	1.78;0.23 *

* = Greater ^{11}C-PIB uptake vs. controls ($p < 0.05$). Not shown for DZ-impaired and MZ-impaired because these subgroups were combined to form the impaired-all group.
° = Similar ^{11}C-PIB uptake with corresponding cognitively impaired co-twin ($p > 0.17$ or greater).

6. DISCUSSION

6.1 THE APPLICABILITY OF ^{11}C-PIB PET

6.1.1 Radiation safety

The validation procedure of ^{11}C-PIB PET for human studies is considerably longer and more complex than can be reviewed in the scope of this thesis. In short, ^{11}C-PIB is a derivative of the histopathological amyloid dye thioflavin T. ^{11}C-PIB, or ^{11}C-6-OH-BTA-1, was selected for further research from several other benzothiazole candidates (Mathis et al. 2002, Mathis et al. 2003). It seemed to readily cross the blood-brain barrier and to bind rapidly and selectively to Aβ with high affinity in nanomolar concentrations (Klunk et al. 2001, Bacskai et al. 2003). These results, along with toxicity assessments, encouraged researchers to perform the first clinical study with ^{11}C-PIB, which in turn demonstrated that ^{11}C-PIB PET could indeed differentiate AD patients from cognitively healthy subjects (Klunk et al. 2004).

However, to validate the clinical use of ^{11}C-PIB and its applicability for repeated scans, the issue of radiation safety also had to be addressed. Before the human dosimetry study (study **I**) presented in this thesis, only one preclinical report where radiation safety had been investigated in baboons had been published (Parsey et al. 2005). Data from two baboons had enabled estimation of human radiation doses, and the critical organ seemed to be the gallbladder. Indeed, the results of study **I** of this thesis are in line with that prediction: the residence time of the gallbladder radioactivity was 0.016 h in study **I** and 0.018 h as estimated from baboon data (Parsey et al. 2005). In other aspects too, there was quite a high degree of consistency between the results of the preclinical study and those of study **I**: the ligand was eliminated mainly via the hepatobiliary and renal systems in both studies, and the effective doses were rather similar: 6.5 μSv/MBq in the preclinical study and 4.7 μSv/MBq in our human study. However, preclinical research cannot entirely replace studies with humans, and this was demonstrated also in these two studies: some possibly important differences were observed. For instance, the increased ^{11}C-PIB uptake in baboon lungs (Parsey et al. 2005) was absent in humans, and the ^{11}C-PIB residence time estimate in the kidneys was 2.3-fold in baboons compared with humans. Conversely, the liver residence time was 2.7 times longer in humans than in baboons. Although the fraction of radioactivity excreted through the renal system was similar between studies (15 % *vs*. 20 %), the urinary bladder residence times differed (0.041 h in the preclinical study and 0.022 h in study **I**). This difference may be accounted for by the different analysis methods in the two studies. The other discrepancies could, however, reflect real differences between the species in physiology, and they underline the need for dosimetry studies to be performed also directly in humans. Another human dosimetry study on ^{11}C-PIB (and the novel amyloid tracer ^{18}F-BAY94-9172) has recently been

published (O'Keefe et al. 2009). In this study, the highest absorbed doses were received by the gallbladder wall, urinary bladder wall, liver, and kidneys – the greatest equivalent doses were thus delivered to the same organs in both human studies. The gallbladder wall's equivalent dose of 44.8 μGy/MBq in the more recent study (O'Keefe et al. 2009) is very close to the value of 41.5 μGy/MBq in study **I**. The estimated effective doses (ED), 5.29 μSv/MBq and 4.74 μSv/MBq, respectively, are also comparable. It is thus justifiable to assume that a human ^{11}C-PIB PET scan would result in a radiation dose of about 2.4 mSv (4.7 μSv/MBq x 500 MBq), and no more than 3.7 mSv (ED 5.3 μSv/MBq x 700 MBq). Both ED estimates are substantially smaller than the estimated maximum radiation burden caused by ^{11}C-radiotracers in general, 11.0 μSv/MBq (Addendum 6 to ICRP Publication 53 2002). Although 500 MBq seems to be a sufficient dose to visualize Aβ plaques, even the greater radiation dose estimate of 3.7 mSv with 700 MBq may be considered as acceptable. For comparison, the published dose of 300 MBq of ^{18}F-BAY94-9172 is expected to yield a radiation burden of 4.4 mSv (O'Keefe et al. 2009). Furthermore, *e.g.* a computed X-ray tomography scan of the body results in a radiation dose of about 10 mSv.

6.1.2 Reproducibility

Some aspects of tracer uptake analysis were already discussed in this thesis in the *Review of the literature* section. Though these addressed the uptake measurements, they did not go into the details of the important issue of reference input. SPM and automated ROI analyses are applied on parametric ^{11}C-PIB PET images, *i.e.* spatially normalized images where the radioactivity concentration in each voxel has already been converted to another more representative and comparable variable. This conversion or normalization is imperative for eliminating the effect of non-specific tracer signal, which can vary greatly depending on factors with great inter-individual variability, such as blood flow. The Graphical Logan analysis method that uses plasma input as its reference has yielded stable ROI results and provided feasible parametric images also with ^{11}C-PIB (Yaqub et al. 2008). ROIs delineated on these kinds of parametric images thus result in uptake values that are comparable between different subjects. However, methods such as the plasma input Logan or the recently evaluated masked-volume-wise PCA method without any modeling assumptions (Razifar et al. 2009) require arterial blood sampling from the subject during PET scanning and the acquisition of imaging data right from the injection until the end of the scan. More simplified and non-invasive methods would be advantageous and the reduction of scanning time would be beneficial both for possibly agitated or otherwise incapacitated subjects as well as for cost-effective PET scanner use.

Image-driven analysis methods are a useful approach to measure specific PET tracer uptake, usually this means the utilization of tracer uptake measurements of a reference region in the same individual. The reference region should be such that it optimally contains *only* non-specifically bound tracer, so that by dividing the radioactivity concentration in

the target region of the PET image with the reference region radioactivity concentration, only specific radioactivity is represented. The cerebellum has proven to contain only small quantities of neuritic Aβ plaques in *post mortem* studies [*e.g.* (Joachim et al. 1989)] and has therefore been chosen as the appropriate ^{11}C-PIB uptake reference region. Late-scan region-to-cerebellum ratios of ^{11}C-PIB uptake have subsequently proven to effectively differentiate AD patients from controls and the test-retest reproducibility has appeared to be good (Lopresti et al. 2005). In some studies, the region-to-cerebellum ratios are expressed as SUV ratios or SUVRs. Region-to-cerebellum ratios or SUVRs have been calculated for data from 40 until 60 minutes after ^{11}C-PIB injection or from 40 to 90 minutes, or from 60 until 90 min post-injection [*e.g.* Klunk et al 2004, Lopresti et al 2005, Kemppainen et al 2006)]. It has so far been customary for ^{11}C-PIB PET scans to last 90 min, but the validation of these late-scan region-to-reference region uptake measurements could in the future result in shorter scanning times with no blood sampling, increasing subject comfort and cost-effectiveness of PET scanner use. In short, obtaining the data at late time points (resulting in higher target-to-cerebellum ratios) but using short scanning sessions, *i.e.* 60 to 90 min after injection (most probably resulting in less movement of the subject and better image quality), could be advantageous. This was one of the rationales for conducting study **II** of this thesis: to validate the voxel-based simplified late-scan region-to-cerebellum ratio parametric image approach *per se*. Another aim was to validate automated ROI analysis in ^{11}C-PIB PET quantitation; this would be preferable to manual ROI analysis, which is laborious and susceptible to operator-induced errors and bias. Automated ROI analysis utilizes the above described parametric images so that all individual images are fitted into a common stereotactic space and a similar ROI set is applied to all of these spatially normalized images.

In the case of the simplified approach evaluated in study **II**, spatial normalization was achieved with the use of an ^{11}C-PIB-ligand-specific common template, although MRI-aided spatial normalization is another alternative. The pros and cons of both methods are under discussion. MRI-aided normalization could perhaps better "correct" the possible corrupting effects of gray matter atrophy in AD, and nonspecific tracer binding to the white matter might be better excluded. However, with a ligand-specific template, possible inaccuracies in between-modalities (PET-MRI) coregistration of the images can be avoided, and the method can be considered as being more efficient as MRI scans are not needed. Nonetheless, the accuracy of spatial normalization is crucial to the reliability of the tracer uptake results. As ligand-specific normalization is simple, it was suitable for the all-in-all simplified analysis process evaluated in study **II**.

Some other parametric image analysis methods could well be more accurate for ^{11}C-PIB uptake quantitation than the proposed late-scan region-to-cerebellum ratio approach. At least in theory, cerebellar Aβ plaques that could appear in very advanced AD might dilute the difference in ^{11}C-PIB uptake between patients and controls. Furthermore, in a follow-up setting, the appearance of cerebellar plaques could mask true increase in a target region ^{11}C-PIB uptake or could even result in decreases in target-to-cerebellum

ratios during follow-up. Other concerns with the cerebellum as a reference region include the possibility of cerebellar atrophy leading to misplacement of its ROI and its possible "contamination" with white matter signal. This issue should be taken into account especially when using automated ROI analysis, although previous studies suggest that cerebellar atrophy is relatively subtle during the course of AD [*e.g.* (Raji et al. 2009)]. The effect of cerebellar atrophy on ^{11}C-PIB region-to-cerebellum ratios during the progression of AD is thus probably minor, but the phenomenon should be studied further and in longitudinal settings.

A recent article reported a comparison of different ^{11}C-PIB reference tissue models and their reproducibility estimates. The test-retest variability of region-to-cerebellum ratios (5.2 % in controls and 7.9 % in patients) was actually greater than those obtained with other parametric methods (Yaquub et al. 2008). However, many of the advantages of the late-scan ratio that have been discussed here are otherwise indisputable. Furthermore, study **II** reported good reproducibility of the method both at the region and at the voxel level, and the reproducibilities were in fact comparable with those previously reported for simplified or multilinear reference tissue models (Yaquub et al. 2008).

Two previous studies had evaluated the reproducibility of manual ROI analysis of late-scan ^{11}C-PIB (40 to 60 and 40 to 90 min post-injection) region-to-cerebellum ratio images (Lopresti et al. 2005, Engler et al. 2006). The VAR values in cortical areas ranged from 3.2 % to 7.3 % in these studies. The manual ROI VAR values ranged from 1.9 % to 9.9 % in study **II**, depending on the subject group and brain region being evaluated. The results are thus comparable between studies. Furthermore and more importantly, the region-level reproducibility of automated ROI analysis was comparable with that of manual ROI analysis in study **II**. In addition, the small VAR values indicated that the voxel-level reproducibility of the parametric images is generally equal to that obtained by manual ROI analysis. It could seem confusing that as opposed to the VAR values, the ICC values were seemingly suboptimal (i.e. they were relatively low) in the control group, as demonstrated in the Results section of this thesis. However, it should be pointed out that this does not mean that within-subject variability would be greater in the controls, but rather that when there is very little if any specific tracer uptake, the between-subject variation also becomes very low, causing the ICC values to decline. These favourable reproducibility observations together with the other advantages of automated ROI analysis thus support the use of automated ROI analysis in favour of conventional manual ROI analysis for ^{11}C-PIB uptake quantitation.

For future clinical (in contrast to current scientific) ^{11}C-PIB PET imaging of patients, it is a noteworthy observation that the visual assessment of ^{11}C-PIB PET images, which was briefly introduced in the *Review of the literature (2.3.2 Findings in Alzheimer's disease)*, also seems reliable (Ng et al. 2007a, Suotunen et al 2010). Visual evaluation of ^{11}C-PIB PET images seems to demonstrate even better agreement between readers, than the clinically much more established visual assessment of ^{18}F-FDG images of AD patients and controls (Ng et al. 2007a).

Table 10. Mean;SD brain ^{11}C-PIB region-to-cerebellum ratios of studies **II-IV**, obtained through automated region-of-interest analysis.

	Study II		**Study III**		**Study IV**	
	AD patients (*n*=6)	Controls (*n*=4)	AD patients (*n*=14)	Controls (*n*=13)	Impaired-all (*n*=17)	Controls (*n*=9)
Medial frontal cortex	NA	NA	1.60;0.34 †	1.30;0.11	1.75;0.33	1.38;0.26
Lateral frontal cortex	1.69;0.25	1.33;0.09	1.43;0.29 †	1.25;0.10	1.82;0.27 †	1.44;0.25
Temporal cortex *	1.61;0.26	1.29;0.08	1.35;0.23	1.27;0.07	1.65;0.19 †	1.32;0.16
Posterior cingulate	1.89;0.23	1.34;0.08	1.71;0.34 †	1.29;0.14	1.90;0.31 †	1.49;0.23
Parietal cortex	1.68;0.23	1.25;0.05	1.35;0.25	1.24;0.10	1.77;0.17 †	1.41;0.21
Occipital cortex	1.39;0.16	1.39;0.09	1.22;0.15	1.31;0.10	1.46;0.11	1.35;0.14
Caudate	1.49;0.29	1.40;0.17	1.47;0.34 †	1.25;0.13	NA	NA
Putamen	1.60;0.20	1.40;0.12	1.53;0.25	1.41;0.13	1.74;0.18	1.43;0.14
White matter	1.78;0.24	1.84;0.21	1.66;0.20	1.89;0.27	1.86;0.18	1.66;0.23
Composite neocortical score	NA	NA	1.49;0.28 †	1.27;0.09	1.78;0.23 †	1.41;0.21

* = lateral temporal cortex in study **II**. NA = not analyzed. When repeated ^{11}C-PIB PET was performed (in studies **III** and **IV**), the values of the baseline scan / scan 1 are shown. † = greater ^{11}C-PIB uptake in the impaired / AD group compared with the control group. Statistics not calculated for Study **II**.

6.1.3 Specificity for AD

The studies of this thesis revealed similar differences in brain ^{11}C-PIB uptake between AD patients and healthy controls as have been reported previously. **Table 10** illustrates the brain ^{11}C-PIB region-to-cerebellum ratios of the cognitively impaired and preserved subjects examined in the studies of this thesis.

The segregation of AD from other dementias is another matter, and was discussed only briefly in the *Review of the literature*. The potential of ^{11}C-PIB PET in differentiating AD from other types of dementia was not within the scope of the experiments of this thesis. However, this is an interesting issue that will significantly affect the future of ^{11}C-PIB PET imaging, and therefore the research results gained thus far on this issue will be reviewed and discussed here in some detail.

In three studies (with relatively small sample sizes), 67-100 % of patients with frontotemporal lobe degeneration (FTLD) were "PIB-negative" (Rabinovici et al. 2007, Rowe et al. 2007, Engler et al. 2008). It has been speculated that the "PIB-positive" FTLD patients of these studies could actually have had AD or mixed pathology at autopsy (which of course still remains unknown). It is thus possible that so called frontal variants of AD could be distinguished from FTLD by means of ^{11}C-PIB PET (Rabinovici et al. 2007). Furthermore, subjects with semantic dementia, which is considered a subtype of FTLD, have shown no increases in ^{11}C-PIB uptake, although there is an overlap in the ^{18}F-FDG uptake patterns between semantic dementia and AD (Drzezga et al. 2008). In conclusion, in FTLD, brain Aβ imaging is generally negative (Rabinovici et al. 2007, Rowe et al. 2007, Drzezga et al. 2008, Engler et al. 2008).

^{11}C-PIB uptake has also been studied in Lewy body diseases; dementia with Lewy bodies (DLB) and Parkinson's disease dementia (PDD). The brain amyloid load appears to be significantly increased in about 44 – 80 % of subjects with DLB, whereas increased ^{11}C-PIB uptake is infrequent in PDD or in non-demented patients with Parkinson's disease (Rowe et al. 2007, Edison et al. 2008b, Gomperts et al. 2008, Johansson et al. 2008, Maetzler et al. 2008, Maetzler et al. 2009, Johansen et al. 2010). The *in vivo* results on DLB patients are generally in accordance with the findings of *post mortem* studies showing AD-type pathology (amyloid plaques and neurofibrillary tangles) in a substantial proportion of patients with DLB (Jellinger et al. 2003). In a recent neuropathological study on very elderly patients, the clinical symptoms of DLB even tended to associate better with severe neurofibrillary pathology than with extensive Lewy-related pathology (Oinas et al. 2009). The autopsy report of a DLB patient indicated that amyloid that was deposited as cerebral amyloid angiopathy, rather than Aβ plaques, had likely been the major source of this subject's ^{11}C-PIB PET signal (Bacskai et al. 2007). Whether this is the case more generally in DLB will need to be clarified with larger samples. To summarize and generalize the results obtained so far on Lewy body diseases, even taking into account the variability between studies, increased ^{11}C-PIB uptake is often seen in DLB but rarely in PDD. To some extent, the variability in the DLB studies is not surprising – the clinical diagnosis of DLB can be difficult with a marked overlap in symptoms with both PDD and AD. Furthermore, these disorders are known to often exhibit mixed pathologies at autopsy (McKeith et al. 2005). The sample sizes in ^{11}C-PIB PET studies with DLB patients have been small, so that even one patient with a misdiagnosis or, more likely, multiple pathologies, could have markedly influenced the results. In any case, because the differentiation of DLB from AD is likely to be somewhat suboptimal with ^{11}C-PIB PET, other supporting measurements such as dopamine transporter imaging, could be helpful and worth investigating (Rinne and Någren 2010).

Small groups of patients with more rare causes of dementia have also been studied with ^{11}C-PIB PET. In investigations of single subjects with either primary progressive aphasia (PPA) (Ng et al. 2007b) or posterior cortical atrophy (PCA) (Ng et al. 2007b, Tenovuo et al. 2008), distinctive focal ^{11}C-PIB uptake patterns, differing from that seen in AD, have been reported. In non-demented subjects with cerebral amyloid angiopathy (CAA), ^{11}C-PIB uptake seems to quantitatively fall between AD patients and controls, but with an occipital predominance (Johnson et al. 2007). Two patients with Creutzfeldt-Jakob disease did not show any marked cortical ^{11}C-PIB uptake (Villemagne et al. 2009).

Only very few studies have investigated ^{11}C-PIB uptake in familial disruptions of brain amyloid metabolism. In two familial forms of AD, caused by point mutations or a deletion in the presenilin-1 gene (Klunk et al. 2007, Koivunen et al. 2008b) and in a family with APP gene duplication (Remes et al. 2008), increased ^{11}C-PIB uptake was observed. However, in all of these groups with genetic alterations leading to overproduction of Aβ, the striatum has been the brain region of predominant ^{11}C-PIB uptake increase. These results imply that even different forms of the same disease entity, *i.e.* familial *versus*

sporadic AD, could in some cases be differentiated from one another by means of ^{11}C-PIB PET. Furthermore, the results of a study on PS1 mutation carrier families suggested that at least in these forms of AD, the disease process could be detected with ^{11}C-PIB PET at a presymptomatic stage (Klunk et al. 2007). The results of study **IV** of this thesis imply that the same could also apply to so called sporadic AD – cognitively preserved monozygotic co-twins of cognitively impaired subjects have an increased risk of developing AD compared to the general population, although they are not "predestined" to suffer this disease like the carriers of AD-associated PS1 mutations. Furthermore, although the present results should be interpreted with caution because of the small sample size and the *post hoc* analysis carried out with the study results, the strong positive association between baseline neocortical ^{11}C-PIB uptake and the subsequent brain volume loss in healthy controls of study **III** may also indicate that increased ^{11}C-PIB uptake could be an antecedent marker of future cognitive decline and AD.

To summarize, there seems to be variations in the ability of ^{11}C-PIB PET in differentiating AD from other current clinical dementia diagnoses. Also, as demonstrated previously by others (Klunk et al. 2004, Mintun et al. 2006, Pike et al. 2007, Rowe et al. 2007, Aizenstein et al. 2008, Jack et al. 2008) and in studies **III** and **IV** of this thesis, a relatively large proportion of cognitively intact subjects show increased brain ^{11}C-PIB uptake compared to the population mean. It has previously been suggested that ^{11}C-PIB could be more of a nonspecific marker of Aβ-related cerebral amyloidosis than a specific indicator of AD (Lockhart et al. 2007), which is indeed logical. Currently, the different dementia diagnoses are conducted largely on a clinical basis, according to the characteristic symptoms of the patient. One could postulate that the dementia diagnosis spectrum will change when new, more objective tools to investigate the specific pathophysiological processes behind these disorders become available. Furthermore, the possibility of mixed pathologies in any dementia patient should not be forgotten. For instance, a recent study on 1,110 consecutive autopsy cases of demented elderly subjects reported that while AD pathology was seen in 82.9%, only 42.9% presented with "pure" AD pathology; AD together with other pathologies was seen in 39.9% of the cases (Jellinger et al. 2010). This underlines a methodological issue concerning the studies of this thesis as well as many other studies; the diagnoses of the subjects were based on conventional clinical evaluation, which is not always correct. This also emphasizes the need of follow-up studies of patients who have had ^{11}C-PIB PET scans, to confirm their diagnoses and to identify possible concomitant pathologies. The identification of concomitant pathologies is also imperative in the search for future disease-modifying therapeutic strategies. ^{11}C-PIB PET, or amyloid imaging in general, could prove useful in identifying those patients (even in the presymptomatic phase), who would benefit from anti-amyloid therapies, regardless of their clinical diagnosis. The results of this thesis – on ^{11}C-PIB PET's applicability and early disease detection potential – may be interpreted as favouring future dementia research based on PET amyloid imaging.

6.1.4 ^{11}C-PIB relative to other amyloid imaging agents

Several other candidate agents for PET (and SPET) amyloid imaging have been investigated in addition to ^{11}C-PIB. They were introduced briefly in the *Review of the literature*. A full evaluation of the role of ^{11}C-PIB in future studies or early disease detection requires a review of some other amyloid agents which will be discussed here in further detail. The focus will be on derivatives of agents used in histopathology, *i.e.* Congo Red, thioflavine, and stilbene derivatives, as well as FDDNP (or [^{18}F] 1,1-dicyano-2-[6-(dimethylamino)-2-naphthalenyl]propene).

Starting with some of the agents familiar from histopathology, the most promising Congo Red derivatives have included the strongly fluorescent compounds X-34 (Styren et al. 2000, Link et al. 2001) and methoxy-X04 (Klunk et al. 2002). Currently the greatest challenge faced by these ligands has been their poor penetrance into brain tissue. In contrast, some of the studied stilbene derivatives, such as ^{11}C-SB-13 ([^{11}C] 4-N-methylamino-4'-hydroxy-stilbene) have proven to be functional, at least to some extent, also in PET studies with humans [*e.g.* (Verhoeff et al. 2004)]. ^{11}C-BF-227 ([^{11}C] 2-(2-(2-[2-dimethylaminothiazol-5-yl]ethenyl)-6-(2-[fluoro]ethoxy)benzoxa-zole), another stilbene derivative, has shown greater binding in AD patients than in controls and some promise in detecting which subjects with MCI will soon convert to AD (*e.g.* better than VBM-MRI) (Waragai et al. 2009), but with a somewhat different regional pattern compared to the other amyloid imaging compounds studied in humans (Kudo et al. 2007). Further studies will need to be conducted with this ligand to elucidate how and why its distribution differs from that of other relatively similar compounds. The recently introduced amyloid imaging agent, ^{18}F-BAY94-9172 ([^{18}F]4-(N-methylamino)-4'-(2-(2-(2-fluoroethoxy)ethoxy)ethoxy)-stilbene), is another promising stilbene derivative. Its advantages include the relatively long half-life of ^{18}F, which increases tracer availability (Rowe et al. 2008), because its use does not require an on-site cyclotron. (The background to the discovery of ^{18}F-labelled amyloid ligands for PET is discussed in detail earlier in this thesis, in the section *2.3.7 Possibilities and prerequisites of in vivo amyloid imaging tracers*).

One ^{18}F-labelled compound, ^{18}F-FDDNP (a derivative of a nonspecific surface dye), binds to amyloid plaques but also to neurofibrillary tangles (NFTs) and prion plaques (Agdeppa et al. 2001, Ye et al. 2005, Boxer et al. 2007). In AD, increased ^{18}F-FDDNP uptake has been seen in the hippocampus and in temporal, parietal and frontal cortices (Shoghi-Jadid et al. 2002, Small et al. 2006). In one study with ^{18}F-FDDNP, a significant difference was observed both between healthy subjects and MCI patients as well as between MCI patients and AD patients. ^{18}F-FDDNP uptake was also inversely correlated with ^{18}F-FDG uptake, and low levels of ^{18}F-FDDNP uptake were associated with better performance in certain memory tasks (Small et al. 2006). The clearance of ^{18}F-FDDNP from tissue, however, varies greatly between different brain regions, complicating the quantitation of tracer uptake. Differences between AD patients and controls in tracer uptake seem to be substantially smaller (10 %) (Small et al. 2006) than for example with ^{11}C-PIB (40-100 %) (see the *Review of the literature*, section *2.3.2 Findings in AD*). In

the future, the binding of ^{18}F-FDDNP to structures other than amyloid plaques may be found to be useful in certain applications. In other situations, conversely, selectivity for amyloid would be a prerequisite for a feasible imaging tracer.

Many new promising PET amyloid imaging tracer candidates emerge continuously (Johnson et al. 2009, Nelissen et al. 2009, Wey et al. 2009). Due to the better availability of SPET over PET, SPET amyloid tracer candidates such as ^{123}I-IMPY (Kung et al. 2004) also arouse increasing interest. The results of this thesis and other extensive research on ^{11}C-PIB's applicability could possibly aid in testing and validating these newer compounds. The required validation procedures were discussed in this thesis more elaborately in the *Review of the literature* in the section *2.3.7 Possibilities and prerequisites of in vivo amyloid imaging tracers*. One of the greatest motivators for identifying PET amyloid imaging tracers beyond ^{11}C-PIB is the better general availability of ^{18}F-labelled compounds. In fact, at the time of writing this thesis, encouraging results have been reported on an ^{18}F-labelled PIB-derivative, ^{18}F-flutemetamol (Nelissen et al. 2009).

6.2 ^{11}C-PIB PET IN DISEASE PROGRESSION AND TREATMENT

6.2.1 ^{11}C-PIB uptake in monitoring disease progression and its potential to show treatment effects

Study **III** of this thesis detected no longitudinal increase in ^{11}C-PIB uptake in AD patients at the group level. The follow-up period was relatively short in relation to the known, very long, disease process of AD. Another two-year follow-up study, with no control group comparison, showed similar results, *i.e.* no changes in ^{11}C-PIB uptake over time (Engler et al. 2006). No longer follow-ups have been published to date, which is understandable given the novelty of *in vivo* amyloid imaging methods. It cannot be said for certain on the basis of the so far published, relatively short, follow-ups, that no tracer uptake increase would occur over longer follow-up periods. However, at present there is a hypothesis that Aβ accumulation may be more rapid in the early phases of the AD process and reach a plateau shortly after or even before clinical AD symptoms begin to appear. The commonly hypothesized timetable of Aβ accumulation was presented in **Figure 4** of the *Review of the literature* and again here as **Figure 26.**

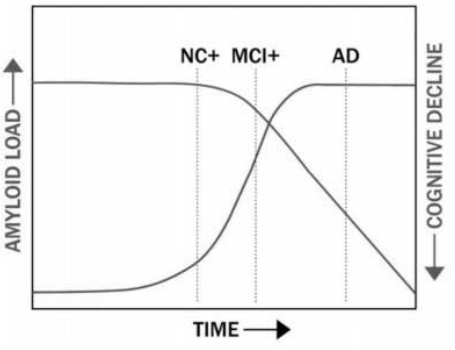

Figure 26. A proposition for the time course of amyloid deposition and cognitive decline in Alzheimer's disease, based *e.g.* on observations with ^{11}C-PIB PET, as suggested by Mathis et al. (Mathis et al. 2007).

Although the mean result of study **III** was no longitudinal change in ^{11}C-PIB uptake in AD over a two-year follow-up, tracer uptake did increase in some of the patients of study **III**. These changes were generally within the test-retest variability range of the method that was estimated in study **II**. On the other hand, the ^{11}C-PIB region-to-cerebellum ratios of some AD patients declined. It is still unclear whether the latter could be a biological phenomenon where Aβ plaques would actually begin to dissolve in more severe AD, or whether methodological limitations may account for this finding. For example, plaques could become inaccessible to the tracer diffusing from the bloodstream within the short time span of PET imaging. Obviously, no equilibrium is reached between the bloodstream and brain tissue during the scan time. In addition, it cannot be ruled out that the apparent decrease would be due to underestimation of tracer uptake caused by brain atrophy not being taken sufficiently into account. Different techniques for eliminating the possible bias caused by decreased brain volume are under development, also in our study group. Also the placement of the reference ROI (cerebellar cortex) is critical, since possible atrophy during disease progression might lead to misplacement of the ROI and its "contamination" by white matter signal. One theoretical possibility is also the appearance of cerebellar Aβ plaques, which would reduce the target-to-cerebellum ratios and could thus mask true increase in the target regions, or could even result in a reduction/decline in the target-to-cerebellum ratio. However, this is probably unlikely, since in study **III**, there was no difference in the cerebellar SUVs between the baseline and follow-up scans.

Cognitive decline and progressive brain atrophy were evident in the AD patients over the two-year follow-up of study **III**. It seems that these measures are more sensitive to monitor disease progression than ^{11}C-PIB uptake, as the latter did not change significantly during two years of AD progression. However, as new therapeutic agents aimed at reducing brain amyloid load emerge, ^{11}C-PIB PET could prove useful in monitoring of specific treatment effects. The power calculations of study **II** give hope that ^{11}C-PIB PET could be a sensitive enough method to monitor treatment effects on brain Aβ load with relatively small sample sizes, although the reductions in Aβ would probably have to be substantial to be captured with ^{11}C-PIB PET. Furthermore, the treatment would have to reduce Aβ *plaques*, possibly in addition to or in equilibrium with soluble forms of Aβ. Promisingly, at the time of completing this thesis, a study report has been published showing that treatment with bapineuzumab for 78 weeks (n=19) reduced AD patients' cortical ^{11}C-PIB retention compared with both baseline and placebo (n=7) (Rinne et al. 2010). ^{11}C-PIB PET thus seems to be a useful means of assessing the effects of potential AD treatments on cortical fibrillar Aβ load *in vivo* also in practice. It should however be noted that ^{18}F-FDG PET and MRI findings are quite likely to correspond better with possible clinical improvement during treatment –different imaging methods can complement each other in monitoring treatment effects.

It is also plausible that monitoring of ^{11}C-PIB uptake in earlier, presymptomatic stages of AD, where for example MRI and ^{18}F-FDG PET findings are not yet detectable, would be

beneficial. The question naturally remains as to who should be screened and followed-up with ^{11}C-PIB PET. The large proportion of cognitively healthy persons with increased ^{11}C-PIB uptake raises many questions and challenges as well as ethical issues for future studies. Study **III** indicates that in presently cognitively normal individuals, increased ^{11}C-PIB uptake could predict ongoing or future brain atrophy. Of course this is not synonymous with future AD, and the sample size in this study was small, and more elaborate and extensive studies will be necessary to resolve this question. However, these observations – as well as the findings of study **IV** showing increased ^{11}C-PIB uptake in cognitively healthy monozygotic co-twins of patients with cognitive impairment - may be interpreted to suggest that increased ^{11}C-PIB uptake could be an early indicator of susceptibility to AD. Many other supporting findings indicating that increased ^{11}C-PIB uptake could be predictive of cognitive decline and AD have also been reported [*e.g.* (Mintun et al. 2006, Kemppainen et al. 2007, Forsberg et al. 2008)].

As a brief conclusion, ^{11}C-PIB PET imaging may not be suitable for monitoring the progression of already manifest AD (study **III**), but does show promise in early disease detection and in the identification of individuals at increased risk for AD (studies **III** and **IV**, see also next chapter). Furthermore, the method is relatively safe (radiation-wise) and reproducible, and could be a feasible means of monitoring the effects of new disease-modifying therapies targeted at amyloid accumulation (studies **I** and **II**).

6.2.2 ^{11}C-PIB uptake relative to other changes in AD – new insights to AD neuropathology?

Brain ^{11}C-PIB uptake does not appear to be strongly associated with dementia severity or different measures of memory performance in AD patients, as reviewed earlier in this thesis. The results of this thesis are in line with previous reports in the sense that the AD progressor and nonprogressor subgroups of study **III** did not display significant differences in their ^{11}C-PIB uptake. This is not unexpected, because neuropathological studies have suggested that amyloid deposition may occur decades before the clinical symptoms of AD appear and that there is no clear quantitative association between cognitive decline and brain amyloid load [*e.g* (Vehmas et al. 2003)]. Furthermore, highly educated patients show more increased ^{11}C-PIB uptake in the lateral frontal cortex than less educated patients with AD with similar degrees of dementia severity (Kemppainen et al. 2008). This can be interpreted to mean that educational and other life-style factors play important modifying roles between brain Aβ deposition and its possible effects on cognition. Whether ^{11}C-PIB uptake is associated with indicators of subtle cognitive decline that could be detected in non-demented individuals is a different matter which is still unclear after quite variable findings so far reported (see section *2.3.6 ^{11}C-PIB PET in relation to CSF biomarkers, MRI findings, ^{18}F-FDG PET findings, inflammation markers and cognitive measures* in the *Review of the literature*). In study **III** of this thesis, one control subject who had increased ^{11}C-PIB uptake already at baseline showed a marked cognitive decline over the follow-up period, although she still performed within the age-

appropriate range at follow-up. In addition, her ^{11}C-PIB uptake increased over time (by 9-13 % in cortical regions), with the change from baseline to follow-up clearly exceeding the test-retest variability range estimated in study **II**. As these observations were made on only one subject, they cannot be generalized. More longitudinal studies with larger samples, standardized neuropsychological assessments and uniform measures are needed. There are in any case strong indications that ^{11}C-PIB PET could provide a tool to detect AD in its presymptomatic phase [*e.g.* (Mintun et al. 2005, Pike et al. 2007, Villemagne et al. 2008, Reiman et al. 2009)], and the results of this thesis support these proposals. In study **IV**, the cognitively intact monozygotic co-twins of subjects with an AD-like impairment showed increased cortical ^{11}C-PIB uptake. A positive family history is the second greatest risk factor for AD after age (Bertram and Tanzi, 2005), and it is unfortunately justifiable to anticipate cognitive problems in the now normally functioning but PIB-positive co-twins of study **IV**. This will be resolved through clinical follow-up of the study subjects.

While ^{11}C-PIB uptake and dementia severity are not associated in a linear fashion, it seems that there is a relationship between ^{18}F-FDG uptake and measures of cognitive decline. As reviewed earlier in this thesis, the predominant sites of brain hypometabolism in AD are different than the regions with greatest amyloid accumulation. Furthermore, the brain regions with greatest grey matter atrophy (*i.e.* neuronal loss) and ^{11}C-PIB binding also differ (Jack et al. 2008). This is demonstrated also in study **III** of this thesis. Plaque and neurofibrillary tangle pathologies also evolve with seemingly separate patterns (Braak and Braak 1991, Braak and Braak 1997). Sites of predominantly increased microglial activation may exist in the vicinity of increased Aβ plaque density, but no quantitative association has been established between these two phenomena (Edison et al. 2008a, Okello et al. 2009a, Wiley et al. 2009). These discrepancies between the different measurable and known pathological changes of AD underline –and make more challenging – the difficulties in trying to reveal the possible causal links between Aβ load, NFTs, inflammatory changes, and both functional and structural neuronal loss. Furthermore, the role of the ApoE gene variation in AD pathogenesis is still unclear.

It has been suggested that different brain regions could be differentially susceptible to the toxic effects of Aβ (Roder et al. 2003, Resende et al. 2007, Frisoni et al. 2009). In neuronal cell cultures with synthetic Aβ exposure and in electrophysiological studies on APP-transgenic mice, it appears that hippocampal neurons are more vulnerable to Aβ-induced apoptosis and impairment in synaptic functioning than for instance frontal neurons (Roder et al. 2003, Resende et al. 2007). It is, however, still unclear whether smaller amounts of Aβ in the MTL could be responsible for the relatively early neuronal loss in that region in AD, or if greater Aβ accumulation elsewhere could indirectly cause these atrophic changes through connections between the neocortex and the MTL. It has also been postulated that soluble forms of Aβ could be more important than insoluble forms (or more specifically, oligomeric forms rather than fibrils) in terms of toxicity [*e.g.* (Walsh et al. 2002, Chafekar et al. 2007)], and this could provide one explanation

for the discrepancy between sites of Aβ plaques and both functional and anatomical neuronal loss. Thus, when continuing studies with ^{11}C-PIB PET, it should be noted that while ^{11}C-PIB labels Aβ plaques, soluble forms of Aβ, whose role could prove important, remain undetected with this method. Other explanations to the anatomical discrepancies include the suggestion that NFTs are more directly associated with neuronal loss, either by mediating the toxic effects of amyloid or simply because they are more important pathological contributors in the first place. It is possible that the increase in NFT load in the entorhinal cortex could be detectable even earlier in the disease process than Aß accumulation (Duyckaerts et al. 1997) but the specific *in vivo* assessment of this phenomenon is unfortunately not possible, to date. Despite the spatial discrepancies, increased amounts of Aβ do seem to be quantitatively associated with greater brain grey matter atrophy [*e.g.* (Jack et al. 2009)]. Furthermore, the results of study **III** may be interpreted to indicate that increased Aβ accumulation may predict subsequent volumetric brain changes. Another recent study reported a strong relationship between brain atrophy and ^{11}C-PIB uptake in subjects with subjective cognitive impairment but not in patients with MCI or AD. The findings suggest a strong relationship between Aβ deposition and brain atrophy very early in the disease process, which could prove an important notion *e.g.* with respect to novel treatment strategies. (Chételat et al. 2010)

With respect to the issue of soluble *vs.* insoluble forms of Aβ, it has been proposed that the decrease of soluble Aβ1-42 in the CSF in AD is a result of brain accumulation and reduced clearance of the polypeptide into the CSF. Decreased Aβ1-42 levels have been observed at an early or even presymptomatic stage of AD (Riemenschneider et al. 2002, Hampel et al. 2004, Moonis et al. 2005), in line with the hypothesis that Aβ deposition occurs years or decades before the appearance of clinical AD symptoms [*e.g.* (Price and Morris 1999)]. *Post mortem* studies have demonstrated that increased Aβ plaques correlate inversely with ventricular CSF Aβ1-42 levels (Strozyk et al. 2003). Longitudinal studies have suggested that CSF soluble Aβ1-42 levels decrease progressively over time (Tapiola et al. 2000). These findings support the hypothesis that there is an interaction between Aβ in the brain parenchyma and in the CSF. However, decreases in CSF Aβ1-42 levels are present in some non-AD non-plaque diseases, as well (CJD, ALS, multiple system atrophy) (Blennow and Hampel 2003) and it has been observed that soluble Aβ1-42 oligomers may reduce gamma secretase activity (Sotthibundhu et al. 2008). These concepts have led to the suggestion that the CSF Aβ1-42 reduction could simply be attributable to reduced production of the polypeptide (de Leon et al. 2007). Studies combining *in vivo* amyloid imaging and CSF Aβ1-42 analyses will hopefully help resolve this issue. At the moment there are some indications that brain parenchymal and CSF Aβ1-42 measures display an inverse correlation (Grimmer et al. 2009), but the relationship needs to be clarified. (See more in the *Review of the literature* section *2.3.6 ^{11}C-PIB PET in relation to CSF biomarkers, MRI findings, ^{18}F-FDG PET findings, inflammation markers and cognitive measures*). If quantities of plaques and soluble Aβ or parenchymal and CSF Aβ do correlate, for example ^{11}C-PIB PET *could* be able to reflect the amount of total Aβ burden, but more studies are, without a doubt, warranted.

Aβ1-42, also in the form of plaques, does seem to induce an inflammatory response, which could be an important contributor to the loss of neurons and brain function in AD. The modified amyloid cascade–neuroinflammation hypothesis was briefly introduced in the *Review of the literature,* but in the following paragraphs, the recent findings combining *in vivo* assessment of microglial activation with amyloid imaging will be reviewed.

In a PET study utilizing both the microglial activation marker ^{11}C-(R)-PK-11195 as well as ^{11}C-PIB, ^{11}C-(R)-PK-11195 uptake was increased in AD patients (n = 13) in the same cortical regions as ^{11}C-PIB uptake, by 20 - 35 % (^{11}C-PIB uptake by 100 %), when compared with controls. The amounts of the two ligands taken up were, however, not associated (Edison et al. 2008a). Another comparative study with smaller samples found no differences in ^{11}C-(R)-PK-11195 uptake between AD patients (n = 6), MCI patients (n = 6) and controls (n = 5) in the first place, although differences in ^{11}C-PIB uptake were evident. Furthermore, ^{11}C-(R)-PK-11195 uptake did not differ between PIB-positive and PIB-negative subjects (Wiley et al. 2009). A similar study on MCI patients demonstrated that ^{11}C-(R)-PK-11195 uptake was increased in 5 of 13 (38 %) subjects. However, again, no correlation between individual ^{11}C-(R)-PK-11195 and ^{11}C-PIB binding was found. Furthermore, in the PIB-negative patients, there were two patients with increased ^{11}C-(R)-PK-11195 uptake but neither of them converted to AD over a 24 – 36 month follow-up, in contrast to 3 out of the 5 PIB-positive subjects (Okello et al. 2009a). One interpretation of these results is that brain microglial activation may be increased in the absence of significant Aβ plaque deposition, a phenomenon known from studies on ^{11}C-(R)-PK-11195 PET retention in other types of brain injury [*e.g.* Banati et al 2000]. This will likely pose additional challenges in trying to establish the role of specific inflammatory responses in AD pathophysiology.

As stated earlier, another factor whose role in the AD process is possibly important, though still unclear, is the ApoE gene variation, and its epsilon 4 allele in particular. A number of different explanations for the role of ApoE in AD pathophysiology have been proposed. Some are associated with APP or amyloid metabolism [*e.g.* (Irizarry et al. 2004, Koistinaho et al. 2004, Manelli et al. 2004)] or the toxicity of amyloid (Manelli et al. 2004), others with different mechanisms such as tau hyperphosphorylation or neuronal oxidative stress or alterations in mitochondrial functions (Strittmatter et al. 1994, Miyata and Smith 1996, Gibson et al. 2000). Difficulties remain in establishing a causal link between the genetic variation of ApoE and the biological processes that might contribute to the risk of developing AD. Furthermore, while the ApoE genotype is associated with AD as a genetic modifier influencing the age of disease onset, its epsilon 4 allele seems to be neither necessary nor sufficient to cause AD (Bertram and Tanzi 2005). In addition, ApoE polymorphism does not seem to affect the incidence of clinical dementia in the very elderly, although, even in this age group, neuropathological AD (*i.e.* increased brain amyloid and NFT load) *is* significantly associated with the ApoE epsilon 4 allele (Polvikoski et al. 2006). In this thesis, ApoE genotyping was carried out in study

IV. In only one discordant dizygotic twin pair, the co-twin with a cognitive deficit and greater ^{11}C-PIB uptake had the epsilon 4 allele unlike his cognitively healthy co-twin. In general, in small samples like that employed in this thesis, the ApoE genotype does not seem to *unambiguously* dictate the extent of ^{11}C-PIB uptake, although studies on non-demented subjects suggest that ^{11}C-PIB uptake is indeed greater in ApoE epsilon 4 carriers (Villemagne et al. 2008, Reiman et al. 2009, Morris et al. 2010). ApoE epsilon 4 thus seems to be somehow related with Aβ deposition, although its relevance to clinical AD is unclear. The results of study **IV** would seem to emphasize the additional importance of *other* genetic factors contributing to increased risk for Aβ deposition and AD. Studies on twins, on individuals with a monogenic AD-causing mutation, and on subjects with a history of AD in the family will be valuable for answering the open questions of AD genetics and will hopefully help to clarify AD pathogenesis.

Brain amyloid accumulation seems to precede some of the other neuropathological changes and the clinical symptoms of the disease (studies **III** and **IV** support this notion) but whether amyloid accumulation is simply one of the more upstream processes of the pathological cascade or the actual initiating event remains unclear. It also remains to be resolved whether neural projections could explain the discrepancies between sites of amyloid accumulation and functional and structural neuronal loss. Another alternative explanation is that the disease mechanism involves completely unknown components.

6.3 THE POTENTIAL OF ^{11}C-PIB PET IN THE EARLY DETECTION OF ALZHEIMER'S DISEASE

A substantial proportion of healthy elderly subjects show AD-like ^{11}C-PIB binding, the value ranges from 10 to 30 % in different studies (Klunk et al. 2004, Mintun et al. 2006, Pike et al. 2007, Rowe et al. 2007, Aizenstein et al. 2008, Jack et al. 2008). Studies **III** and **IV** of this thesis were in line with these values: 15-33 % of the controls showed increased ^{11}C-PIB uptake, depending on the examined brain region, when using the often-employed 1.5-cut-off limit for "PIB-positivity" (Aizenstein et al. 2008, Jack et al. 2008). (Whether or not a general cut-off limit can even be feasibly established and applied for ^{11}C-PIB retention, and if so, what should this limit value be, are interesting questions of their own.)

The percentage of healthy controls with increased ^{11}C-PIB uptake seems to increase with age – in one study, 20 %, 35 % and 50 % of the subjects displayed PIB-positive scans in the 61-70, 71-80 and 81+ age groups, respectively (Villemagne et al. 2008). This is in agreement with *post mortem* data on Aβ deposition in normal aging [*e.g.* (Davies et al. 1988)]. In general, several *post mortem* reports have shown that about 30 % of non-demented persons over the age of 75 exhibit cortical Aβ plaques on histopathological examination [*e.g.* (Price and Morris 1999, Price et al. 2009)]. Furthermore, and quite interestingly, this prevalence of amyloid plaques in the non-demented elderly is almost equivalent to the estimated prevalence of dementia at age 85 (Ferri et al. 2005), which

could be interpreted to support the hypothesis that amyloid accumulation precedes clinical dementia symptoms by several years [*e.g* (Price and Morris 1999)].

Increased ^{11}C-PIB uptake has been proposed to be predictive of conversion to AD in MCI subjects (Forsberg et al. 2008, Koivunen et al. 2008a, Okello et al. 2009b, Wolk et al. 2009). Due to the limited history of *in vivo* amyloid imaging, the same cannot yet be said about the possible value of ^{11}C-PIB PET in predicting future AD in completely healthy individuals. For example, subtle memory problems do seem to be associated with increased ^{11}C-PIB uptake in seemingly cognitively healthy individuals in some studies (Pike et al. 2007, Mormino et al. 2009), but contrasting results to these have also been reported (Aizenstein et al. 2008, Jack et al. 2008). As was discussed in the previous section *6.2.2 ^{11}C-PIB uptake relative to other changes in AD – new insights to AD neuropathology?* of this *Discussion*, one healthy control subject in study **III** suffered a marked cognitive decline in conjunction with elevated and increasing ^{11}C-PIB uptake. In addition, the correlation between baseline ^{11}C-PIB uptake and subsequent brain atrophy rates in the healthy controls of study **III** could possibly indicate future AD in subjects that are now healthy, but these are rather speculative observations in small samples. It is thus evident that it is important to continue investigations of ^{11}C-PIB uptake in normal aging as well as in what has been thought to be but may not be normal aging.

To generalize, unfortunately it is still unclear whether a person can have marked brain Aβ load without ever developing clinical symptoms of AD. As a possibly confusing factor, ^{11}C-PIB uptake seems to be greater in the presence of the ApoE epsilon 4 allele in normal aging (Villemagne et al. 2008, Reiman et al. 2009), but this does not seem to be necessarily associated with cognitive symptoms (Villemagne et al. 2008). It has also been suggested that some of the ^{11}C-PIB uptake seen in control subjects may be attributable to amyloid deposits in cerebral blood vessels (Svedberg et al. 2009). This possibility, along with other explanations for PIB-positivity in healthy individuals, should be investigated further and its clinical relevance clarified.

The variation in the proportions of PIB-positive non-demented subjects between different studies (Klunk et al. 2004, Mintun et al. 2006, Pike et al. 2007, Rowe et al. 2007, Aizenstein et al. 2008, Jack et al. 2008) cannot be considered “alarming”, given the prominent role of chance in these small samples. However, one important methodological issue to be addressed before concluding on the proportion of PIB-positive healthy subjects in the general population, is selection bias – individuals with increased risk (either related to genetic or environmental risk factors, or presenting as subtle memory problems) are likely to be more eager to participate in ^{11}C-PIB PET studies, also as healthy controls. This was definitely a phenomenon that could not be completely excluded in studies **II-IV** of this thesis, although attempts were made to avoid this bias. In controlled proportions, individuals who are classified as healthy, with either subtle symptoms or no cognitive symptoms and with either increased familial risk or no special familial risk for cognitive disorders, are all interesting amyloid imaging study candidates in research aimed at understanding AD. By enriching the PIB-positive proportion of healthy study

subjects for instance through enrolment of genetically predisposed individuals, a more profound understanding of the evolution of brain Aβ accumulation could be gained in the relatively near future.

Study **IV** of this thesis demonstrated that cognitively preserved monozygotic co-twins of subjects with an AD-like cognitive impairment showed increased ^{11}C-PIB uptake in their cerebral cortex and striatum when compared with healthy non-twin control subjects and cognitively preserved dizygotic co-twins. In addition, similar ^{11}C-PIB uptake patterns were observed within the cognitively discordant monozygotic twin pairs in some typical brain regions. The cognitively preserved dizygotic co-twins showed no such ^{11}C-PIB uptake increases, and their values were in the same range as those of healthy unrelated control subjects. Previous, similar study designs with monozygotic twins have demonstrated similar findings on glucose metabolism assessed with ^{18}F-FDG PET (Järvenpää et al. 2003, Virta et al. 2009). In contrast, MRI studies detected no reductions in hippocampal volumes in healthy monozygotic co-twins of AD patients (Järvenpää et al. 2004). The monozygotic twin ^{11}C-PIB uptake results of study **IV**, together with the ^{18}F-FDG and MRI study results, support the amyloid cascade hypothesis by reinforcing the concept that Aβ pathology and metabolic impairments precede brain atrophy and memory impairment in AD. Furthermore, a *post mortem* study in three monozygotic twin pairs with AD has suggested that despite the variation in the age of disease onset, presentation and duration, the amyloid and neurofibrillary tangle pathologies are concordant between affected co-twins (Brickell et al. 2007). Although all of this should be interpreted with caution; as the monozygotic co-twins of the cognitively impaired subjects are at increased genetic risk for AD and they do show increased ^{11}C-PIB uptake although they are still healthy, it seems plausible that ^{11}C-PIB uptake could – perhaps in conjunction with other indicators - be predictive of future AD.

7. CONCLUSIONS

The following general conclusions may be drawn from the studies presented in this thesis:

I An adequate Aβ-imaging dose of the radiotracer ^{11}C-PIB for 3-dimensional brain PET imaging results in an acceptable effective radiation dose which allows repeated studies in the same individuals.

II Assessment of brain ^{11}C-PIB uptake is reproducible even when simplified analysis methods and a short scanning protocol are used. ^{11}C-PIB appears suitable for PET studies aiming to quantitate brain Aβ accumulation for monitoring the effects of anti-amyloid treatments.

III Brain ^{11}C-PIB uptake does not seem to increase markedly during two years of Alzheimer's disease (AD) progression. Increased cortical ^{11}C-PIB uptake may predict ongoing brain atrophy in cognitively normal individuals, and may be a useful method for patient selection and follow-up in early-phase intervention trials of new therapeutic agents.

IV Cognitively preserved persons who have a monozygotic twin with an AD-like cognitive impairment appear to have increased ^{11}C-PIB uptake compared to other cognitively healthy persons. Genetic factors thus seem to play an important modifying role in the development of AD-like Aβ plaque pathology. AD might be detectable in high-risk individuals in its presymptomatic phase with ^{11}C-PIB PET, which would have important consequences for future diagnostics and research on disease-modifying treatments.

8. ACKNOWLEDGEMENTS

This work was carried out at Turku PET Centre during the years 2003-2010. I am grateful for having been able to work there on and off between my medical studies as well as full-time when that became possible. The flexible and friendly staff allowed this to happen. I want to thank Juhani Knuuti, Director of Turku PET Centre, for keeping the strings in his hands at this excellent facility. I wish to express my gratitude to my daily co-workers, the core personnel of Turku PET Centre: especially Tuula Tolvanen and Mika Teräs for their expertise and patience in matters of PET physics and instrumentation; Vesa Oikonen for modeling know-how; Rami Mikkola and Marko Tättäläinen for computer assistance. Tarja Keskitalo, Minna Aatsinki, Marjo Tähti, Anne-Mari Jokinen, Hannele Lehtinen, Outi Numminen, Kaleva Mölsä and Heidi Betlehem for being skilful radiographers and great company during the PET sessions. Medical laboratory technologists Sanna Suominen, Heidi Partanen, Eija Nirhamo, Emilia Puhakka and Leena Tokoi are thanked for all their work and humour in the laboratory. I also thank Mirja Jyrkinen and Sinikka Lehtola for help with important secretarial matters.

The studies that form this thesis were done in collaboration with several experts. Without them this thesis would not have been possible. Tuula Tolvanen is thanked for her great contribution and guidance in study **I**. I thank Sargo Aalto for ^{11}C-PIB quantitation in studies **II-IV** and for valuable comments on several scientific issues and for making me figure things out on my own. Mika Scheinin and Marita Kailajärvi enabled the collaboration with Clinical Research Services Turku (CRST), which was important in study **III**. All friendly CRST staff members, especially Tita Kaila and Mia Koutu, are also warmly acknowledged. Nina Kemppainen is thanked for paving the road for me in ^{11}C-PIB PET studies and for her comments on publications **II** and **III**. Matti Viitanen is thanked for his key role in originally finding the patients for study **III**. Ian Wilson is thanked for his contribution in ^{11}C-PIB's landing in Turku. Juha Koikkalainen and Jyrki Lötjönen of VTT, Tampere, are gratefully acknowledged for making study **III** a multi-modality investigation, which gave the study great value. The staff of the radiochemistry laboratory of the University of Turku is thanked for the production and delivery of the radiotracer. Especially Eveliina Arponen, Johanna Rokka, Semi Helin and, above all, Kjell Någren are thanked for ^{11}C-PIB production. Mira Karrasch deserves a great thanks for organizing the neuropsychological assessments for the studies, as well as for teaching me their interpretation. Sanna Knuts, Heidi Lehto, Anna Ikonen, Minja Westerlund, Veronika Solovian, Anniina Järvinen and Jenny Halin (and others) are thanked for carrying out this testing – it must be hard work. Ulla Kulmala-Gråhn, Maarit Mantere and Kristiina Saanakorpi are acknowledged for their work at the Finnish Twin Registy and for conducting the telephone interviews of the subjects in study **IV**. Jaakko Kaprio and Markku Koskenvuo are valued for their life-long work with the Finnish Twin Cohort and their strong input in study **IV**. Ismo Räihä's contribution to study **IV** is also acknowledged. Tero Vahlberg and Sanna Hinkka-Yli-Salomäki are thanked for their assistance in statistical matters.

I also want to thank all of my research subjects. They were willing to undergo invasive research procedures and to spend a lot of time for the benefit of science, with no promise of personal gain from the research. Public trust in medical science and willingness to participate in research are valuable assets that we scientists should be thankful for.

In these four studies as well as in my research career as a whole, the greatest help of all came from my supervisor, Juha O. Rinne. He fathered the ideas in the first place, he brought ^{11}C-PIB PET studies to Finland, and he guided me through thick and thin. In the midst of everything, he saw the big picture. I have never met a person more friendly, optimistic and patient than he. He is a great role model – not only in science but also in life.

Under the soft but determined supervision of Juha were also my fellow researchers, whom I wish to thank for sharing this experience. Jere Virta is acknowledged for help both in methodology and in meditation. Pekka Jokinen, Terhi Tuokkola, Jaana Koivunen, Eero Rissanen, Jyri Virta and Timo Suotunen are particularly thanked for sharing the scanning workload and for good talks and a great atmosphere. The other researchers at Turku PET Centre are warmly thanked as well – whether be it for teaching me, singing for me or drinking coffee or champagne with me on different occasions. Nina Savisto and the rest of the gang organizing the memorable 2008 XI Turku PET Symposium are also very warmly remembered.

I am grateful to Aapo Ahonen and Raimo Sulkava, the official reviewers of this thesis, for their constructive comments, and to Ewen MacDonald for revising the language.

My wonderful circle of friends, consisting largely of the "KS" group, is thanked for keeping it real. To my parents, Mika and Marjukka, as well as my brothers, Matias and Lauri, I owe so much for their never-ending support, company, and valuable advice. I think my father Mika can pretty much be blamed for me becoming a scientist. Jami's family is warmly thanked for encouragement, good times and for their patience on me keeping their boy in Turku. Jami himself I cannot even be *grateful* to because this is what love means - you taught me that, and replaced luck.

This study has been financially supported by the Päivikki and Sakari Sohlberg Foundation, the Sigrid Jusélius Foundation, the Niilo Huolma Fellowship of the Medical Faculty of the University of Turku, the Finnish Medical Society Duodecim, the Regional Trust of the Finnish Cultural Foundation, the Finnish Alzheimer's Disease Research Foundation, the Turku University Foundation and by clinical research grants from Turku University Central Hospital. I am also very thankful for the Alawi-Mandell award granted to me by the Society of Nuclear Medicine and the Junior Faculty Award of the 9th AD/PD Congress. All of these sources of support are gratefully acknowledged.

Noora Scheinin

Turku, May 2010

9. REFERENCES

Addendum 6 to ICRP Publication 53: *Radiation Doses of Radiopharmaceuticals* **2002**. Available at: www.icrp.org/docs/Add_5-7_to_P53.pdf. Accessed October 3, 2001.

Agdeppa, E.; Kepe, V.; Liu, J.; Flores-Torres, S.; Satyamurthy, N.; Petric, A.; Cole, G.; Small, G.; Huang, S.; Barrio, J., Binding characteristics of radiofluorinated 6-dialkylamino-2-naphthylethylidene derivatives as positron emission tomography imaging probes for beta-amyloid plaques in Alzheimer's disease. *J Neurosci* **2001,** *21* (24), RC189.

Aggarwal, N.; Wilson, R.; Beck, T.; Bienias, J.; Berry-Kravis, E.; Bennett, D., The apolipoprotein E epsilon4 allele and incident Alzheimer's disease in persons with mild cognitive impairment. *Neurocase* **2005,** *11* (1), 3-7.

Aizenstein, H.; Nebes, R.; Saxton, J.; Price, J.; Mathis, C.; Tsopelas, N.; Ziolko, S.; James, J.; Snitz, B.; Houck, P.; Bi, W.; Cohen, A.; Lopresti, B.; DeKosky, S.; Halligan, E.; Klunk, W., Frequent amyloid deposition without significant cognitive impairment among the elderly. *Arch Neurol* **2008,** *65* (11), 1509-17.

Anchisi, D.; Borroni, B.; Franceschi, M.; Kerrouche, N.; Kalbe, E.; Beuthien-Beumann, B.; Cappa, S.; Lenz, O.; Ludecke, S.; Marcone, A.; Mielke, R.; Ortelli, P.; Padovani, A.; Pelati, O.; Pupi, A.; Scarpini, E.; Weisenbach, S.; Herholz, K.; Salmon, E.; Holthoff, V.; Sorbi, S.; Fazio, F.; Perani, D., Heterogeneity of brain glucose metabolism in mild cognitive impairment and clinical progression to Alzheimer disease. *Arch Neurol* **2005,** *62* (11), 1728-33.

Archer, H. A.; Edison, P.; Brooks, D. J.; Barnes, J.; Frost, C.; Yeatman, T.; Fox, N. C.; Rossor, M. N., Amyloid load and cerebral atrophy in Alzheimer's disease: An C-11-PIB positron emission tomography study. *Annals of Neurology* **2006,** *60* (1), 145-147.

Areosa, S.; Sherriff, F., Memantine for dementia. *Cochrane Database Syst Rev* **2003,** (3), CD003154.

Arlicot, N.; Katsifis, A.; Garreau, L.; Mattner, F.; Vergote, J.; Duval, S.; Kousignian, I.; Bodard, S.; Guilloteau, D.; Chalon, S., Evaluation of CLINDE as potent translocator protein (18 kDa) SPECT radiotracer reflecting the degree of neuroinflammation in a rat model of microglial activation. *Eur J Nucl Med Mol Imaging* **2008,** *35* (12), 2203-11.

Arnáiz, E.; Jelic, V.; Almkvist, O.; Wahlund, L.; Winblad, B.; Valind, S.; Nordberg, A., Impaired cerebral glucose metabolism and cognitive functioning predict deterioration in mild cognitive impairment. *Neuroreport* **2001,** *12* (4), 851-5.

Bacskai, B.; Frosch, M.; Freeman, S.; Raymond, S.; Augustinack, J.; Johnson, K.; Irizarry, M.; Klunk, W.; Mathis, C.; Dekosky, S.; Greenberg, S.; Hyman, B.; Growdon, J., Molecular imaging with Pittsburgh Compound B confirmed at autopsy: a case report. *Arch Neurol* **2007,** *64* (3), 431-4.

Bacskai, B.; Hickey, G.; Skoch, J.; Kajdasz, S.; Wang, Y.; Huang, G.; Mathis, C.; Klunk, W.; Hyman, B., Four-dimensional multiphoton imaging of brain entry, amyloid binding, and clearance of an amyloid-beta ligand in transgenic mice. *Proc Natl Acad Sci U S A* **2003,** *100* (21), 12462-7.

Banati, R.; Newcombe, J.; Gunn, R.; Cagnin, A.; Turkheimer, F.; Heppner, F.; Price, G.; Wegner, F.; Giovannoni, G.; Miller, D.; Perkin, G.; Smith, T.; Hewson, A.; Bydder, G.; Kreutzberg, G.; Jones, T.; Cuzner, M.; Myers, R., The peripheral benzodiazepine binding site in the brain in multiple sclerosis: quantitative in vivo imaging of microglia as a measure of disease activity. *Brain* **2000,** *123 (Pt 11)*, 2321-37.

Barber, R.; Ballard, C.; McKeith, I.; Gholkar, A.; O'Brien, J., MRI volumetric study of dementia with Lewy bodies: a comparison with AD and vascular dementia. *Neurology* **2000,** *54* (6), 1304-9.

Barrow, C., Advances in the Development of Abeta-Related Therapeutic Strategies for Alzheimer's Disease. *Drug News Perspect* **2002,** *15* (2), 102-109.

Bartzokis, G.; Lu, P.; Mintz, J., Human brain myelination and amyloid beta deposition in Alzheimer's disease. *Alzheimers Dement* **2007,** *3* (2), 122-125.

Bayer, A.; Bullock, R.; Jones, R.; Wilkinson, D.; Paterson, K.; Jenkins, L.; Millais, S.; Donoghue, S., Evaluation of the safety and immunogenicity of synthetic Abeta42 (AN1792) in patients with AD. *Neurology* **2005,** *64* (1), 94-101.

Bertram, L.; Tanzi, R., Alzheimer's disease: one disorder, too many genes? *Hum Mol Genet* **2004a,** *13 Spec No 1*, R135-41.

Bertram, L.; Tanzi, R., The current status of Alzheimer's disease genetics: what do we tell the patients? *Pharmacol Res* **2004b,** *50* (4), 385-96.

Bertram, L.; Tanzi, R., The genetic epidemiology of neurodegenerative disease. *J Clin Invest* **2005,** *115* (6), 1449-57.

Birks, J., Cholinesterase inhibitors for Alzheimer's disease. *Cochrane Database Syst Rev* **2006,** (1), CD005593.

Bittner, D.; Grön, G.; Schirrmeister, H.; Reske, S.; Riepe, M., [18F]FDG-PET in patients with Alzheimer's disease: marker of disease spread. *Dement Geriatr Cogn Disord* **2005,** *19* (1), 24-30.

Blennow, K.; Hampel, H., CSF markers for incipient Alzheimer's disease. *Lancet Neurol* **2003,** *2* (10), 605-13.

Boccardi, M.; Laakso, M.; Bresciani, L.; Galluzzi, S.; Geroldi, C.; Beltramello, A.; Soininen, H.; Frisoni, G., The MRI pattern of frontal and temporal brain atrophy in fronto-temporal dementia. *Neurobiol Aging* **2003,** *24* (1), 95-103.

Bolmont, T.; Clavaguera, F.; Meyer-Luehmann, M.; Herzig, M.; Radde, R.; Staufenbiel, M.; Lewis, J.; Hutton, M.; Tolnay, M.; Jucker, M., Induction of tau pathology by intracerebral infusion of amyloid-beta -containing brain extract and by amyloid-beta deposition in APP x Tau transgenic mice. *Am J Pathol* **2007,** *171* (6), 2012-20.

Boxer, A.; Rabinovici, G.; Kepe, V.; Goldman, J.; Furst, A.; Huang, S.; Baker, S.; O'neil, J.; Chui, H.; Geschwind, M.; Small, G.; Barrio, J.; Jagust, W.; Miller, B., Amyloid imaging in distinguishing atypical prion disease from Alzheimer disease. *Neurology* **2007,** *69* (3), 283-90.

Braak, H.; Braak, E., Neuropathological stageing of Alzheimer-related changes. *Acta Neuropathol* **1991,** *82* (4), 239-59.

Braak, H.; Braak, E., Staging of Alzheimer-related cortical destruction. *Int Psychogeriatr* **1997,** *9 Suppl 1*, 257-61; discussion 269-72.

Brickell, K.; Leverenz, J.; Steinbart, E.; Rumbaugh, M.; Schellenberg, G.; Nochlin, D.; Lampe, T.; Holm, I.; Van Deerlin, V.; Yuan, W.; Bird, T., Clinicopathological concordance and discordance in three monozygotic twin pairs with familial Alzheimer's disease. *J Neurol Neurosurg Psychiatry* **2007,** *78* (10), 1050-5.

Brion, J., Neurofibrillary tangles and Alzheimer's disease. *Eur Neurol* **1998,** *40* (3), 130-40.

Buckner, R. L.; Snyder, A. Z.; Shannon, B. J.; LaRossa, G.; Sachs, R.; Fotenos, A. F.; Sheline, Y. I.; Klunk, W. E.; Mathis, C. A.; Morris, J. C.; Mintun, M. A., Molecular, structural, and functional characterization of Alzheimer's disease: Evidence for a relationship between default activity, amyloid, and memory. *Journal of Neuroscience* **2005,** *25* (34), 7709-7717.

Busse, A.; Angermeyer, M.; Riedel-Heller, S., Progression of mild cognitive impairment to dementia: a challenge to current thinking. *Br J Psychiatry* **2006,** *189*, 399-404.

Cagnin, A.; Brooks, D.; Kennedy, A.; Gunn, R.; Myers, R.; Turkheimer, F.; Jones, T.; Banati, R., In-vivo measurement of activated microglia in dementia. *Lancet* **2001,** *358* (9280), 461-7.

Campion, D.; Dumanchin, C.; Hannequin, D.; Dubois, B.; Belliard, S.; Puel, M.; Thomas-Anterion, C.; Michon, A.; Martin, C.; Charbonnier, F.; Raux, G.; Camuzat, A.; Penet, C.; Mesnage, V.; Martinez, M.; Clerget-Darpoux, F.; Brice, A.; Frebourg, T., Early-onset autosomal dominant Alzheimer disease: prevalence, genetic heterogeneity, and mutation spectrum. *Am J Hum Genet* **1999,** *65* (3), 664-70.

Caroli, A.; Testa, C.; Geroldi, C.; Nobili, F.; Barnden, L.; Guerra, U.; Bonetti, M.; Frisoni, G., Cerebral perfusion correlates of conversion to Alzheimer's disease in amnestic mild cognitive impairment. *J Neurol* **2007,** *254* (12), 1698-707.

Chafekar, S.; Hoozemans, J.; Zwart, R.; Baas, F.; Scheper, W., Abeta 1-42 induces mild endoplasmic reticulum stress in an aggregation state-dependent manner. *Antioxid Redox Signal* **2007,** *9* (12), 2245-54.

Chang, C.; Silverman, D., Accuracy of early diagnosis and its impact on the management and course of Alzheimer's disease. *Expert Rev Mol Diagn* **2004,** *4* (1), 63-9.

Chételat, G.; Desgranges, B.; de la Sayette, V.; Viader, F.; Eustache, F.; Baron, J., Mild cognitive impairment: Can FDG-PET predict who is to rapidly convert to Alzheimer's disease? *Neurology* **2003,** *60* (8), 1374-7.

Chételat, G.; Landeau, B.; Eustache, F.; Mézenge, F.; Viader, F.; de la Sayette, V.; Desgranges, B.; Baron, J., Using voxel-based morphometry to map the structural changes associated with rapid conversion in MCI: a longitudinal MRI study. *Neuroimage* **2005,** *27* (4), 934-46.

Chételat, G.; Villemagne V.L.; Bourgeat P.; Pike K.E.; Jones G.; Ames D.; Ellis K.A.; Szoeke C.; Martins R.N.; O'Keefe G.J.; Salvado O.; Masters C.L.; Rowe C.C., *Ann Neurol* **2010,** *67* (3), 317-24.

Choo, I.; Lee, D.; Youn, J.; Jhoo, J.; Kim, K.; Lee, D.; Lee, J.; Woo, J., Topographic patterns of brain functional impairment progression according to clinical severity staging in 116 Alzheimer disease patients: FDG-PET study. *Alzheimer Dis Assoc Disord* **2007,** *21* (2), 77-84.

Collie, A.; Maruff, P., The neuropsychology of preclinical Alzheimer's disease and mild cognitive impairment. *Neurosci Biobehav Rev* **2000,** *24* (3), 365-74.

Cook, R.; Schneck, S.; Clark, D., Twins with Alzheimer's disease. *Arch Neurol* **1981,** *38* (5), 300-1.

Dai, W.; Lopez, O.; Carmichael, O.; Becker, J.; Kuller, L.; Gach, H., Mild cognitive impairment and alzheimer disease: patterns of altered cerebral blood flow at MR imaging. *Radiology* **2009,** *250* (3), 856-66.

Davies, L.; Wolska, B.; Hilbich, C.; Multhaup, G.; Martins, R.; Simms, G.; Beyreuther, K.; Masters, C., A4 amyloid protein deposition and the diagnosis of Alzheimer's disease: prevalence in aged brains determined by immunocytochemistry compared with conventional neuropathologic techniques. *Neurology* **1988,** *38* (11), 1688-93.

de Leon, M.; Convit, A.; Wolf, O.; Tarshish, C.; DeSanti, S.; Rusinek, H.; Tsui, W.; Kandil, E.; Scherer, A.; Roche, A.; Imossi, A.; Thorn, E.; Bobinski, M.; Caraos, C.; Lesbre, P.; Schlyer, D.; Poirier, J.; Reisberg, B.; Fowler, J., Prediction of cognitive decline in normal elderly subjects with 2-[(18)F]fluoro-2-deoxy-D-glucose/poitron-emission tomography (FDG/PET). *Proc Natl Acad Sci U S A* **2001,** *98* (19), 10966-71.

de Leon, M.; DeSanti, S.; Zinkowski, R.; Mehta, P.; Pratico, D.; Segal, S.; Rusinek, H.; Li, J.; Tsui, W.; Saint Louis, L.; Clark, C.; Tarshish, C.; Li, Y.; Lair, L.; Javier, E.; Rich, K.; Lesbre, P.; Mosconi, L.; Reisberg, B.; Sadowski, M.; DeBernadis, J.; Kerkman, D.; Hampel, H.; Wahlund, L.; Davies, P., Longitudinal CSF and MRI biomarkers improve the diagnosis of mild cognitive impairment. *Neurobiol Aging* **2006,** *27* (3), 394-401.

de Leon, M.; Mosconi, L.; Blennow, K.; DeSanti, S.; Zinkowski, R.; Mehta, P.; Pratico, D.; Tsui, W.; Saint

Louis, L.; Sobanska, L.; Brys, M.; Li, Y.; Rich, K.; Rinne, J.; Rusinek, H., Imaging and CSF studies in the preclinical diagnosis of Alzheimer's disease. *Ann N Y Acad Sci* **2007,** *1097*, 114-45.

DeCarli, C.; Frisoni, G.; Clark, C.; Harvey, D.; Grundman, M.; Petersen, R.; Thal, L.; Jin, S.; Jack, C. J.; Scheltens, P., Qualitative estimates of medial temporal atrophy as a predictor of progression from mild cognitive impairment to dementia. *Arch Neurol* **2007,** *64* (1), 108-15.

Diehl-Schmid, J.; Grimmer, T.; Drzezga, A.; Bornschein, S.; Riemenschneider, M.; Förstl, H.; Schwaiger, M.; Kurz, A., Decline of cerebral glucose metabolism in frontotemporal dementia: a longitudinal 18F-FDG-PET-study. *Neurobiol Aging* **2007,** *28* (1), 42-50.

Drzezga, A.; Grimmer, T.; Henriksen, G.; Stangier, I.; Pemeczky, R.; Diehl-Schmid, J.; Mathis, C. A.; Klunck, W. E.; Price, J.; DeKosky, S.; Wester, H. J.; Schwaiger, M.; Kurz, A., Imaging of amyloid plaques and cerebral glucose metabolism in semantic dementia and Alzheimer's disease. *Neuroimage* **2008,** *39* (2), 619-633.

Drzezga, A.; Grimmer, T.; Henriksen, G.; Mühlau, M.; Perneczky, R.; Miederer, I.; Praus, C.; Sorg, C.; Wohlschläger, A.; Riemenschneider, M.; Wester, H.; Foerstl, H.; Schwaiger, M.; Kurz, A., Effect of APOE genotype on amyloid plaque load and gray matter volume in Alzheimer disease. *Neurology* **2009,** *72* (17), 1487-94.

Drzezga, A.; Grimmer, T.; Riemenschneider, M.; Lautenschlager, N.; Siebner, H.; Alexopoulus, P.; Minoshima, S.; Schwaiger, M.; Kurz, A., Prediction of individual clinical outcome in MCI by means of genetic assessment and (18)F-FDG PET. *J Nucl Med* **2005,** *46* (10), 1625-32.

Dubois, B.; Feldman, H.; Jacova, C.; Dekosky, S.; Barberger-Gateau, P.; Cummings, J.; Delacourte, A.; Galasko, D.; Gauthier, S.; Jicha, G.; Meguro, K.; O'brien, J.; Pasquier, F.; Robert, P.; Rossor, M.; Salloway, S.; Stern, Y.; Visser, P.; Scheltens, P., Research criteria for the diagnosis of Alzheimer's disease: revising the NINCDS-ADRDA criteria. *Lancet Neurol* **2007,** *6* (8), 734-46.

Duyckaerts, C.; Hauw, J., Prevalence, incidence and duration of Braak's stages in the general population: can we know? *Neurobiol Aging* **1997,** *18* (4), 362-9; discussion 389-92.

Edison, P.; Okello, A.; Archer, H.; Hinz, R.; Fox, N.; Kennedy, A.; Rossor, M.; Brooks, D. J., Amyloid deposition and cerebral glucose metabolism in Alzheimer's disease: A longitudinal 11C-PIB and 18F-FDG PET study. *Journal of Neurology Neurosurgery and Psychiatry* **2007b,** *78* (2), 220-220.

Edison, P.; Archer, H.; Gerhard, A.; Hinz, R.; Pavese, N.; Turkheimer, F.; Hammers, A.; Tai, Y.; Fox, N.; Kennedy, A.; Rossor, M.; Brooks, D., Microglia, amyloid, and cognition in Alzheimer's disease: An [11C](R)PK11195-PET and [11C]PIB-PET study. *Neurobiol Dis* **2008a,** *32* (3), 412-9.

Edison, P.; Archer, H.; Hinz, R.; Hammers, A.; Pavese, N.; Tai, Y.; Hotton, G.; Cutler, D.; Fox, N.; Kennedy, A.; Rossor, M.; Brooks, D., Amyloid, hypometabolism, and cognition in Alzheimer disease: an [11C]PIB and [18F]FDG PET study. *Neurology* **2007a,** *68* (7), 501-8.

Edison, P.; Rowe, C.; Rinne, J.; Ng, S.; Ahmed, I.; Kemppainen, N.; Villemagne, V.; O'Keefe, G.; Någren, K.; Chaudhury, K.; Masters, C.; Brooks, D., Amyloid load in Parkinson's disease dementia and Lewy body dementia measured with [11C]PIB positron emission tomography. *J Neurol Neurosurg Psychiatry* **2008b,** *79* (12), 1331-8.

Engler, H.; Forsberg, A.; Almkvist, O.; Blomquist, G.; Larsson, E.; Savitcheva, I.; Wall, A.; Ringheim, A.; Langstrom, B.; Nordberg, A., Two-year follow-up of amyloid deposition in patients with Alzheimer's disease. *Brain* **2006,** *129*, 2856-2866.

Engler, H.; Santillo, A. F.; Wang, S. X.; Lindau, M.; Savitcheva, I.; Nordberg, A.; Lannfelt, L.; Langstrom, B.; Kilander, L., In vivo amyloid imaging with PET in frontotemporal dementia. *European Journal of Nuclear Medicine and Molecular Imaging* **2008,** *35* (1), 100-106.

Ewers, M.; Buerger, K.; Teipel, S.; Scheltens, P.; Schröder, J.; Zinkowski, R.; Bouwman, F.; Schönknecht, P.; Schoonenboom, N.; Andreasen, N.; Wallin, A.; DeBernardis, J.; Kerkman, D.; Heindl, B.; Blennow, K.; Hampel, H., Multicenter assessment of CSF-phosphorylated tau for the prediction of conversion of MCI. *Neurology* **2007,** *69* (24), 2205-12.

Ewers, M.; Zhong, Z.; Bürger, K.; Wallin, A.; Blennow, K.; Teipel, S.; Shen, Y.; Hampel, H., Increased CSF-BACE 1 activity is associated with ApoE-epsilon 4 genotype in subjects with mild cognitive impairment and Alzheimer's disease. *Brain* **2008,** *131* (Pt 5), 1252-8.

Fagan, A. M.; Mintun, M. A.; Mach, R. H.; Lee, S. Y.; Dence, C. S.; Shah, A. R.; LaRossa, G. N.; Spinner, M. L.; Klunk, W. E.; Mathis, C. A.; DeKosky, S. T.; Morris, J. C.; Holtzman, D. M., Inverse relation between in vivo amyloid imaging load and cerebrospinal fluid A beta(42) in humans. *Annals of Neurology* **2006,** *59* (3), 512-519.

Farrer, L.; Cupples, L.; Haines, J.; Hyman, B.; Kukull, W.; Mayeux, R.; Myers, R.; Pericak-Vance, M.; Risch, N.; van Duijn, C., Effects of age, sex, and ethnicity on the association between apolipoprotein E genotype and Alzheimer disease. A meta-analysis. APOE and Alzheimer Disease Meta Analysis Consortium. *JAMA* **1997,** *278* (16), 1349-56.

Fein, G.; Di Sclafani, V.; Tanabe, J.; Cardenas, V.; Weiner, M.; Jagust, W.; Reed, B.; Norman, D.; Schuff, N.; Kusdra, L.; Greenfield, T.; Chui, H., Hippocampal and cortical atrophy predict dementia in subcortical ischemic vascular disease. *Neurology* **2000,** *55* (11), 1626-35.

Ferri, C.; Prince, M.; Brayne, C.; Brodaty, H.; Fratiglioni, L.; Ganguli, M.; Hall, K.; Hasegawa, K.; Hendrie, H.; Huang, Y.; Jorm, A.; Mathers, C.; Menezes, P.;

Rimmer, E.; Scazufca, M., Global prevalence of dementia: a Delphi consensus study. *Lancet* **2005,** *366* (9503), 2112-7.

Fleisher, A.; Sowell, B.; Taylor, C.; Gamst, A.; Petersen, R.; Thal, L., Clinical predictors of progression to Alzheimer disease in amnestic mild cognitive impairment. *Neurology* **2007,** *68* (19), 1588-95.

Forsberg, A.; Engler, H.; Almkvist, O.; Blomquist, G.; Hagman, G.; Wall, A.; Ringheim, A.; Långström, B.; Nordberg, A., PET imaging of amyloid deposition in patients with mild cognitive impairment. *Neurobiol Aging* **2008,** *29* (10), 1456-65.

Friedland, R.; Kalaria, R.; Berridge, M.; Miraldi, F.; Hedera, P.; Reno, J.; Lyle, L.; Marotta, C., Neuroimaging of vessel amyloid in Alzheimer's disease. *Ann N Y Acad Sci* **1997,** *826*, 242-7.

Frisoni, G.; Lorenzi, M.; Caroli, A.; Kemppainen, N.; Någren, K.; Rinne, J., In vivo mapping of amyloid toxicity in Alzheimer disease. *Neurology* **2009,** *72* (17), 1504-11.

Friston K.J.; Worsley K.J.; Poline J.B.; Frith C.D.; Franckowiak R.S.J., Statistical parametric maps in functional brain imaging. A general approach. *Hum Brain Mapp* **1995,** *2*, 189-210.

Ganguli, M.; Dodge, H.; Shen, C.; DeKosky, S., Mild cognitive impairment, amnestic type: an epidemiologic study. *Neurology* **2004,** *63* (1), 115-21.

Gatz, M.; Pedersen, N.; Berg, S.; Johansson, B.; Johansson, K.; Mortimer, J.; Posner, S.; Viitanen, M.; Winblad, B.; Ahlbom, A., Heritability for Alzheimer's disease: the study of dementia in Swedish twins. *J Gerontol A Biol Sci Med Sci* **1997,** *52* (2), M117-25.

Gatz, M.; Reynolds, C.; Fratiglioni, L.; Johansson, B.; Mortimer, J.; Berg, S.; Fiske, A.; Pedersen, N., Role of genes and environments for explaining Alzheimer disease. *Arch Gen Psychiatry* **2006,** *63* (2), 168-74.

Gibson, G.; Haroutunian, V.; Zhang, H.; Park, L.; Shi, Q.; Lesser, M.; Mohs, R.; Sheu, R.; Blass, J., Mitochondrial damage in Alzheimer's disease varies with apolipoprotein E genotype. *Ann Neurol* **2000,** *48* (3), 297-303.

Gilman, S.; Koller, M.; Black, R.; Jenkins, L.; Griffith, S.; Fox, N.; Eisner, L.; Kirby, L.; Rovira, M.; Forette, F.; Orgogozo, J., Clinical effects of Abeta immunization (AN1792) in patients with AD in an interrupted trial. *Neurology* **2005,** *64* (9), 1553-62.

Gomperts, S.; Rentz, D.; Moran, E.; Becker, J.; Locascio, J.; Klunk, W.; Mathis, C.; Elmaleh, D.; Shoup, T.; Fischman, A.; Hyman, B.; Growdon, J.; Johnson, K., Imaging amyloid deposition in Lewy body diseases. *Neurology* **2008,** *71* (12), 903-10.

Graham, M.; Peterson, L.; Link, J.; Evans, M.; Rasey, J.; Koh, W.; Caldwell, J.; Krohn, K., Fluorine-18-fluoromisonidazole radiation dosimetry in imaging studies. *J Nucl Med* **1997,** *38* (10), 1631-6.

Grimmer, T.; Henriksen, G.; Wester, H.; Förstl, H.; Klunk, W.; Mathis, C.; Kurz, A.; Drzezga, A., Clinical severity of Alzheimer's disease is associated with PIB uptake in PET. *Neurobiol Aging* **2008,** *30* (12),1902-9.

Grimmer, T.; Riemenschneider, M.; Förstl, H.; Henriksen, G.; Klunk, W.; Mathis, C.; Shiga, T.; Wester, H.; Kurz, A.; Drzezga, A., Beta amyloid in Alzheimer's disease: increased deposition in brain is reflected in reduced concentration in cerebrospinal fluid. *Biol Psychiatry* **2009,** *65* (11), 927-34.

Haense, C.; Buerger, K.; Kalbe, E.; Drzezga, A.; Teipel, S.; Markiewicz, P.; Herholz, K.; Heiss, W.; Hampel, H., CSF total and phosphorylated tau protein, regional glucose metabolism and dementia severity in Alzheimer's disease. *Eur J Neurol* **2008,** *15* (11), 1155-62.

Hampel, H.; Bürger, K.; Teipel, S.; Bokde, A.; Zetterberg, H.; Blennow, K., Core candidate neurochemical and imaging biomarkers of Alzheimer's disease. *Alzheimers Dement* **2008,** *4* (1), 38-48.

Hampel, H.; Teipel, S.; Fuchsberger, T.; Andreasen, N.; Wiltfang, J.; Otto, M.; Shen, Y.; Dodel, R.; Du, Y.; Farlow, M.; Möller, H.; Blennow, K.; Buerger, K., Value of CSF beta-amyloid1-42 and tau as predictors of Alzheimer's disease in patients with mild cognitive impairment. *Mol Psychiatry* **2004,** *9* (7), 705-10.

Hansson, O.; Zetterberg, H.; Buchhave, P.; Londos, E.; Blennow, K.; Minthon, L., Association between CSF biomarkers and incipient Alzheimer's disease in patients with mild cognitive impairment: a follow-up study. *Lancet Neurol* **2006,** *5* (3), 228-34.

Hansson, O.; Zetterberg, H.; Vanmechelen, E.; Vanderstichele, H.; Andreasson, U.; Londos, E.; Wallin, A.; Minthon, L.; Blennow, K., Evaluation of plasma Abeta(40) and Abeta(42) as predictors of conversion to Alzheimer's disease in patients with mild cognitive impairment. *Neurobiol Aging* **2010**, *31*(3), 357-67.

Hardy, J., Amyloid, the presenilins and Alzheimer's disease. *Trends Neurosci* **1997,** *20* (4), 154-9.

Hardy, J.; Selkoe, D., The amyloid hypothesis of Alzheimer's disease: progress and problems on the road to therapeutics. *Science* **2002,** *297* (5580), 353-6.

Herholz, K., PET studies in dementia. *Ann Nucl Med* **2003,** *17* (2), 79-89.

Herholz, K.; Carter, S.; Jones, M., Positron emission tomography imaging in dementia. *Br J Radiol* **2007,** *80 Spec No 2*, S160-7.

Hof, P.; Bouras, C.; Perl, D.; Sparks, D.; Mehta, N.; Morrison, J., Age-related distribution of neuropathologic changes in the cerebral cortex of patients with Down's syndrome. Quantitative regional analysis and comparison with Alzheimer's disease. *Arch Neurol* **1995,** *52* (4), 379-91.

Hoffman, J.; Welsh-Bohmer, K.; Hanson, M.; Crain, B.; Hulette, C.; Earl, N.; Coleman, R., FDG PET imaging in patients with pathologically verified dementia. *J Nucl Med* **2000,** *41* (11), 1920-8.

Howell, R.; Wessels, B.; Loevinger, R.; Watson, E.; Bolch, W.; Brill, A.; Charkes, N.; Fisher, D.; Hays, M.; Robertson, J.; Siegel, J.; Thomas, S., The MIRD perspective 1999. Medical Internal Radiation Dose Committee. *J Nucl Med* **1999,** *40* (1), 3S-10S.

ICRP. *1990 Recommendations of the International Commission on RadiologicalProtection*. ICRP publication 60. Oxford, U.K.: Pergamon Press; **1991**.

Ikonomovic, M. D.; Klunk, W. E.; Abrahamson, E. E.; Mathis, C. A.; Price, J. C.; Tsopelas, N. D.; Lopresti, B. J.; Ziolko, S.; Bi, W. Z.; Paljug, W. R.; Debnath, M. L.; Hope, C. E.; Isanski, B. A.; Hamilton, R. L.; DeKosky, S. T., Post-mortem correlates of in vivo PiB-PET amyloid imaging in a typical case of Alzheimer's disease. *Brain* **2008,** *131*, 1630-1645.

Irizarry, M.; Deng, A.; Lleo, A.; Berezovska, O.; Von Arnim, C.; Martin-Rehrmann, M.; Manelli, A.; LaDu, M.; Hyman, B.; Rebeck, G., Apolipoprotein E modulates gamma-secretase cleavage of the amyloid precursor protein. *J Neurochem* **2004,** *90* (5), 1132-43.

Ishii, K.; Sakamoto, S.; Sasaki, M.; Kitagaki, H.; Yamaji, S.; Hashimoto, M.; Imamura, T.; Shimomura, T.; Hirono, N.; Mori, E., Cerebral glucose metabolism in patients with frontotemporal dementia. *J Nucl Med* **1998,** *39* (11), 1875-8.

Jack, C. R.; Lowe, V. J.; Senjem, M. L.; Weigand, S. D.; Kemp, B. J.; Shiung, M. M.; Knopman, D. S.; Boeve, B. F.; Klunk, W. E.; Mathis, C. A.; Petersen, R. C., C-II PiB and structural MRI provide complementary information in imaging of Alzheimers disease and amnestic mild cognitive impairment. *Brain* **2008,** *131*, 665-680.

Jack, C. J.; Lowe, V.; Weigand, S.; Wiste, H.; Senjem, M.; Knopman, D.; Shiung, M.; Gunter, J.; Boeve, B.; Kemp, B.; Weiner, M.; Petersen, R., Serial PIB and MRI in normal, mild cognitive impairment and Alzheimer's disease: implications for sequence of pathological events in Alzheimer's disease. *Brain* **2009,** *132* (Pt 5), 1355-65.

Jagust, W.; Friedland, R.; Budinger, T.; Koss, E.; Ober, B., Longitudinal studies of regional cerebral metabolism in Alzheimer's disease. *Neurology* **1988,** *38* (6), 909-12.

Järvenpää, T.; Laakso, M.; Rossi, R.; Koskenvuo, M.; Kaprio, J.; Räihä, I.; Kurki, T.; Laine, M.; Frisoni, G.; Rinne, J., Hippocampal MRI volumetry in cognitively discordant monozygotic twin pairs. *J Neurol Neurosurg Psychiatry* **2004,** *75* (1), 116-20.

Järvenpää, T.; Räihä, I.; Kaprio, J.; Koskenvuo, M.; Laine, M.; Kurki, T.; Vahlberg, T.; Viljanen, T.; Ahonen, K.; Rinne, J., Regional cerebral glucose metabolism in monozygotic twins discordant for Alzheimer's disease. *Dement Geriatr Cogn Disord* **2003,** *16* (4), 245-52.

Järvenpää, T.; Rinne, J.; Räihä, I.; Koskenvuo, M.; Löppönen, M.; Hinkka, S.; Kaprio, J., Characteristics of two telephone screens for cognitive impairment. *Dement Geriatr Cogn Disord* **2002,** *13* (3), 149-55.

Jellinger, K.; Attems, J., Prevalence of dementia disorders in the oldest-old: an autopsy study. *Acta Neuropathol* **2010,** *119* (4), 421-33.

Jellinger, K.; Seppi, K.; Wenning, G., Clinical and neuropathological correlates of Lewy body disease. *Acta Neuropathol* **2003,** *106* (2), 188-9; author reply 190.

Joachim, C.; Morris, J.; Selkoe, D., Diffuse senile plaques occur commonly in the cerebellum in Alzheimer's disease. *Am J Pathol* **1989,** *135* (2), 309-19.

Johansen, K.; White, L.; Sando, S.; Aasly, J., Biomarkers: Parkinson disease with dementia and dementia with Lewy bodies. *Parkinsonism Relat Disord* **2010**. Epub ahead of print.

Johansson, A.; Savitcheva, I.; Forsberg, A.; Engler, H.; Långström, B.; Nordberg, A.; Askmark, H., [(11)C]-PIB imaging in patients with Parkinson's disease: preliminary results. *Parkinsonism Relat Disord* **2008,** *14* (4), 345-7.

Johnson, A.; Jeppsson, F.; Sandell, J.; Wensbo, D.; Neelissen, J.; Juréus, A.; Ström, P.; Norman, H.; Farde, L.; Svensson, S., AZD2184: a radioligand for sensitive detection of beta-amyloid deposits. *J Neurochem* **2009,** *108* (5), 1177-86.

Johnson, K. A.; Gregas, M.; Becker, J. A.; Kinnecom, C.; Salat, D. H.; Moran, E. K.; Smith, E. E.; Rosand, J.; Rentz, D. M.; Klunk, W. E.; Mathis, C. A.; Price, J. C.; DeKosky, S. T.; Fischman, A. J.; Greenberg, S. M., Imaging of amyloid burden and distribution in cerebral amyloid angiopathy. *Annals of Neurology* **2007,** *62* (3), 229-234.

Jorm, A.; Jolley, D., The incidence of dementia: a meta-analysis. *Neurology* **1998,** *51* (3), 728-33.

Kaprio, J.; Koskenvuo, M., Genetic and environmental factors in complex diseases: the older Finnish Twin Cohort. *Twin Res* **2002,** *5* (5), 358-65.

Kato, H.; Yoshikawa, T.; Oku, N.; Imaizumi, M.; Takasawa, M.; Kimura, Y.; Kajimoto, K.; Tanaka, M.; Kitagawa, K.; Hori, M.; Hatazawa, J., Statistical parametric analysis of cerebral blood flow in vascular dementia with small-vessel disease using Tc-HMPAO SPECT. *Cerebrovasc Dis* **2008,** *26* (5), 556-62.

Kawachi, T.; Ishii, K.; Sakamoto, S.; Sasaki, M.; Mori, T.; Yamashita, F.; Matsuda, H.; Mori, E., Comparison of the diagnostic performance of FDG-PET and VBM-MRI in very mild Alzheimer's disease. *Eur J Nucl Med Mol Imaging* **2006,** *33* (7), 801-9.

Kemppainen, N. M.; Aalto, S.; Karrasch, M.; Nagren, K.; Savisto, N.; Konen, V.; Viitanen, M.; Parkkola, F.; Rinne, J. O., Cognitive reserve hypothesis: Pittsburgh Compound B and fluorodeoxyglucose positron emission tomography in relation to education in mild Alzheimer's disease. *Annals of Neurology* **2008,** *63* (1), 112-118.

Kemppainen, N.; Aalto, S.; Wilson, I.; Någren, K.; Helin, S.; Brück, A.; Oikonen, V.; Kailajärvi, M.; Scheinin, M.; Viitanen, M.; Parkkola, R.; Rinne, J., Voxel-based analysis of PET amyloid ligand [11C]PIB uptake in Alzheimer disease. *Neurology* **2006,** *67* (9), 1575-80.

Kemppainen, N.; Aalto, S.; Wilson, I.; Någren, K.; Helin, S.; Brück, A.; Oikonen, V.; Kailajärvi, M.; Scheinin, M.; Viitanen, M.; Parkkola, R.; Rinne, J., PET amyloid ligand [11C]PIB uptake is increased in

mild cognitive impairment. *Neurology* **2007,** *68* (19), 1603-6.

Khachaturian, A.; Corcoran, C.; Mayer, L.; Zandi, P.; Breitner, J., Apolipoprotein E epsilon4 count affects age at onset of Alzheimer disease, but not lifetime susceptibility: The Cache County Study. *Arch Gen Psychiatry* **2004,** *61* (5), 518-24.

Klunk, W. E.; Engler, H.; Nordberg, A.; Wang, Y. M.; Blomqvist, G.; Holt, D. P.; Bergstrom, M.; Savitcheva, I.; Huang, G. F.; Estrada, S.; Ausen, B.; Debnath, M. L.; Barletta, J.; Price, J. C.; Sandell, J.; Lopresti, B. J.; Wall, A.; Koivisto, P.; Antoni, G.; Mathis, C. A.; Langstrom, B., Imaging brain amyloid in Alzheimer's disease with Pittsburgh Compound-B. *Annals of Neurology* **2004,** *55* (3), 306-319.

Klunk, W.; Bacskai, B.; Mathis, C.; Kajdasz, S.; McLellan, M.; Frosch, M.; Debnath, M.; Holt, D.; Wang, Y.; Hyman, B., Imaging Abeta plaques in living transgenic mice with multiphoton microscopy and methoxy-X04, a systemically administered Congo red derivative. *J Neuropathol Exp Neurol* **2002,** *61* (9), 797-805.

Klunk, W.; Mathis, C., The future of amyloid-beta imaging: a tale of radionuclides and tracer proliferation. *Curr Opin Neurol* **2008,** *21* (6), 683-7.

Klunk, W.; Price, J.; Mathis, C.; Tsopelas, N.; Lopresti, B.; Ziolko, S.; Bi, W.; Hoge, J.; Cohen, A.; Ikonomovic, M.; Saxton, J.; Snitz, B.; Pollen, D.; Moonis, M.; Lippa, C.; Swearer, J.; Johnson, K.; Rentz, D.; Fischman, A.; Aizenstein, H.; DeKosky, S., Amyloid deposition begins in the striatum of presenilin-1 mutation carriers from two unrelated pedigrees. *J Neurosci* **2007,** *27* (23), 6174-84.

Klunk, W.; Wang, Y.; Huang, G.; Debnath, M.; Holt, D.; Mathis, C., Uncharged thioflavin-T derivatives bind to amyloid-beta protein with high affinity and readily enter the brain. *Life Sci* **2001,** *69* (13), 1471-84.

Klunk, W.; Wang, Y.; Huang, G.; Debnath, M.; Holt, D.; Shao, L.; Hamilton, R.; Ikonomovic, M.; DeKosky, S.; Mathis, C., The binding of 2-(4'-methylaminophenyl) benzothiazole to postmortem brain homogenates is dominated by the amyloid component. *J Neurosci* **2003,** *23* (6), 2086-92.

Koistinaho, M.; Lin, S.; Wu, X.; Esterman, M.; Koger, D.; Hanson, J.; Higgs, R.; Liu, F.; Malkani, S.; Bales, K.; Paul, S., Apolipoprotein E promotes astrocyte colocalization and degradation of deposited amyloid-beta peptides. *Nat Med* **2004,** *10* (7), 719-26.

Koivunen, J.; Pirttilä, T.; Kemppainen, N.; Aalto, S.; Herukka, S.; Jauhianen, A.; Hänninen, T.; Hallikainen, M.; Någren, K.; Rinne, J.; Soininen, H., PET amyloid ligand [11C]PIB uptake and cerebrospinal fluid beta-amyloid in mild cognitive impairment. *Dement Geriatr Cogn Disord* **2008a,** *26* (4), 378-83.

Koivunen, J.; Verkkoniemi, A.; Aalto, S.; Paetau, A.; Ahonen, J.; Viitanen, M.; Någren, K.; Rokka, J.; Haaparanta, M.; Kalimo, H.; Rinne, J., PET amyloid ligand [11C]PIB uptake shows predominantly striatal increase in variant Alzheimer's disease. *Brain* **2008b,** *131* (Pt 7), 1845-53.

Kreutzberg, G., Microglia: a sensor for pathological events in the CNS. *Trends Neurosci* **1996,** *19* (8), 312-8.

Kudo, Y.; Okamura, N.; Furumoto, S.; Tashiro, M.; Furukawa, K.; Maruyama, M.; Itoh, M.; Iwata, R.; Yanai, K.; Arai, H., 2-(2-[2-Dimethylaminothiazol-5-yl]ethenyl)-6- (2-[fluoro]ethoxy)benzoxazole: a novel PET agent for in vivo detection of dense amyloid plaques in Alzheimer's disease patients. *J Nucl Med* **2007,** *48* (4), 553-61.

Kung, M.; Hou, C.; Zhuang, Z.; Skovronsky, D.; Kung, H., Binding of two potential imaging agents targeting amyloid plaques in postmortem brain tissues of patients with Alzheimer's disease. *Brain Res* **2004,** *1025* (1-2), 98-105.

Lambert, J.; Amouyel, P., Genetic heterogeneity of Alzheimer's disease: complexity and advances. *Psychoneuroendocrinology* **2007,** *32 Suppl 1*, S62-70.

Larrieu, S.; Letenneur, L.; Orgogozo, J.; Fabrigoule, C.; Amieva, H.; Le Carret, N.; Barberger-Gateau, P.; Dartigues, J., Incidence and outcome of mild cognitive impairment in a population-based prospective cohort. *Neurology* **2002,** *59* (10), 1594-9.

Leinonen, V.; Alafuzoff, I.; Aalto, S.; Suotunen, T.; Savolainen, S.; Någren, K.; Tapiola, T.; Pirttilä, T.; Rinne, J.; Jääskeläinen, J.; Soininen, H.; Rinne, J., Assessment of beta-amyloid in a frontal cortical brain biopsy specimen and by positron emission tomography with carbon 11-labeled Pittsburgh Compound B. *Arch Neurol* **2008,** *65* (10), 1304-9.

Li, Y.; Rinne, J.; Mosconi, L.; Pirraglia, E.; Rusinek, H.; DeSanti, S.; Kemppainen, N.; Någren, K.; Kim, B.; Tsui, W.; de Leon, M., Regional analysis of FDG and PIB-PET images in normal aging, mild cognitive impairment, and Alzheimer's disease. *Eur J Nucl Med Mol Imaging* **2008,** *35* (12), 2169-81.

Likeman, M.; Anderson, V.; Stevens, J.; Waldman, A.; Godbolt, A.; Frost, C.; Rossor, M.; Fox, N., Visual assessment of atrophy on magnetic resonance imaging in the diagnosis of pathologically confirmed young-onset dementias. *Arch Neurol* **2005,** *62* (9), 1410-5.

Link, C.; Johnson, C.; Fonte, V.; Paupard, M.; Hall, D.; Styren, S.; Mathis, C.; Klunk, W., Visualization of fibrillar amyloid deposits in living, transgenic Caenorhabditis elegans animals using the sensitive amyloid dye, X-34. *Neurobiol Aging* **2001,** *22* (2), 217-26.

Lockhart, A.; Lamb, J.; Osredkar, T.; Sue, L.; Joyce, J.; Ye, L.; Libri, V.; Leppert, D.; Beach, T., PIB is a non-specific imaging marker of amyloid-beta (Abeta) peptide-related cerebral amyloidosis. *Brain* **2007,** *130* (Pt 10), 2607-15.

Logan, J., Graphical analysis of PET data applied to reversible and irreversible tracers. *Nucl Med Biol* **2000,** *27* (7), 661-70.

Logan, J.; Fowler, J.; Volkow, N.; Wang, G.; Ding, Y.; Alexoff, D., Distribution volume ratios without blood sampling from graphical analysis of PET data. *J Cereb Blood Flow Metab* **1996,** *16* (5), 834-40.

Logan, J.; Fowler, J.; Volkow, N.; Wolf, A.; Dewey, S.; Schlyer, D.; MacGregor, R.; Hitzemann, R.; Bendriem, B.; Gatley, S., Graphical analysis of reversible radioligand binding from time-activity measurements applied to [N-11C-methyl]-(-)-cocaine PET studies in human subjects. *J Cereb Blood Flow Metab* **1990,** *10* (5), 740-7.

Lopresti, B. J.; Klunk, W. E.; Mathis, C. A.; Hoge, J. A.; Ziolko, S. K.; Lu, X. L.; Meltzer, C. C.; Schimmel, K.; Tsopelas, N. D.; DeKosky, S. T.; Price, J. C., Simplified quantification of Pittsburgh compound B amyloid imaging PET studies: A comparative analysis. *Journal of Nuclear Medicine* **2005,** *46* (12), 1959-1972.

Lötjönen, J.; Wolz, R.; Koikkalainen, J.; Thurfjell, L.; Waldemar, G.; Soininen, H.; Rueckert, D., Fast and robust multi-atlas segmentation of brain magnetic resonance images. *Neuroimage* **2010,** *49* (3), 2352-65.

Lowe, V.; Kemp, B.; Jack, C. J.; Senjem, M.; Weigand, S.; Shiung, M.; Smith, G.; Knopman, D.; Boeve, B.; Mullan, B.; Petersen, R., Comparison of 18F-FDG and PiB PET in cognitive impairment. *J Nucl Med* **2009,** *50* (6), 878-86.

Maetzler, W.; Liepelt, I.; Reimold, M.; Reischl, G.; Solbach, C.; Becker, C.; Schulte, C.; Leyhe, T.; Keller, S.; Melms, A.; Gasser, T.; Berg, D., Cortical PIB binding in Lewy body disease is associated with Alzheimer-like characteristics. *Neurobiol Dis* **2009,** *34* (1), 107-12.

Maetzler, W.; Reimold, M.; Liepelt, I.; Solbach, C.; Leyhe, T.; Schweitzer, K.; Eschweiler, G.; Mittelbronn, M.; Gaenslen, A.; Uebele, M.; Reischl, G.; Gasser, T.; Machulla, H.; Bares, R.; Berg, D., [11C]PIB binding in Parkinson's disease dementia. *Neuroimage* **2008,** *39* (3), 1027-33.

Manelli, A.; Stine, W.; Van Eldik, L.; LaDu, M., ApoE and Abeta1-42 interactions: effects of isoform and conformation on structure and function. *J Mol Neurosci* **2004,** *23* (3), 235-46.

Markesbery, W.; Schmitt, F.; Kryscio, R.; Davis, D.; Smith, C.; Wekstein, D., Neuropathologic substrate of mild cognitive impairment. *Arch Neurol* **2006,** *63* (1), 38-46.

Martins, I.; Hone, E.; Foster, J.; Sünram-Lea, S.; Gnjec, A.; Fuller, S.; Nolan, D.; Gandy, S.; Martins, R., Apolipoprotein E, cholesterol metabolism, diabetes, and the convergence of risk factors for Alzheimer's disease and cardiovascular disease. *Mol Psychiatry* **2006,** *11* (8), 721-36.

Mathis, C.; Bacskai, B.; Kajdasz, S.; McLellan, M.; Frosch, M.; Hyman, B.; Holt, D.; Wang, Y.; Huang, G.; Debnath, M.; Klunk, W., A lipophilic thioflavin-T derivative for positron emission tomography (PET) imaging of amyloid in brain. *Bioorg Med Chem Lett* **2002,** *12* (3), 295-8.

Mathis, C.; Lopresti, B.; Klunk, W., Impact of amyloid imaging on drug development in Alzheimer's disease. *Nucl Med Biol* **2007,** *34* (7), 809-22.

Mathis, C.; Wang, Y.; Holt, D.; Huang, G.; Debnath, M.; Klunk, W., Synthesis and evaluation of 11C-labeled 6-substituted 2-arylbenzothiazoles as amyloid imaging agents. *J Med Chem* **2003,** *46* (13), 2740-54.

Matsuda, H., Role of neuroimaging in Alzheimer's disease, with emphasis on brain perfusion SPECT. *J Nucl Med* **2007,** *48* (8), 1289-300.

Mattsson, N.; Zetterberg, H.; Hansson, O.; Andreasen, N.; Parnetti, L.; Jonsson, M.; Herukka, S.; van der Flier, W.; Blankenstein, M.; Ewers, M.; Rich, K.; Kaiser, E.; Verbeek, M.; Tsolaki, M.; Mulugeta, E.; Rosén, E.; Aarsland, D.; Visser, P.; Schröder, J.; Marcusson, J.; de Leon, M.; Hampel, H.; Scheltens, P.; Pirttilä, T.; Wallin, A.; Jönhagen, M.; Minthon, L.; Winblad, B.; Blennow, K., CSF biomarkers and incipient Alzheimer disease in patients with mild cognitive impairment. *JAMA* **2009,** *302* (4), 385-93.

McEvoy, L.; Fennema-Notestine, C.; Roddey, J.; Hagler, D. J.; Holland, D.; Karow, D.; Pung, C.; Brewer, J.; Dale, A., Alzheimer disease: quantitative structural neuroimaging for detection and prediction of clinical and structural changes in mild cognitive impairment. *Radiology* **2009,** *251* (1), 195-205.

McGeer, P.; McGeer, E., Inflammation, autotoxicity and Alzheimer disease. *Neurobiol Aging* **2001,** *22* (6), 799-809.

McKeith, I.; Dickson, D.; Lowe, J.; Emre, M.; O'Brien, J.; Feldman, H.; Cummings, J.; Duda, J.; Lippa, C.; Perry, E.; Aarsland, D.; Arai, H.; Ballard, C.; Boeve, B.; Burn, D.; Costa, D.; Del Ser, T.; Dubois, B.; Galasko, D.; Gauthier, S.; Goetz, C.; Gomez-Tortosa, E.; Halliday, G.; Hansen, L.; Hardy, J.; Iwatsubo, T.; Kalaria, R.; Kaufer, D.; Kenny, R.; Korczyn, A.; Kosaka, K.; Lee, V.; Lees, A.; Litvan, I.; Londos, E.; Lopez, O.; Minoshima, S.; Mizuno, Y.; Molina, J.; Mukaetova-Ladinska, E.; Pasquier, F.; Perry, R.; Schulz, J.; Trojanowski, J.; Yamada, M., Diagnosis and management of dementia with Lewy bodies: third report of the DLB Consortium. *Neurology* **2005,** *65* (12), 1863-72.

McKhann, G.; Drachman, D.; Folstein, M.; Katzman, R.; Price, D.; Stadlan, E., Clinical diagnosis of Alzheimer's disease: report of the NINCDS-ADRDA Work Group under the auspices of Department of Health and Human Services Task Force on Alzheimer's Disease. *Neurology* **1984,** *34* (7), 939-44.

Meyer, M.; Tschanz, J.; Norton, M.; Welsh-Bohmer, K.; Steffens, D.; Wyse, B.; Breitner, J., APOE genotype predicts when--not whether--one is predisposed to develop Alzheimer disease. *Nat Genet* **1998,** *19* (4), 321-2.

Mielke, R.; Herholz, K.; Grond, M.; Kessler, J.; Heiss, W., Clinical deterioration in probable Alzheimer's disease correlates with progressive metabolic impairment of association areas. *Dementia* **1994,** *5* (1), 36-41.

Mikhno, A.; Devanand, D.; Pelton, G.; Cuasay, K.; Gunn, R.; Upton, N.; Lai, R.; Libri, V.; Mann, J.; Parsey, R., Voxel-based analysis of 11C-PIB scans for diagnosing Alzheimer's disease. *J Nucl Med* **2008,** *49* (8), 1262-9.

Minoshima, S.; Giordani, B.; Berent, S.; Frey, K.; Foster, N.; Kuhl, D., Metabolic reduction in the posterior cingulate cortex in very early Alzheimer's disease. *Ann Neurol* **1997,** *42* (1), 85-94.

Mintun, M. A.; LaRossa, G. N.; Sheline, Y. I.; Lee, S. Y.; Dence, C. S.; Robert, M. H.; Klunk, W. E.; Mathis, C. A.; DeKosky, S. T.; Morris, J. C., Distribution of [11C] PIB in a nondemented population: Implication for use as an antecedent marker of Alzheimer's disease. *Neuropsychopharmacology* **2005,** *30*, S223-S223.

Mintun, M.; Larossa, G.; Sheline, Y.; Dence, C.; Lee, S.; Mach, R.; Klunk, W.; Mathis, C.; DeKosky, S.; Morris, J., [11C]PIB in a nondemented population: potential antecedent marker of Alzheimer disease. *Neurology* **2006,** *67* (3), 446-52.

Misra, C.; Fan, Y.; Davatzikos, C., Baseline and longitudinal patterns of brain atrophy in MCI patients, and their use in prediction of short-term conversion to AD: results from ADNI. *Neuroimage* **2009,** *44* (4), 1415-22.

Miyata, M.; Smith, J., Apolipoprotein E allele-specific antioxidant activity and effects on cytotoxicity by oxidative insults and beta-amyloid peptides. *Nat Genet* **1996,** *14* (1), 55-61.

Moonis, M.; Swearer, J.; Dayaw, M.; St George-Hyslop, P.; Rogaeva, E.; Kawarai, T.; Pollen, D., Familial Alzheimer disease: decreases in CSF Abeta42 levels precede cognitive decline. *Neurology* **2005,** *65* (2), 323-5.

Mormino, E.; Kluth, J.; Madison, C.; Rabinovici, G.; Baker, S.; Miller, B.; Koeppe, R.; Mathis, C.; Weiner, M.; Jagust, W., Episodic memory loss is related to hippocampal-mediated beta-amyloid deposition in elderly subjects. *Brain* **2009,** *132* (Pt 5), 1310-23.

Morris, J.; Storandt, M.; Miller, J.; McKeel, D.; Price, J.; Rubin, E.; Berg, L., Mild cognitive impairment represents early-stage Alzheimer disease. *Arch Neurol* **2001,** *58* (3), 397-405.

Morris, J..C.; Roe C.M.; Xiong C.; Fagan A.M.; Goate A.M.; Holtzman D.M.; Mintun M.A., APOE predicts amyloid-beta but not tau Alzheimer pathology in cognitively normal aging. *Ann Neurol* **2010,** *67* (1), 122-31.

Mosconi, L., Brain glucose metabolism in the early and specific diagnosis of Alzheimer's disease. FDG-PET studies in MCI and AD. *Eur J Nucl Med Mol Imaging* **2005,** *32* (4), 486-510.

Mosconi, L.; Brys, M.; Glodzik-Sobanska, L.; De Santi, S.; Rusinek, H.; de Leon, M., Early detection of Alzheimer's disease using neuroimaging. *Exp Gerontol* **2007,** *42* (1-2), 129-38.

Mosconi, L.; Perani, D.; Sorbi, S.; Herholz, K.; Nacmias, B.; Holthoff, V.; Salmon, E.; Baron, J.; De Cristofaro, M.; Padovani, A.; Borroni, B.; Franceschi, M.; Bracco, L.; Pupi, A., MCI conversion to dementia and the APOE genotype: a prediction study with FDG-PET. *Neurology* **2004,** *63* (12), 2332-40.

Näslund, J.; Haroutunian, V.; Mohs, R.; Davis, K.; Davies, P.; Greengard, P.; Buxbaum, J., Correlation between elevated levels of amyloid beta-peptide in the brain and cognitive decline. *JAMA* **2000,** *283* (12), 1571-7.

Nelissen, N.; Van Laere, K.; Thurfjell, L.; Owenius, R.; Vandenbulcke, M.; Koole, M.; Bormans, G.; Brooks, D.; Vandenberghe, R., Phase 1 Study of the Pittsburgh Compound B Derivative 18F-Flutemetamol in Healthy Volunteers and Patients with Probable Alzheimer Disease. *J Nucl Med* **2009,** *50* (8), 1251-1259.

Nestor, P.; Graham, N.; Fryer, T.; Williams, G.; Patterson, K.; Hodges, J., Progressive non-fluent aphasia is associated with hypometabolism centred on the left anterior insula. *Brain* **2003,** *126* (Pt 11), 2406-18.

Newberg, A.; Wintering, N.; Plössl, K.; Hochold, J.; Stabin, M.; Watson, M.; Skovronsky, D.; Clark, C.; Kung, M.; Kung, H., Safety, biodistribution, and dosimetry of 123I-IMPY: a novel amyloid plaque-imaging agent for the diagnosis of Alzheimer's disease. *J Nucl Med* **2006,** *47* (5), 748-54.

Ng, S.; Villemagne, V.; Masters, C.; Rowe, C., Evaluating atypical dementia syndromes using positron emission tomography with carbon 11 labeled Pittsburgh Compound B. *Arch Neurol* **2007b,** *64* (8), 1140-4.

Ng, S.; Villemagne, V.; Berlangieri, S.; Lee, S.; Cherk, M.; Gong, S.; Ackermann, U.; Saunder, T.; Tochon-Danguy, H.; Jones, G.; Smith, C.; O'Keefe, G.; Masters, C.; Rowe, C., Visual assessment versus quantitative assessment of 11C-PIB PET and 18F-FDG PET for detection of Alzheimer's disease. *J Nucl Med* **2007a,** *48* (4), 547-52.

Nordberg, A., PET imaging of amyloid in Alzheimer's disease. *Lancet Neurology* **2004,** *3* (9), 519-527.

O'Keefe, G.; Saunder, T.; Ng, S.; Ackerman, U.; Tochon-Danguy, H.; Chan, J.; Gong, S.; Dyrks, T.; Lindemann, S.; Holl, G.; Dinkelborg, L.; Villemagne, V.; Rowe, C., Radiation dosimetry of beta-amyloid tracers 11C-PiB and 18F-BAY94-9172. *J Nucl Med* **2009,** *50* (2), 309-15.

Oinas, M.; Polvikoski, T.; Sulkava, R.; Myllykangas, L.; Juva, K.; Notkola, I.; Rastas, S.; Niinistö, L.; Kalimo, H.; Paetau, A., Neuropathologic findings of dementia with lewy bodies (DLB) in a population-based Vantaa 85+ study. *J Alzheimers Dis* **2009,** *18* (3), 677-89.

Okello, A.; Edison, P.; Archer, H.; Turkheimer, F.; Kennedy, J.; Bullock, R.; Walker, Z.; Kennedy, A.; Fox, N.; Rossor, M.; Brooks, D., Microglial activation and amyloid deposition in mild cognitive impairment: a PET study. *Neurology* **2009a,** *72* (1), 56-62.

Okello, A.; Koivunen, J.; Edison, P.; Archer, H.; Turkheimer, F.; Någren, K.; Bullock, R.; Walker, Z.; Kennedy, A.; Fox, N.; Rossor, M.; Rinne, J.; Brooks, D., Conversion of amyloid positive and negative MCI to AD over 3 years. An 11C-PIB PET study. *Neurology* **2009b,** *73* (10), 744-5.

Olichney, J.; Hansen, L.; Galasko, D.; Saitoh, T.; Hofstetter, C.; Katzman, R.; Thal, L., The apolipoprotein E epsilon 4 allele is associated with increased neuritic plaques and cerebral amyloid angiopathy in Alzheimer's disease and Lewy body variant. *Neurology* **1996,** *47* (1), 190-6.

Parsey, R.; Sokol, L.; Bélanger, M.; Kumar, J.; Simpson, N.; Wang, T.; Pratap, M.; Van Heertum, R.; John Mann, J., Amyloid plaque imaging agent [C-11]-6-OH-BTA-1: biodistribution and radiation dosimetry in baboon. *Nucl Med Commun* **2005,** *26* (10), 875-80.

Patlak, C.; Blasberg, R.; Fenstermacher, J., Graphical evaluation of blood-to-brain transfer constants from multiple-time uptake data. *J Cereb Blood Flow Metab* **1983,** *3* (1), 1-7.

Patwardhan, M.; McCrory, D.; Matchar, D.; Samsa, G.; Rutschmann, O., Alzheimer disease: operating characteristics of PET--a meta-analysis. *Radiology* **2004,** *231* (1), 73-80.

Pedersen, N.; Gatz, M.; Berg, S.; Johansson, B., How heritable is Alzheimer's disease late in life? Findings from Swedish twins. *Ann Neurol* **2004,** *55* (2), 180-5.

Petersen, R., Mild cognitive impairment: transition between aging and Alzheimer's disease. *Neurologia* **2000,** *15* (3), 93-101.

Petersen, R., Mild cognitive impairment as a diagnostic entity. *J Intern Med* **2004,** *256* (3), 183-94.

Petersen, R.; Doody, R.; Kurz, A.; Mohs, R.; Morris, J.; Rabins, P.; Ritchie, K.; Rossor, M.; Thal, L.; Winblad, B., Current concepts in mild cognitive impairment. *Arch Neurol* **2001,** *58* (12), 1985-92.

Petersen, R.; Parisi, J.; Dickson, D.; Johnson, K.; Knopman, D.; Boeve, B.; Jicha, G.; Ivnik, R.; Smith, G.; Tangalos, E.; Braak, H.; Kokmen, E., Neuropathologic features of amnestic mild cognitive impairment. *Arch Neurol* **2006,** *63* (5), 665-72.

Pike, K. E.; Savage, G.; Villemagne, V. L.; Ng, S.; Moss, S. A.; Maruff, P.; Mathis, C. A.; Klunk, W. E.; Masters, C. L.; Rowe, C. C., beta-amyloid imaging and memory in non-demented individuals: evidence for preclinical Alzheimer's disease. *Brain* **2007,** *130*, 2837-2844.

Polvikoski, T.; Sulkava, R.; Haltia, M.; Kainulainen, K.; Vuorio, A.; Verkkoniemi, A.; Niinistö, L.; Halonen, P.; Kontula, K., Apolipoprotein E, dementia, and cortical deposition of beta-amyloid protein. *N Engl J Med* **1995,** *333* (19), 1242-7.

Polvikoski, T.; Sulkava, R.; Rastas, S.; Sutela, A.; Niinistö, L.; Notkola, I.; Verkkoniemi, A.; Viramo, P.; Juva, K.; Haltia, M., Incidence of dementia in very elderly individuals: a clinical, neuropathological and molecular genetic study. *Neuroepidemiology* **2006,** *26* (2), 76-82.

Price, J. C.; Klunk, W. E.; Lopresti, B. J.; Lu, X. L.; Hoge, J. A.; Ziolko, S. K.; Holt, D. P.; Meltzer, C. C.; DeKosky, S. T.; Mathis, C. A., Kinetic modeling of amyloid binding in humans using PET imaging and Pittsburgh Compound-B. *Journal of Cerebral Blood Flow and Metabolism* **2005,** *25* (11), 1528-1547.

Price, J.; Davis, P.; Morris, J.; White, D., The distribution of tangles, plaques and related immunohistochemical markers in healthy aging and Alzheimer's disease. *Neurobiol Aging* **1991,** *12* (4), 295-312.

Price, J.; McKeel, D. J.; Buckles, V.; Roe, C.; Xiong, C.; Grundman, M.; Hansen, L.; Petersen, R.; Parisi, J.; Dickson, D.; Smith, C.; Davis, D.; Schmitt, F.; Markesbery, W.; Kaye, J.; Kurlan, R.; Hulette, C.; Kurland, B.; Higdon, R.; Kukull, W.; Morris, J., Neuropathology of nondemented aging: presumptive evidence for preclinical Alzheimer disease. *Neurobiol Aging* **2009,** *30* (7), 1026-36.

Price, J.; Morris, J., Tangles and plaques in nondemented aging and "preclinical" Alzheimer's disease. *Ann Neurol* **1999,** *45* (3), 358-68.

Rabinovici, G.; Furst, A.; O'Neil, J.; Racine, C.; Mormino, E.; Baker, S.; Chetty, S.; Patel, P.; Pagliaro, T.; Klunk, W.; Mathis, C.; Rosen, H.; Miller, B.; Jagust, W., 11C-PIB PET imaging in Alzheimer disease and frontotemporal lobar degeneration. *Neurology* **2007,** *68* (15), 1205-12.

Raiha, I.; Kaprio, J.; Koskenvuo, M.; Rajala, T.; Sourander, L., Alzheimer's disease in Finnish twins. *Lancet* **1996,** *347* (9001), 573-8.

Raji, C.; Becker, J.; Tsopelas, N.; Price, J.; Mathis, C.; Saxton, J.; Lopresti, B.; Hoge, J.; Ziolko, S.; DeKosky, S.; Klunk, W., Characterizing regional correlation, laterality and symmetry of amyloid deposition in mild cognitive impairment and Alzheimer's disease with Pittsburgh Compound B. *J Neurosci Methods* **2008,** *172* (2), 277-82.

Raji, C.A.; Lopez O.L.; Kuller L.H.; Carmichael O.T.; Becker, J.T., Age, Alzheimer disease, and brain structure. *Neurology* **2009,** *73* (22), 1899-905.

Ray, S.; Britschgi, M.; Herbert, C.; Takeda-Uchimura, Y.; Boxer, A.; Blennow, K.; Friedman, L.; Galasko, D.; Jutel, M.; Karydas, A.; Kaye, J.; Leszek, J.; Miller, B.; Minthon, L.; Quinn, J.; Rabinovici, G.; Robinson, W.; Sabbagh, M.; So, Y.; Sparks, D.; Tabaton, M.; Tinklenberg, J.; Yesavage, J.; Tibshirani, R.; Wyss-Coray, T., Classification and prediction of clinical Alzheimer's diagnosis based on plasma signaling proteins. *Nat Med* **2007,** *13* (11), 1359-62.

Razifar, P.; Ringheim, A.; Engler, H.; Hall, H.; Långström, B., Masked-Volume-Wise PCA and "reference Logan" illustrate similar regional differences in kinetic behavior in human brain PET study using [11C]-PIB. *BMC Neurol* **2009,** *9*, 2.

Reiman, E.; Caselli, R.; Yun, L.; Chen, K.; Bandy, D.; Minoshima, S.; Thibodeau, S.; Osborne, D., Preclinical evidence of Alzheimer's disease in persons homozygous for the epsilon 4 allele for apolipoprotein E. *N Engl J Med* **1996,** *334* (12), 752-8.

Reiman, E.; Chen, K.; Liu, X.; Bandy, D.; Yu, M.; Lee, W.; Ayutyanont, N.; Keppler, J.; Reeder, S.; Langbaum, J.; Alexander, G.; Klunk, W.; Mathis, C.; Price, J.; Aizenstein, H.; DeKosky, S.; Caselli, R., Fibrillar amyloid-beta burden in cognitively normal people at 3 levels of genetic risk for Alzheimer's disease. *Proc Natl Acad Sci U S A* **2009,** *106* (16), 6820-5.

Reitz, C.; Mayeux, R., Endophenotypes in normal brain morphology and Alzheimer's disease: a review. *Neuroscience* **2009,** *164* (1), 174-90.

Remes, A.; Laru, L.; Tuominen, H.; Aalto, S.; Kemppainen, N.; Mononen, H.; Någren, K.; Parkkola, R.; Rinne, J., Carbon 11-labeled pittsburgh compound

B positron emission tomographic amyloid imaging in patients with APP locus duplication. *Arch Neurol* **2008,** *65* (4), 540-4.

Resende, R.; Pereira, C.; Agostinho, P.; Vieira, A.; Malva, J.; Oliveira, C., Susceptibility of hippocampal neurons to Abeta peptide toxicity is associated with perturbation of Ca2+ homeostasis. *Brain Res* **2007,** *1143*, 11-21.

Ridha, B.; Barnes, J.; Bartlett, J.; Godbolt, A.; Pepple, T.; Rossor, M.; Fox, N., Tracking atrophy progression in familial Alzheimer's disease: a serial MRI study. *Lancet Neurol* **2006,** *5* (10), 828-34.

Riemenschneider, M.; Lautenschlager, N.; Wagenpfeil, S.; Diehl, J.; Drzezga, A.; Kurz, A., Cerebrospinal fluid tau and beta-amyloid 42 proteins identify Alzheimer disease in subjects with mild cognitive impairment. *Arch Neurol* **2002,** *59* (11), 1729-34.

Ries, M.; Carlsson, C.; Rowley, H.; Sager, M.; Gleason, C.; Asthana, S.; Johnson, S., Magnetic resonance imaging characterization of brain structure and function in mild cognitive impairment: a review. *J Am Geriatr Soc* **2008,** *56* (5), 920-34.

Rinne, J.; Brooks, D.; Rossor, M.; Fox, N.; Bullock, R.; Klunk, W.; Mathis, C.; Blennow, K.; Barakos, J.; Okello, A.; Rodriguez Martinez de Liano, S.; Liu, E.; Koller, M.; Gregg, K.; Schenk, D.; Black, R.; Grundman, M., 11C-PiB PET assessment of change in fibrillar amyloid-beta load in patients with Alzheimer's disease treated with bapineuzumab: a phase 2, double-blind, placebo-controlled, ascending-dose study. *Lancet Neurol* **2010,** *9* (4), 363-72.

Rinne, J.; Någren, K., Positron emission tomography in at risk patients and in the progression of mild cognitive impairment to Alzheimer's disease. *J Alzheimers Dis* **2010,** *19* (1), 291-300.

Ritchie, K.; Dupuy, A., The current status of apo E4 as a risk factor for Alzheimer's disease: an epidemiological perspective. *Int J Geriatr Psychiatry* **1999,** *14* (9), 695-700.

Roder, S.; Danober, L.; Pozza, M.; Lingenhoehl, K.; Wiederhold, K.; Olpe, H., Electrophysiological studies on the hippocampus and prefrontal cortex assessing the effects of amyloidosis in amyloid precursor protein 23 transgenic mice. *Neuroscience* **2003,** *120* (3), 705-20.

Rovelet-Lecrux, A.; Hannequin, D.; Raux, G.; Le Meur, N.; Laquerrière, A.; Vital, A.; Dumanchin, C.; Feuillette, S.; Brice, A.; Vercelletto, M.; Dubas, F.; Frebourg, T.; Campion, D., APP locus duplication causes autosomal dominant early-onset Alzheimer disease with cerebral amyloid angiopathy. *Nat Genet* **2006,** *38* (1), 24-6.

Rowe, C.; Ackerman, U.; Browne, W.; Mulligan, R.; Pike, K.; O'Keefe, G.; Tochon-Danguy, H.; Chan, G.; Berlangieri, S.; Jones, G.; Dickinson-Rowe, K.; Kung, H.; Zhang, W.; Kung, M.; Skovronsky, D.; Dyrks, T.; Holl, G.; Krause, S.; Friebe, M.; Lehman, L.; Lindemann, S.; Dinkelborg, L.; Masters, C.; Villemagne, V., Imaging of amyloid beta in Alzheimer's disease with 18F-BAY94-9172, a novel PET tracer: proof of mechanism. *Lancet Neurol* **2008,** *7* (2), 129-35.

Rowe, C.; Ng, S.; Ackermann, U.; Gong, S.; Pike, K.; Savage, G.; Cowie, T.; Dickinson, K.; Maruff, P.; Darby, D.; Smith, C.; Woodward, M.; Merory, J.; Tochon-Danguy, H.; O'Keefe, G.; Klunk, W.; Mathis, C.; Price, J.; Masters, C.; Villemagne, V., Imaging beta-amyloid burden in aging and dementia. *Neurology* **2007,** *68* (20), 1718-25.

Sarna, S.; Kaprio, J.; Sistonen, P.; Koskenvuo, M., Diagnosis of twin zygosity by mailed questionnaire. *Hum Hered* **1978,** *28* (4), 241-54.

Scheltens, P.; Leys, D.; Barkhof, F.; Huglo, D.; Weinstein, H.; Vermersch, P.; Kuiper, M.; Steinling, M.; Wolters, E.; Valk, J., Atrophy of medial temporal lobes on MRI in "probable" Alzheimer's disease and normal ageing: diagnostic value and neuropsychological correlates. *J Neurol Neurosurg Psychiatry* **1992,** *55* (10), 967-72.

Schmechel, D.; Saunders, A.; Strittmatter, W.; Crain, B.; Hulette, C.; Joo, S.; Pericak-Vance, M.; Goldgaber, D.; Roses, A., Increased amyloid beta-peptide deposition in cerebral cortex as a consequence of apolipoprotein E genotype in late-onset Alzheimer disease. *Proc Natl Acad Sci U S A* **1993,** *90* (20), 9649-53.

Schuff, N.; Woerner, N.; Boreta, L.; Kornfield, T.; Shaw, L.; Trojanowski, J.; Thompson, P.; Jack, C. J.; Weiner, M., MRI of hippocampal volume loss in early Alzheimer's disease in relation to ApoE genotype and biomarkers. *Brain* **2009,** *132* (Pt 4), 1067-77.

Shoghi-Jadid, K.; Small, G.; Agdeppa, E.; Kepe, V.; Ercoli, L.; Siddarth, P.; Read, S.; Satyamurthy, N.; Petric, A.; Huang, S.; Barrio, J., Localization of neurofibrillary tangles and beta-amyloid plaques in the brains of living patients with Alzheimer disease. *Am J Geriatr Psychiatry* **2002,** *10* (1), 24-35.

Silbert, L.; Quinn, J.; Moore, M.; Corbridge, E.; Ball, M.; Murdoch, G.; Sexton, G.; Kaye, J., Changes in premorbid brain volume predict Alzheimer's disease pathology. *Neurology* **2003,** *61* (4), 487-92.

Silverman, D., Brain 18F-FDG PET in the diagnosis of neurodegenerative dementias: comparison with perfusion SPECT and with clinical evaluations lacking nuclear imaging. *J Nucl Med* **2004,** *45* (4), 594-607.

Silverman, D.; Small, G.; Chang, C.; Lu, C.; Kung De Aburto, M.; Chen, W.; Czernin, J.; Rapoport, S.; Pietrini, P.; Alexander, G.; Schapiro, M.; Jagust, W.; Hoffman, J.; Welsh-Bohmer, K.; Alavi, A.; Clark, C.; Salmon, E.; de Leon, M.; Mielke, R.; Cummings, J.; Kowell, A.; Gambhir, S.; Hoh, C.; Phelps, M., Positron emission tomography in evaluation of dementia: Regional brain metabolism and long-term outcome. *JAMA* **2001,** *286* (17), 2120-7.

Sleegers, K.; Brouwers, N.; Gijselinck, I.; Theuns, J.; Goossens, D.; Wauters, J.; Del-Favero, J.; Cruts, M.; van Duijn, C.; Van Broeckhoven, C., APP duplication is sufficient to cause early onset Alzheimer's dementia with cerebral amyloid angiopathy. *Brain* **2006,** *129* (Pt 11), 2977-83.

Small, G.; Ercoli, L.; Silverman, D.; Huang, S.; Komo, S.; Bookheimer, S.; Lavretsky, H.; Miller,

K.; Siddarth, P.; Rasgon, N.; Mazziotta, J.; Saxena, S.; Wu, H.; Mega, M.; Cummings, J.; Saunders, A.; Pericak-Vance, M.; Roses, A.; Barrio, J.; Phelps, M., Cerebral metabolic and cognitive decline in persons at genetic risk for Alzheimer's disease. *Proc Natl Acad Sci U S A* **2000,** *97* (11), 6037-42.

Small, G.; Kepe, V.; Ercoli, L.; Siddarth, P.; Bookheimer, S.; Miller, K.; Lavretsky, H.; Burggren, A.; Cole, G.; Vinters, H.; Thompson, P.; Huang, S.; Satyamurthy, N.; Phelps, M.; Barrio, J., PET of brain amyloid and tau in mild cognitive impairment. *N Engl J Med* **2006,** *355* (25), 2652-63.

Small, G.; Mazziotta, J.; Collins, M.; Baxter, L.; Phelps, M.; Mandelkern, M.; Kaplan, A.; La Rue, A.; Adamson, C.; Chang, L., Apolipoprotein E type 4 allele and cerebral glucose metabolism in relatives at risk for familial Alzheimer disease. *JAMA* **1995,** *273* (12), 942-7.

Smith, G.; de Leon, M.; George, A.; Kluger, A.; Volkow, N.; McRae, T.; Golomb, J.; Ferris, S.; Reisberg, B.; Ciaravino, J., Topography of cross-sectional and longitudinal glucose metabolic deficits in Alzheimer's disease. Pathophysiologic implications. *Arch Neurol* **1992,** *49* (11), 1142-50.

Snyder W.S.; Cook M.J.; Nasset E.S.; Karhausen L.R.; Howells G.P.; Tipton I.H., *Report of the Task Group on Reference Man*. New York, NY: Pergamon Press; **1974**.

Sotthibundhu, A.; Sykes, A.; Fox, B.; Underwood, C.; Thangnipon, W.; Coulson, E., Beta-amyloid(1-42) induces neuronal death through the p75 neurotrophin receptor. *J Neurosci* **2008,** *28* (15), 3941-6.

Stabin, M., MIRDOSE: personal computer software for internal dose assessment in nuclear medicine. *J Nucl Med* **1996,** *37* (3), 538-46.

Strittmatter, W.; Saunders, A.; Goedert, M.; Weisgraber, K.; Dong, L.; Jakes, R.; Huang, D.; Pericak-Vance, M.; Schmechel, D.; Roses, A., Isoform-specific interactions of apolipoprotein E with microtubule-associated protein tau: implications for Alzheimer disease. *Proc Natl Acad Sci U S A* **1994,** *91* (23), 11183-6.

Strittmatter, W.; Saunders, A.; Schmechel, D.; Pericak-Vance, M.; Enghild, J.; Salvesen, G.; Roses, A., Apolipoprotein E: high-avidity binding to beta-amyloid and increased frequency of type 4 allele in late-onset familial Alzheimer disease. *Proc Natl Acad Sci U S A* **1993,** *90* (5), 1977-81.

Strozyk, D.; Blennow, K.; White, L.; Launer, L., CSF Abeta 42 levels correlate with amyloid-neuropathology in a population-based autopsy study. *Neurology* **2003,** *60* (4), 652-6.

Styren, S.; Hamilton, R.; Styren, G.; Klunk, W., X-34, a fluorescent derivative of Congo red: a novel histochemical stain for Alzheimer's disease pathology. *J Histochem Cytochem* **2000,** *48* (9), 1223-32.

Suemoto, T.; Okamura, N.; Shiomitsu, T.; Suzuki, M.; Shimadzu, H.; Akatsu, H.; Yamamoto, T.; Kudo, Y.; Sawada, T., In vivo labeling of amyloid with BF-108. *Neurosci Res* **2004,** *48* (1), 65-74.

Sultana, R.; Perluigi, M.; Butterfield, D., Oxidatively modified proteins in Alzheimer's disease (AD), mild cognitive impairment and animal models of AD: role of Abeta in pathogenesis. *Acta Neuropathol* **2009,** *118* (1), 131-50.

Sunderland, T.; Linker, G.; Mirza, N.; Putnam, K.; Friedman, D.; Kimmel, L.; Bergeson, J.; Manetti, G.; Zimmermann, M.; Tang, B.; Bartko, J.; Cohen, R., Decreased beta-amyloid1-42 and increased tau levels in cerebrospinal fluid of patients with Alzheimer disease. *JAMA* **2003,** *289* (16), 2094-103.

Sunderland, T.; Mirza, N.; Putnam, K.; Linker, G.; Bhupali, D.; Durham, R.; Soares, H.; Kimmel, L.; Friedman, D.; Bergeson, J.; Csako, G.; Levy, J.; Bartko, J.; Cohen, R., Cerebrospinal fluid beta-amyloid1-42 and tau in control subjects at risk for Alzheimer's disease: the effect of APOE epsilon4 allele. *Biol Psychiatry* **2004,** *56* (9), 670-6.

Suotunen, T.; Hirvonen, J.; Immonen-Räihä, P.; Aalto, S.; Lisinen, I.; Arponen, E.; Teräs, M.; Koski, K.; Sulkava, R.; Seppänen, M.; Rinne, J., Visual assessment of [(11) C]PIB PET in patients with cognitive impairment. *Eur J Nucl Med Mol Imaging* **2010**. Epub ahead of print.

Svedberg, M.; Hall, H.; Hellström-Lindahl, E.; Estrada, S.; Guan, Z.; Nordberg, A.; Långström, B., [(11) C]PIB-amyloid binding and levels of Abeta40 and Abeta42 in postmortem brain tissue from Alzheimer patients. *Neurochem Int* **2009,** *54* (5-6), 347-57.

Tapiola, T.; Pirttilä, T.; Mikkonen, M.; Mehta, P.; Alafuzoff, I.; Koivisto, K.; Soininen, H., Three-year follow-up of cerebrospinal fluid tau, beta-amyloid 42 and 40 concentrations in Alzheimer's disease. *Neurosci Lett* **2000,** *280* (2), 119-22.

Tenovuo, O.; Kemppainen, N.; Aalto, S.; Någren, K.; Rinne, J., Posterior cortical atrophy: a rare form of dementia with in vivo evidence of amyloid-beta accumulation. *J Alzheimers Dis* **2008,** *15* (3), 351-5.

Terwel, D.; Muyllaert, D.; Dewachter, I.; Borghgraef, P.; Croes, S.; Devijver, H.; Van Leuven, F., Amyloid activates GSK-3beta to aggravate neuronal tauopathy in bigenic mice. *Am J Pathol* **2008,** *172* (3), 786-98.

Thal, D.; Rüb, U.; Orantes, M.; Braak, H., Phases of A beta-deposition in the human brain and its relevance for the development of AD. *Neurology* **2002,** *58* (12), 1791-800.

Theuns, J.; Brouwers, N.; Engelborghs, S.; Sleegers, K.; Bogaerts, V.; Corsmit, E.; De Pooter, T.; van Duijn, C.; De Deyn, P.; Van Broeckhoven, C., Promoter mutations that increase amyloid precursor-protein expression are associated with Alzheimer disease. *Am J Hum Genet* **2006,** *78* (6), 936-46.

Tzourio-Mazoyer, N.; Landeau, B.; Papathanassiou, D.; Crivello, F.; Etard, O.; Delcroix, N.; Mazoyer, B.; Joliot, M., Automated anatomical labeling of activations in SPM using a macroscopic anatomical parcellation of the MNI MRI single-subject brain. *Neuroimage* **2002,** *15* (1), 273-89.

van de Pol, L.; Hensel, A.; Barkhof, F.; Gertz, H.; Scheltens, P.; van der Flier, W., Hippocampal atrophy

in Alzheimer disease: age matters. *Neurology* **2006,** *66* (2), 236-8.

Vehmas, A.; Kawas, C.; Stewart, W.; Troncoso, J., Immune reactive cells in senile plaques and cognitive decline in Alzheimer's disease. *Neurobiol Aging 24* (2), 321-31.

Verhoeff, N.; Wilson, A.; Takeshita, S.; Trop, L.; Hussey, D.; Singh, K.; Kung, H.; Kung, M.; Houle, S., In-vivo imaging of Alzheimer disease beta-amyloid with [11C]SB-13 PET. *Am J Geriatr Psychiatry* **2004,** *12* (6), 584-95.

Versijpt, J.; Dumont, F.; Van Laere, K.; Decoo, D.; Santens, P.; Audenaert, K.; Achten, E.; Slegers, G.; Dierckx, R.; Korf, J., Assessment of neuroinflammation and microglial activation in Alzheimer's disease with radiolabelled PK11195 and single photon emission computed tomography. A pilot study. *Eur Neurol* **2003,** *50* (1), 39-47.

Villemagne, V.; McLean, C.; Reardon, K.; Boyd, A.; Lewis, V.; Klug, G.; Jones, G.; Baxendale, D.; Masters, C.; Rowe, C.; Collins, S., 11C-PiB PET studies in typical sporadic Creutzfeldt-Jakob disease. *J Neurol Neurosurg Psychiatry* **2009**, *80* (9), 998-1001.

Villemagne, V.; Pike, K.; Darby, D.; Maruff, P.; Savage, G.; Ng, S.; Ackermann, U.; Cowie, T.; Currie, J.; Chan, S.; Jones, G.; Tochon-Danguy, H.; O'Keefe, G.; Masters, C.; Rowe, C., Abeta deposits in older non-demented individuals with cognitive decline are indicative of preclinical Alzheimer's disease. *Neuropsychologia* **2008,** *46* (6), 1688-97.

Virta, J.; Aalto, S.; Järvenpää, T.; Karrasch, M.; Kaprio, J.; Koskenvuo, M.; Räihä, I.; Viljanen, T.; Rinne, J., Voxel-based analysis of cerebral glucose metabolism in mono- and dizygotic twins discordant for Alzheimer disease. *J Neurol Neurosurg Psychiatry* **2009,** *80* (3), 259-66.

Virta, J.; Karrasch, M.; Kaprio, J.; Koskenvuo, M.; Räihä, I.; Viljanen, T.; Rinne, J., Cerebral glucose metabolism in dizygotic twin pairs discordant for Alzheimer's disease. *Dement Geriatr Cogn Disord* **2008,** *25* (1), 9-16.

Wadghiri, Y.; Sigurdsson, E.; Sadowski, M.; Elliott, J.; Li, Y.; Scholtzova, H.; Tang, C.; Aguinaldo, G.; Pappolla, M.; Duff, K.; Wisniewski, T.; Turnbull, D., Detection of Alzheimer's amyloid in transgenic mice using magnetic resonance microimaging. *Magn Reson Med* **2003,** *50* (2), 293-302.

Wahlund, L.; Julin, P.; Johansson, S.; Scheltens, P., Visual rating and volumetry of the medial temporal lobe on magnetic resonance imaging in dementia: a comparative study. *J Neurol Neurosurg Psychiatry* **2000,** *69* (5), 630-5.

Wahlund, L.; Julin, P.; Lindqvist, J.; Scheltens, P., Visual assessment of medical temporal lobe atrophy in demented and healthy control subjects: correlation with volumetry. *Psychiatry Res* **1999,** *90* (3), 193-9.

Walsh, D.; Klyubin, I.; Fadeeva, J.; Cullen, W.; Anwyl, R.; Wolfe, M.; Rowan, M.; Selkoe, D., Naturally secreted oligomers of amyloid beta protein potently inhibit hippocampal long-term potentiation in vivo. *Nature* **2002,** *416* (6880), 535-9.

Walsh, D.; Selkoe, D., A beta oligomers - a decade of discovery. *J Neurochem* **2007,** *101* (5), 1172-84.

Waragai, M.; Okamura, N.; Furukawa, K.; Tashiro, M.; Furumoto, S.; Funaki, Y.; Kato, M.; Iwata, R.; Yanai, K.; Kudo, Y.; Arai, H., Comparison study of amyloid PET and voxel-based morphometry analysis in mild cognitive impairment and Alzheimer's disease. *J Neurol Sci* **2009,** *285* (1-2), 100-8.

Wey, S.; Weng, C.; Lin, K.; Yao, C.; Yen, T.; Kung, H.; Skovronsky, D.; Kung, M., Validation of an (18) F-labeled biphenylalkyne as a positron emission tomography imaging agent for beta-amyloid plaques. *Nucl Med Biol* **2009,** *36* (4), 411-7.

Wiley, C.; Lopresti, B.; Venneti, S.; Price, J.; Klunk, W.; DeKosky, S.; Mathis, C., Carbon 11-labeled Pittsburgh Compound B and carbon 11-labeled (R)-PK11195 positron emission tomographic imaging in Alzheimer disease. *Arch Neurol* **2009,** *66* (1), 60-7.

Winblad, B.; Palmer, K.; Kivipelto, M.; Jelic, V.; Fratiglioni, L.; Wahlund, L.; Nordberg, A.; Bäckman, L.; Albert, M.; Almkvist, O.; Arai, H.; Basun, H.; Blennow, K.; de Leon, M.; DeCarli, C.; Erkinjuntti, T.; Giacobini, E.; Graff, C.; Hardy, J.; Jack, C.; Jorm, A.; Ritchie, K.; van Duijn, C.; Visser, P.; Petersen, R., Mild cognitive impairment--beyond controversies, towards a consensus: report of the International Working Group on Mild Cognitive Impairment. *J Intern Med* **2004,** *256* (3), 240-6.

Wolk, D.; Price, J.; Saxton, J.; Snitz, B.; James, J.; Lopez, O.; Aizenstein, H.; Cohen, A.; Weissfeld, L.; Mathis, C.; Klunk, W.; DeKoskym, S., Amyloid imaging in mild cognitive impairment subtypes. *Ann Neurol* **2009,** *65* (5), 557-68.

Yaqub, M.; Tolboom, N.; Boellaard, R.; van Berckel, B.; van Tilburg, E.; Luurtsema, G.; Scheltens, P.; Lammertsma, A., Simplified parametric methods for [11C]PIB studies. *Neuroimage* **2008,** *42* (1), 76-86.

Ye, L.; Morgenstern, J.; Gee, A.; Hong, G.; Brown, J.; Lockhart, A., Delineation of positron emission tomography imaging agent binding sites on beta-amyloid peptide fibrils. *J Biol Chem* **2005,** *280* (25), 23599-604.

Zaknun, J.; Leblhuber, F.; Schücktanz, H., Value of cerebral blood flow quantification in the diagnosis of dementia. *Nucl Med Commun* **2008,** *29* (3), 260-9.

Zetterberg, H.; Andreasson, U.; Hansson, O.; Wu, G.; Sankaranarayanan, S.; Andersson, M.; Buchhave, P.; Londos, E.; Umek, R.; Minthon, L.; Simon, A.; Blennow, K., Elevated cerebrospinal fluid BACE1 activity in incipient Alzheimer disease. *Arch Neurol* **2008,** *65* (8), 1102-7.

Ziolko, S. K.; Weissfeld, L. A.; Klunk, W. E.; Mathis, C. A.; Hoge, J. A.; Lopresti, B. J.; DeKosky, S. T.; Price, J. C., Evaluation of voxel-based methods for the statistical analysis of PIBPET amyloid imaging studies in Alzheimer's disease. *Neuroimage* **2006,** *33* (1), 94-102.